



**US Army Corps  
of Engineers**  
Waterways Experiment  
Station

Wetlands Research Program Technical Report WRP-CP-10

## **Open-Channel Flow Through Simulated Vegetation: Turbulence Modeling and Sediment Transport**

by Fabian Lopez, Marcelo Garcia

DMC QUALITY IMPROVED 4



August 1997 – Final Report  
Approved For Public Release; Distribution Is Unlimited



The following two letters used as part of the number designating technical reports of research published under the Wetlands Research Program identify the area under which the report was prepared:

	<u>Task</u>		<u>Task</u>
CP	Critical Processes	RE	Restoration & Establishment
DE	Delineation & Evaluation	SM	Stewardship & Management

**The contents of this report are not to be used for advertising, publication, or promotional purposes. Citation of trade names does not constitute an official endorsement or approval of the use of such commercial products.**



**Wetlands Research Program**

Technical Report WRP-CP-10  
August 1997

# **Open-Channel Flow Through Simulated Vegetation: Turbulence Modeling and Sediment Transport**

by Fabian Lopez, Marcelo Garcia

Hydrosystems Laboratory  
Department of Civil Engineering  
University of Illinois at Urbana-Champaign  
Urbana, IL 61801

**Final report**

Approved for public release; distribution is unlimited

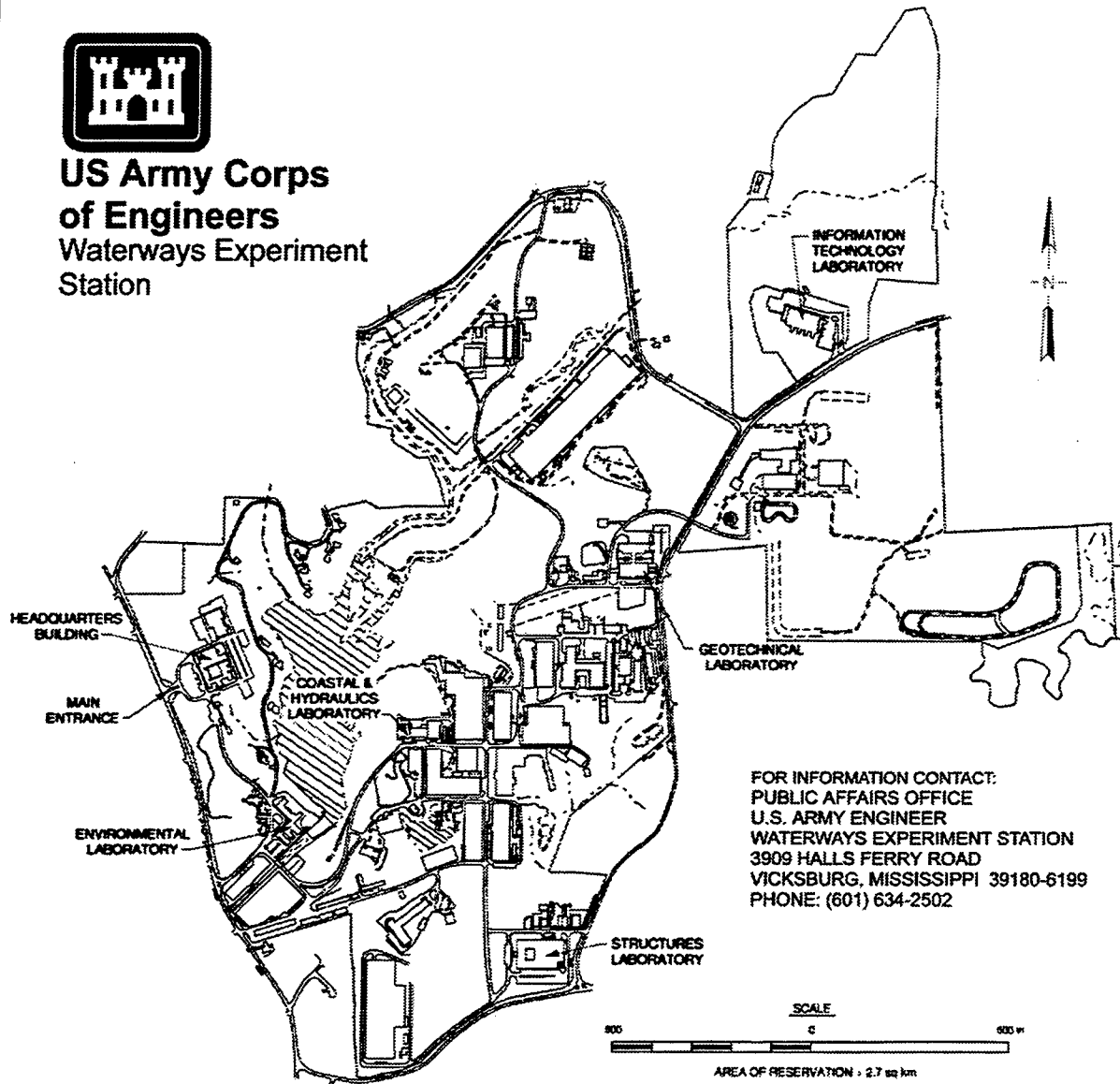
Prepared for U.S. Army Corps of Engineers  
Washington, DC 20314-1000

Monitored by U.S. Army Engineer Waterways Experiment Station  
3909 Halls Ferry Road, Vicksburg, MS 39180-6199

Under Work Unit 32752



**US Army Corps  
of Engineers**  
Waterways Experiment  
Station



**Waterways Experiment Station Cataloging-in-Publication Data**

Lopez, Fabian.

Open-channel flow through simulated vegetation : turbulence modeling and sediment transport / by Fabian Lopez, Marcelo Garcia ; prepared for U.S. Army Corps of Engineers ; monitored by U.S. Army Engineer Waterways Experiment Station..

123 p. : ill. ; 28 cm. -- (Technical report ; WRP-CP-10) (Wetlands Research Program technical report ; WRP-CP-10)

Includes bibliographic references.

1. Turbulence. 2. Sediment transport. 3. Channels (Hydraulic engineering) I. Garcia, Marcelo. II. United States. Army. Corps of Engineers. III. U.S. Army Engineer Waterways Experiment Station. IV. Wetlands Research Program (U.S.) V. Title. VI. Title: Turbulence modeling and sediment transport. VII. Series: Wetlands Research Program technical report ; WRP-CP-10. VIII. Series: Technical report (U.S. Army Engineer Waterways Experiment Station) ; WRP-CP-10.

TA7 W34 no. WRP-CP-10



# Critical Processes

## *Open-Channel Flow Through Simulated Vegetation: Turbulence Modeling and Sediment Transport (TR WRP-CP-10)*

### **ISSUE:**

In recent years, vegetated floodplains and wetlands have been regarded as constituents of the ecosystem where significant transport processes take place during floods. In this sense, sedimentation has been identified as a major contributor to nonpoint source pollution. Engineering tools are thus needed for estimating both the mean flow and turbulence structure as well as the suspended sediment transport capacity of vegetated waterways.

### **RESEARCH OBJECTIVE:**

The two-equation turbulence model based on the  $k-\epsilon$  closure scheme was developed to simulate the flow and turbulence characteristics of open-channel flows through nonemergent vegetation. Once the performance of the model was verified, the flow structure of vegetated open channels was numerically simulated. Simulated rigid and flexible plants were used to validate the model. Finally, dimensional analysis allowed identification of the dimensionless parameters that govern suspended sediment transport processes in the presence of vegetation, and thus helped in the design of numerical experiments to investigate the role of different flow properties, sediment characteristics, and vegetation parameters upon the transport capacity.

### **SUMMARY:**

The two-equation turbulence model was found to accurately represent the mean flow and turbulence

structure of open channels through simulated vegetation, thus providing the necessary information to estimate suspended sediment transport processes. A reduction of the averaged streamwise momentum transfer toward the bed (i.e., shear stress) induced by the vegetation was identified as the main reason for lower suspended sediment transport capacities in vegetated waterways compared with those observed in nonvegetated channels under similar flow conditions. Simulated profiles of kinematic eddy viscosity were used to solve the sediment diffusion equation, yielding distributions of relative sediment concentration slightly in excess of the ones predicted by the Rousean formula. A power law was found to provide a very good collapse of all the numerically generated data for suspended sediment transport rates in vegetated channels.

### **AVAILABILITY OF REPORT:**

This report is available on Interlibrary Loan Service from the U.S. Army Engineer Waterways Experiment Station (WES) Library, 3909 Halls Ferry Road, Vicksburg, MS 39180-6199, telephone (601) 634-2355.

To purchase a copy, call the National Technical Information Service (NTIS) at (703) 487-4650. For help in identifying a title for sale, call (703) 487-4780.

NTIS report numbers may also be requested from the WES librarians.

### **About the Authors:**

Dr. Marcelo Garcia is an Associate Professor at the University of Illinois at Urbana-Champaign. Dr. Fabian Lopez is with the National Institute of Science and Hydrologic Technique, Argentina. **Point of Contact** at the U.S. Army Engineer Waterways Experiment Station is Mr. Brad Hall, Research Hydraulic Engineer at the Coastal and Hydraulics Laboratory, (601) 634-3392.

# Contents

---

<b>Preface</b> .....	<b>xi</b>
<b>1 Introduction</b> .....	<b>1</b>
Background .....	1
Purpose of Study .....	2
<b>2 Literature Review</b> .....	<b>4</b>
<b>3 Theoretical Considerations</b> .....	<b>10</b>
Governing Equations for Flow Through Vegetation .....	10
Continuity Equation .....	12
Momentum Equations .....	13
Energy (Second-Order Moment) Equations .....	14
Modeling of Form-Drag Forces in Open-Channel Flows .....	19
Turbulence Modeling by a First-Level, Two-Equation Closure Scheme .....	21
Boundary Conditions and Constants for Open-Channel Flow Through Vegetation .....	25
Estimation of Reynolds Stress Tensor Components .....	26
Limitations of Turbulence Models Based on Flux-Gradient Approximations .....	29
Numerical Algorithm .....	30
<b>4 Turbulence Structure in Open-Channel Flows Without Vegetation</b> .....	<b>34</b>
Mean Flow .....	34
Second-order Moments .....	35
Energy Budget Terms .....	35
Eddy Viscosity and Mixing Length .....	35
Turbulent Scales .....	39
Validity of Flux Gradient Assumptions .....	39
<b>5 Suspended Sediment Transport in Open-Channel Flows without Vegetation</b> .....	<b>45</b>
Equation for Vertical Sediment Diffusion .....	45

Buoyancy Effects upon Suspended Sediment Transport Capacity .....	46
Vertical Profile of Suspended Sediment Concentration .....	50
Suspended Sediment Transport Capacity .....	50
<b>6 Turbulence Structure in Vegetated Open-Channel Flows</b>	<b>56</b>
Experiments in Open-Channel Flows with Simulated Vegetation .....	56
Mean Flow Characteristics .....	57
Second-order Moments .....	58
Reynolds stresses .....	58
Turbulent kinetic energy and turbulence intensities .....	64
Energy Budget Terms .....	64
Spatially averaged time-mean values .....	64
Budget of total turbulent kinetic energy .....	70
Eddy Viscosity and Mixing Length .....	70
Turbulent Length Scales .....	70
Momentum Transfer to the Bed .....	70
Manning's Resistance Coefficient .....	70
Impact of Wall Functions .....	78
Validity of Gradient-Flux Assumptions for Flow through Vegetation .....	78
Final Remarks .....	81
<b>7 Suspended Sediment Transport in Vegetated Open Channels</b>	<b>82</b>
Dimensional Analysis of Sediment Transport in Vegetated Open Channels ..	82
Experiments by Tollner, Barfield and Hayes (1982) .....	83
Vertical Profiles of Suspended Sediment Concentration .....	86
Suspended Sediment Transport Capacity .....	86
Suspended Sediment Transport Capacity as function of $H/h_p$ .....	86
Suspended Sediment Transport Capacity as function of $Ha$ .....	90
Relative Transport Capacity of Suspended Sediment .....	90
Final Remarks .....	96
<b>8 Summary and Conclusions</b> .....	<b>98</b>
<b>References</b> .....	<b>100</b>
<b>Appendix A Notation</b> .....	<b>A1</b>

# List of Figures

---

Figure 3.1 Schematic of flow through vegetation .....	12
Figure 3.2 Schematic of pressure field .....	20
Figure 3.3 Definition diagram for cylinder density. ....	20
Figure 3.4 Variation of $C\mu$ with the ratio $P/\epsilon$ .....	28
Figure 3.5 Definition of control volume. ....	31
Figure 4.1 Observed and predicted vertical distributions of mean velocity for experiments on transitionally rough and hydraulically smooth bed conditions. ....	35
Figure 4.2 Observed and predicted vertical distribution of dimensionless rms value of streamwise velocity fluctuations .....	36
Figure 4.3 Observed and predicted vertical distribution of rms value of vertical velocity fluctuations, smooth-bed condition. ....	37
Figure 4.4 Observed and predicted vertical distribution of dimensionless energy budget terms. ....	38
Figure 4.5 Observed and predicted vertical distribution of dimensionless kinematic eddy viscosity and mixing length, smooth-bed condition. ...	39
Figure 4.6 Observed and predicted vertical distribution of dimensionless streamwise macro-length scale, smooth and transitionally rough bed conditions. ....	41
Figure 4.7 Observed and predicted vertical distribution of dimensionless Taylor's micro-scale .....	42
Figure 4.8 Observed and predicted vertical distribution of dimensionless Kolmogorov micro-scale. ....	43
Figure 4.9 Evaluation of Corrsin's criteria according to equations 40 and 42. ....	44

Figure 5.1 Suspended sediment transport capacity as function of Rouse number and different buoyancy effects together with predictions by Einstein's (1950) formula .....	51
Figure 5.2 Relative water discharge as function of Rouse number and different buoyancy effects .....	52
Figure 5.3 Dimensionless vertical profile of suspended sediment concentration for different mean diameters .....	53
Figure 5.4 Estimated suspended sediment transport capacity for different mean diameters .....	54
Figure 5.5 Estimated suspended sediment transport capacity for different mean flow depths .....	55
Figure 6.1 Observed and predicted vertical distribution of mean velocity, rigid conditions .....	59
Figure 6.2 Observed and predicted vertical distribution of mean velocity, flexible conditions .....	60
Figure 6.3 Observed and predicted vertical distribution of mean velocity in semilog scale. ....	61
Figure 6.4 Observed and predicted vertical distribution of Reynolds stresses, rigid conditions .....	62
Figure 6.5 Observed and predicted vertical distribution of Reynolds stresses, flexible conditions. ....	63
Figure 6.6 Observed and predicted vertical distribution of streamwise turbulence intensity, rigid condition. ....	65
Figure 6.7 Observed and predicted vertical distribution of streamwise turbulence intensity, flexible condition. ....	66
Figure 6.8 Observed and predicted vertical distribution of total streamwise turbulence intensity .....	67
Figure 6.9 Observed and predicted vertical distribution of different terms in the spatially averaged, temporal-mean, turbulent kinetic energy budget for $(C_{fk}, C_{fe})=(0.0,0.0)$ .....	68
Figure 6.10 Observed and predicted vertical distribution of different terms in the spatially-averaged, temporal-mean, turbulent kinetic energy budget for $(C_{fk}, C_{fe})=(0.25,0.33)$ . ....	69

Figure 6.11 Observed and predicted vertical distribution of different terms in the total turbulent kinetic energy budget. ....	71
Figure 6.12 Observed and predicted vertical distribution of eddy viscosity, rigid condition .....	72
Figure 6.13 Observed and predicted vertical distribution of mixing length, rigid condition .....	73
Figure 6.14 Observed and predicted vertical distribution of eddy viscosity and mixing length, flexible vegetation. ....	74
Figure 6.15 Observed (symbols) and predicted (thin lines) vertical distribution of dimensionless length scales for Exp1. ....	75
Figure 6.16 Momentum transfer towards the bed vs. dimensionless plant density. ....	76
Figure 6.17 Computed values of Manning's resistance coefficient as a function of plant density. ....	77
Figure 6.18 Computed values of flow depth and Manning's resistance coefficient as a function of density measured as number of plants per square meter. ....	77
Figure 6.19 Impact of different wall functions .....	79
Figure 6.20 Evaluation of Corrsin's criteria for flow through vegetation	80
Figure 7.1 Numerical simulation of experimental observations by Tollner, Barfield and Hayes (1982) .....	85
Figure 7.2 Observed and predicted vertical distribution of dimensionless suspended sediment concentration, condition I. ....	87
Figure 7.3 Observed and predicted vertical distribution of dimensionless suspended sediment concentration, condition II .....	88
Figure 7.4 Computed suspended transport capacity as a function of $u_*/w_s$ , $Re_p$ and $H/hp$ , for $Ha = 0.70$ .....	89
Figure 7.5 Computed suspended transport capacity as a function of the parameters $u_*/w_s$ , $Re_p^b$ and $H/hp$ , for $Ha = 0.70$ .....	91
Figure 7.6 Computed suspended transport capacity as a function of parameter $u_*/w_s$ , $Re_p^b (H/hp)^{0.38}$ , for $Ha = 0.70$ .....	92
Figure 7.7 Computed suspended transport capacity as a function of $u_*/w_s$ and $Re_p$ , for $Ha = 0.70$ and $H/hp = 3.5$ . ....	93

Figure 7.8 Computed suspended transport capacity as a function of $u^*/w_s$ , $R_{ep}$ and $Ha$ , for $H/hp = 3.5$ .....	94
Figure 7.9 Computed relative transport in suspension as a function of density and sediment size for constant water discharge, channel slope, and plant height. ....	95
Figure 7.10 Suspended sediment transport capacity as a function of parameter $u^*/w_s R_{ep}^b (H/hp)^{0.38}$ , for $Ha = 0.70$ . Computations by the k- $\omega$ model compared to best-fit line from k- $\epsilon$ model. ....	97

# Preface

---

The work described in this report was authorized by Headquarters, U.S. Army Corps of Engineers (HQUSACE), as part of the Critical Processes Task Area of the Wetlands Research Program (WRP). The work was performed under Work Unit 32752, "Sedimentation," for which Mr. Brad Hall was Principal Investigator. Mr. Dick Dibuono (CECW-EH-W) was the WRP Technical Monitor for this work.

Mr. Dave Mathis (CERC-C) was the WRP Coordinator at the Directorate of Research and Development, HQUSACE; Mr. William L. Klesch (CECW-PO) served as the WRP Technical Monitors' Representative; Dr. Russell F. Theriot, U.S. Army Engineer Waterways Experiment Station (WES), was the WRP Program Manager. Mr. Jack Davis was the Task Area Manager.

The work was performed at The University of Illinois at Urbana-Champaign at Urbana, IL. This report was prepared by Drs. Fabian Lopez and Marcelo Garcia, under Contract No. DACW39-94-K-0010, and under the general supervision of Messrs. Richard A. Sager, Acting Director, Hydraulics Laboratory, WES; William McAnally, Chief, Waterways and Estuaries Division, Hydraulics Laboratory; and Michael J. Trawle, Chief, Rivers and Streams Branch, Waterways and Estuaries Division; and under the direct supervision of Mr. Brad R. Hall, Rivers and Streams Branch. Messrs. McAnally and Hall performed the technical review of the report.

This report is being published by the WES Coastal and Hydraulics Laboratory (CHL). The CHL was formed in October 1996 with the merger of the WES Coastal Engineering Research Center and Hydraulics Laboratory. Dr. James R. Houston is the Director of the CHL and Messrs. Richard A. Sagar and Charles C. Calhoun, Jr., are the Assistant Directors.

Technical Director of WES was Dr. Robert W. Whalin. Commander was COL Bruce K. Howard, EN.

*The contents of this report are not to be used for advertising, publication, or promotional purposes. Citation of trade names does not constitute an official endorsement or approval of the use of such commercial products.*

# 1 Introduction

---

## Background

Historically, vegetation in streams and rivers has been considered by hydraulic engineers as a source of flow resistance, and as such it has usually been eliminated with the goal of improving water conveyance. This explains why earlier research interests were focused primarily on the estimation of resistance laws, mean velocity distributions, and the determination of approximate rules for the partition of the total action of gravity between friction drag due to bed roughness and form drag due to plants. In recent years, however, plants in aquatic environments have reached a different status, and vegetation is no longer regarded merely as an obstruction to the movement of water, but rather as a means of providing stabilization of banks and channels and habitat and food for animals, as well as pleasing landscapes for recreational use (Haslam and Wolseley 1981). The preservation of vegetation is nowadays considered of great relevance for the ecology of rivers. In recent years, such unprecedented environmental concerns have motivated the onset of several studies concentrating on the characterization of turbulent transport processes in natural flow conditions. In particular, there has been an increasing need for the understanding of retention processes in wetlands, by which suspended solids and/or chemical contaminants (pesticides, heavy metals, etc.) are being deposited and retained within a natural or artificial waterway. In particular, vegetated floodplains and wetlands have been regarded lately as constituents of the ecosystem where significant transport processes take place during floods. In this sense, sedimentation has been identified as a major source of nonpoint source pollution impairment in U.S. rivers and lakes, where excessive sedimentation results in the destruction of fish habitat, decreased recreational use, and loss of

water storage capacity (U.S. Environmental Protection Agency 1993). In Illinois for instance, field studies conducted in riverine wetlands have indicated sediment-trapping efficiencies ranging from 60 to 85 percent (Demissie 1990), and estimates by the U.S. Department of Agriculture (USDA) indicate that annual offsite costs of sediment derived from cropland erosion alone are of the order of \$2 to \$6 billion, with an additional \$1 billion arising from loss in compared productivity (USDA 1987).

All these have prompted the development of engineering tools for the estimation of contaminant and sediment transport, for the assessment of environmental impacts, for the evaluation of design alternatives, and for the management of wetlands. Although some general models based on rather crude assumptions have been developed, they have benefited very little from advances in the knowledge of turbulence in the presence of vegetation from other research areas such as atmospheric sciences. As a result, very few physically based models exist to help engineers evaluate transport processes and in particular the sediment retention capabilities of vegetated waterways.

## **Purpose of Study**

The overall objective of the present work is to investigate the effect of vegetation on the mean flow properties and on the turbulence structure in open-channel flows and the implications of the resulting flow structure for the entrainment, transport, and deposition of suspended sediment. The working hypothesis is that if vegetation-induced roughness increases flow resistance via momentum diffusion, the same roughness should also reduce the diffusion of suspended sediment. In particular, it is important to know if the suspended sediment distribution is significantly different from the Rousean distribution for equilibrium open-channel suspensions, and if it is, what are the implications for the advective and diffusive transport of sediment in vegetated channels.

To achieve such objectives, knowledge about turbulence characteristics in the presence of vegetation coming from atmospheric boundary layers will be coupled with advances in the numerical simulation of free-surface flows. This integration will be used to produce a two-equation turbulence closure scheme for modeling the complex turbulence structure of flows through vegetation and for estimating related transport processes in plant environments. The numerical model will then provide quantitative information about the role played by flow parameters, sediment properties, and vegetation characteristics in the suspended sediment transport capacity of vegetated free-surface flows, and therefore will facilitate the assessment of the factors that influence the sediment-trapping

ability of wetlands, as well as the conditions under which previously deposited sediment/pollutants might be reentrained into suspension and exported out of a given system.

## 2 Literature Review

---

Mean flow and turbulence characteristics in the presence of vegetation have received a lot of attention in the last few years, specially for the case of atmospheric flows over plant canopies. One of the main motivations for such studies has been the need for understanding related transport processes in natural environments, such as the transport of pollutants, heat, carbon dioxide, etc. Regarding free-surface flows in streams, engineering research on vegetated open-channel flows has traditionally been limited to the estimation of resistance laws. In general, the investigations may be classified into two groups corresponding to the study of rigid and flexible vegetation, respectively. An extensive bibliography on the subject, with more than 350 references, has been collected by Dawson and Charlton (1988). Brief review of some of the previous work follows.

Pioneering work on open-channel flow through vegetation was performed by Ree and Palmer (1949; see also Palmer 1945), who developed a method for estimating water discharge capacity. They employed the often-used Manning's coefficient, concluding that the  $n-UR_h$  relationship depends on the physical properties of the grass and is thus independent of channel geometry and flow conditions. Here  $U$  is the mean velocity and  $R_h$  is the hydraulic radius.<sup>1</sup>

A series of studies has been conducted at the University of Waterloo, Canada, to determine the flow characteristics of vegetated open channels. In their early investigation, Kowen, Unny, and Hill (1969) used artificial styrene made roughness elements glued to the bottom of a laboratory flume to study flow over simulated, flexible vegetation. Pitot tube technique allowed them to measure

---

<sup>1</sup>. For convenience, symbols and unusual abbreviations are listed and defined in the Notation (Appendix A).

velocity distributions. These authors found a good fit to their experimental results with a modified form of the logarithmic law by adjusting the values of the roughness parameter and the origin intercept. In the case of flexible elements they found the roughness parameter to be 12 percent larger than the deflected height of the elements. They suggested, however, the use of a log law using the undeflected height of the plants, and by comparing it with experimental field data they concluded that both the origin intercept and the slope were functions of both vegetation density and plant flexibility. It is interesting to note that almost all researchers suggest the use of a logarithmic law for the vertical profile of mean velocities above the plants, hence implicitly assuming the existence of an equilibrium layer, i.e., with production of turbulence being locally balanced by dissipation.

Kowen and Unny (1973) conducted a series of experiments simulating vegetation by using plastic strips of different thicknesses. They proposed the existence of three basic flow regimes: (a) erect, when the plastic strips are erect and stationary; (b) waving, when the strips undergo a waving motion; and (c) prone, when the strips are bent over. Similar regimes were observed by Gourlay (1970) for Kikuyu grass. Despite these kinematical classifications, the hydraulic behavior of simulated vegetation showed the existence of only two regimes, because the frictional coefficient for both erect and waving "plants" indicated identical values, whereas much lower friction factors (by a factor of five) were observed for the prone cases. These observations clearly indicate the existence of a common turbulence structure for flow in vegetated channels for both erect and waving plants, whereas a different turbulence dynamic probably dictates the behavior of prone or bent-over vegetation. This latter fact is herein interpreted as a consequence of the reduced turbulent diffusivity coefficient for momentum at the top of the plants due to the vertical blockage exerted by the inclined elements. These investigators also introduced a stiffness parameter,  $MEI$ , where  $M$  is the relative density of the plants and  $EI$  is the stem flexural rigidity.

Numerical predictions of sediment transport capacities in vegetated free-surface flows were attempted by Li and Shen (1973) based on a superposition technique for the wakes generated behind isolated elements, a procedure originally proposed by Petryk (1969). They assumed local drag coefficients for open channels of about 1.2, and their results showed mean drag coefficients close to 1.1 for staggered arrangements independent of plant density, while the mean drag coefficient for square, parallel patterns showed increasing values for increasing spacing. They applied this method for the estimation of bed load, and compared the relative effect on sediment yields by various combinations of tall vegetation.

Also in line with the use of Manning's coefficient as a measure of flow resistance, Petryk and Bosmajian (1975) developed a quantitative procedure for predicting this coefficient as a function of flow depth and vegetation characteristics. Their method considered flow depths that were less than or equal to the maximum plant height, and its most useful application is in predicting the variation of Manning's  $n$  with depth.

Among the attempts to build models that provide more information about the flow structure, not only about the overall flow resistance, Reid and Whitaker (1976) developed a numerical algorithm for wind-driven flow through and above vegetative obstructions. Accordingly, they divided the water column into two layers, one within the canopy, and one above it and averaged the governing equations within each layer. The main drawback of this approach is the need to specify the interfacial stress at the top of the plants.

In the area of atmospheric boundary layers, Wilson and Shaw (1977), recognizing some of the limitations of first-level turbulence closure schemes, developed a higher-order closure model for atmospheric flows above plant canopies. At the same time these authors were the first to recognize the necessity of spatial as well as temporal averaging of the governing equations for the proper one-dimensional representation of the problem.

More recently Kowen and Li (1980) proposed a new methodology for the design of channels with vegetative linings, thus improving the traditional  $n-UR_h$  method. The originality of this new method consists in introducing some biomechanical concepts and proposing a field methodology for estimating the flexural stiffness of natural vegetation: a "board drop test" and a vegetation height method.

Hino (1981) was probably one of the first researchers to address the importance of vegetation in open channels from an ecohydrodynamic point of view. He also pointed out the particular mathematical and numerical difficulties that arise in the case of free-surface flows, which transform the problem into a nonlinear two-point boundary-value problem with an implicitly posed boundary condition at the bottom, and presented some numerical results as well as perturbation solutions using a mixing-length closure scheme.

Raupach and Shaw (1982), based on previous work by Wilson and Shaw (1977), first proposed a mathematical procedure for obtaining the momentum and energy equations in multi-connected flows clearly stating the rules for the commutation of spatial averaging operators and spatial differentiation. Their work allows for the identification of different momentum and energy dispersive

terms arising as a consequence of the three-dimensional nature of the flow structure as well as of the noncommutation of the operators mentioned.

One of the few laboratory works on the sedimentology of erect vegetation in open channels was conducted by Tollner, Barfield, and Hayes (1982; Tollner 1974), which reported good predictions of sediment transport capacity using parameters similar to the ones proposed by Graf (1971), but with the channel width replaced by the element spacing. Their results were, however, obtained in a relatively short (2.10 m) and narrow (0.13 m) channel, where the achievement of equilibrium conditions (at least for suspended sediment profiles) becomes questionable.

The primitive nature of the closure scheme used by Reid and Whitaker (1976) motivated Burke and Stolzenbach (1983; Burke 1982), who were probably one of the first to propose the use of a two-equation turbulence closure scheme for free-surface flows through obstructions. In this kind of closure the eddy viscosity is assumed proportional to the product of a characteristic length and a velocity scale, both obtained by solving two transport equations, so that they do not have to be specified a priori for each problem. The presence of vegetation was accounted for in the turbulent kinetic energy and dissipation equations by the introduction of drag-related source terms, but no mathematical derivation was presented to justify these assumptions. While their model predictions were generally in good agreement with experimental observations, they recognize the lack of knowledge about the value of the drag coefficient of the elements in open-channels but did not explain satisfactorily the overestimation of the turbulent kinetic energy.

Another simpler yet useful attempt to close the turbulence problem is the one due to Christensen (1985), who used the mixing length approach to compute eddy viscosities, and thus developed an explicit formula for the velocity profile over a flexible roughness layer to be used in heavily vegetated rivers and channels.

In light of the proposed averaging procedure by Raupach and Shaw (1982), Raupach et al. (1986) conducted a series of experiments aimed at characterizing the turbulence structure of atmospheric flows over a vegetated canopy. They used a laboratory wind tunnel with a model plant canopy made of aluminium strips, where velocity measurements were taken at several points both above and within the roughness elements using a special three-dimensional hot-wire anemometer. They were thus able to estimate the different terms composing the turbulent kinetic energy balance within the canopy. From their observations, the importance of the inertial transport term atop of the simulated canopy becomes

noticeable, which represents a major loss near the top of the canopy but constitutes the principal gain mechanism lower down.

Saowapon and Kowen (1989) have advanced an analytical model for predicting vertical velocity profiles in vegetated channels that accounts for the flexibility of the plants. While the results of both the Christensen (1985) and Saowapon and Kowen (1989) models look rather encouraging when compared against laboratory observations, it is clear that the algebraic scheme used to compute eddy viscosities (i.e. a mixing length approach) provides only limited information on the effect of roughness elements on the diffusion of momentum (and eventually sediment).

Kadlec (1990) obtained a power law resistance function for overland flow over *Spartina* grass in terms of depth and friction slope. The exponent on the depth appears to describe both the vertical vegetation stem density and the bottom elevation distribution and takes a value close to three. This fact seems to indicate a strong depth-dependent behavior in wetlands, where depth-time variations are strongly regulated by a condition of small and slowly varying depths.

The Kanazawa University group (Tsujimoto et al. 1991<sup>a</sup> and 1991<sup>b</sup>; Tsujimoto 1993; Shimizu and Tsujimoto 1993) has reported several open-channel turbulence measurements in the presence of vegetation. A series of experimental as well as numerical studies has been conducted concerning both rigid and flexible emergent and nonemergent vegetation. Their results for rigid vegetation show that an almost uniform mean velocity distribution prevails when the mean flow depth is smaller than the vegetation height, with negligible turbulent momentum exchange and small turbulent intensities. On the other hand, shear-dominated flows seem to prevail for nonemergent vegetation, even below the top of the plants, as a consequence of active momentum exchange between the faster surface flow and the flow within the simulated vegetation. In this latter case, a peak in the Reynolds stress distribution is observed at the top of the roughness elements. The corresponding results for flexible vegetation show that the mean velocity profile is no longer as uniform as with rigid elements for emergent vegetation, showing slightly decreasing values as the free surface is approached. Turbulent intensities are still negligible. On the other hand, nonemergent results indicate the existence of a deflection point near the top of the elements, with a corresponding peak in the vertical distribution of turbulent intensities. Concerning the numerical model, relatively good agreement with the experimental observations was obtained with a modified version of the standard high-Reynolds-number  $k-\epsilon$  model, also with drag-related source terms accounting for the presence of vegetation. Weighting factors in these source

terms were fit to reproduce observed distributions of mean velocity and Reynolds stresses. Although the numerical code is very similar to the one employed by Burke and Stolzenbach (1983), the weighting factors in both schemes are radically different, the most striking aspect being the value of 0.07 obtained by Tsujimoto et al. for the drag-related turbulence production term compared to the value of 1.0 used by Burke and Stolzenbach. It is worth mentioning that with the value of 0.07, Tsujimoto et al. obtained a very good fit for the measured turbulence intensities. In a more recent work, however, Tsujimoto and Shimizu (1994) report good agreements with experimental observations by using the same weighting factors as Burke and Stolzenbach. It is therefore not clear at all why very low values of the weighting coefficients yield good agreement with the observed turbulent kinetic energy profiles, whereas from a physical point of view the coefficient of the work done by the flow against form-drag forces should be equal to unity (and thus very close to 1.0 in the numerical model). Note that both approaches give a similar degree of fit to observed profiles of mean velocities and Reynolds stresses, which should be attributed to the fact that eddy viscosity is computed as proportional to the ratio between  $k$  and  $\epsilon$ , so that certain combinations of the weighting coefficients in the drag-related source terms in  $k$  and  $\epsilon$  equations yield similar values of eddy viscosity.

Finally, concerning field results, Freeman, Hall and Abraham (1994) performed several field tests to determine Manning's  $n$  values and sediment trap efficiencies for stands of bulrushes. Their results indicate resistance coefficients substantially higher than the ones suggested by the U.S. Geological Survey (Arcement and Schneider 1989). Manning's  $n$  was observed to be in a range between 0.26 and 0.70, with values increasing linearly with vegetation density.

# 3 Theoretical Considerations

---

As seen in the previous chapter, most attempts to numerically simulate open-channel flows in the presence of vegetation have used either very simplified or more complex closure schemes, but with the common basis of artificially introducing the effect of vegetation by adding body forces. As will be shown in this chapter, this approach has led to some inconsistencies when numerical results are compared against experimental observations. To overcome such difficulties, the governing equations are herein first derived for a free-surface flow through obstacles, adapting expressions originally developed for atmospheric flows through plant canopies. Through this derivation, it will be shown that the presence of vegetation generates dispersive fluxes of momentum and energy as well as viscous and form-drag forces. Since the latter is usually parameterized using a drag coefficient, the second part of this chapter deals with the evaluation of this coefficient in open channels. Once the governing equations that mathematically define the problem are obtained, the third part of the chapter introduces the assumptions needed in order to close the turbulence problem at first level using a two-equation algorithm. Finally, some limitations of the assumptions introduced are presented, followed by a brief description of the numerical method employed to solve the resulting system of nonlinear partial differential equations.

## Governing Equations for Flow Through Vegetation

This section deals with open-channel flow in the presence of vegetation. Therefore the analysis presented is a slight modification of the approach proposed by Raupach and Shaw (1982) for atmospheric flows through plant

canopies. From a mathematical point of view, the flow of water through and above plants presents new challenges due to the three-dimensionality of the turbulence, thus representing a highly nonhomogeneous flow field. Since from an engineering perspective a one-dimensional description of the problem is commonly desirable, the need for spatially averaging (at least horizontally) naturally arises in the problem. In an earlier work, Wilson and Shaw (1977) already noted that the traditional approach of arbitrarily introducing form-drag as an extra body force in the momentum equation incorrectly describes the effect of wake turbulence. But it was not until the work of Raupach and Shaw (1982) that the complete set of equations became available.

Wilson and Shaw (1977) offered two averaging schemes for the conservation equations. In the first one, hereafter termed Scheme I, the equations describing the instantaneous flow field are averaged over a plane large enough to eliminate fluctuations due to both the turbulent scales and the canopy structure. Consider an open-channel flow through a regular array of vertical, rigid cylinders simulating vegetation such as depicted in Figure 3.1. Freezing the flow at any given instant and analyzing the instantaneous velocity field will show the existence of spatial variations due to the canopy (for example, differences between  $u_1^1$ ,  $u_1^2$  and  $u_1^3$ , where  $u_i^j$  represents the component along the  $i$ -axis,  $x_i$ , of the instantaneous velocity at location  $j$ ) as well as spatial variations at similar locations in the flow due to the intrinsic nature of turbulence (for example, differences between  $u_1^1$ ,  $u_1^4$  and  $u_1^5$ ). Therefore, if the channel is sufficiently wide and long, a large enough horizontal area has to be chosen so that averages of the instantaneous flow field performed over that plane will provide mean values independent of spatial variations due to the canopy structure and the turbulence. In the second averaging procedure proposed by Wilson and Shaw (1977), hereafter called Scheme II, the three-dimensional flow structure is locally time-averaged first in the usual way to filter fluctuations due to the turbulence, and then spatially averaged to eliminate variations due to the canopy structure. Referring to the experiment, at each location there would be a fluctuating velocity series in the time domain. First a temporal average would thus be performed at each location to get rid of turbulent fluctuations, and then the time-mean data would be spatially averaged to filter spatial variations. It is readily seen that for regularly arranged plants the extent of the spatial filter in the first scheme has to be much larger than in the second one.

In the following discussion, angle brackets and overbars will indicate horizontal and temporal averages, respectively, and double and single primes will indicate spatial and temporal fluctuations, respectively, from their corresponding mean values. The formal definition of a horizontal average of a variable  $\psi$  is (see Figure 3.1):

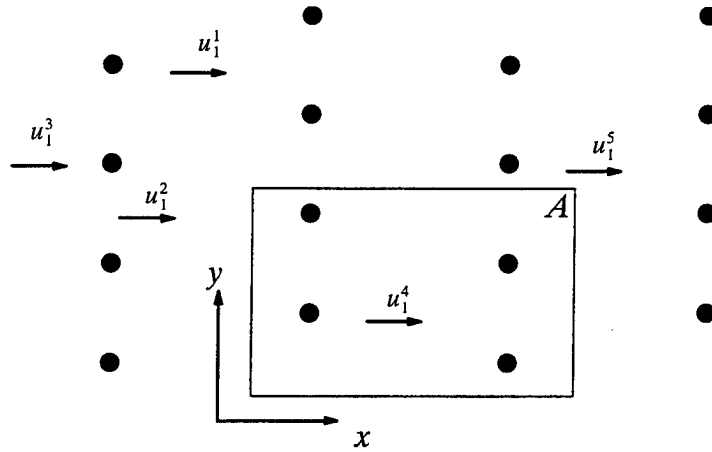


Figure 3.1 Schematic of flow through vegetation

$$\langle \psi \rangle = \frac{1}{A} \iint \psi(x, y) dx dy \quad (1)$$

where

$A$  = horizontal area of rectangle shown in Figure 3.1

From a mathematical point of view the spatial averaging operator in a flow through obstacles satisfies all but one of the commutation properties required for a turbulence averaging operator (Monin and Yaglom 1971; Schlichting 1979). This exception concerns the commutation between averaging and differentiation operations. Raupach and Shaw (1982) clearly show how Green's theorem may be used to demonstrate that if  $\Psi$  is constant at the fluid-element interface, then horizontal averaging and spatial differentiation commute (i.e.  $\langle \partial \psi / \partial x_i \rangle = \partial \langle \psi \rangle / \partial x_i$ ), and otherwise they do not commute. In particular, three cases of interest result: spatial differentiation and horizontal averaging do not commute for pressure, and neither do Laplacian operators and horizontal averaging for velocity, but first-order spatial differentiation and horizontal averaging do commute for velocity and its higher order moments.

### Continuity Equation

The instantaneous continuity equation for an incompressible, homogeneous and steady flow is (tensor notation will be used):

$$\frac{\partial u_i}{\partial x_i} = 0 \quad (2)$$

Because of the rules enumerated in the preceding section, both schemes yield essentially identical results when Equation 2 is considered, i.e.:

$$\begin{array}{c} \text{Scheme I} \\ \frac{\partial}{\partial x_i} \langle u_i \rangle = 0 \end{array} \quad \left| \quad \begin{array}{c} \text{Scheme II} \\ \frac{\partial}{\partial x_i} \langle \bar{u}_i \rangle = 0 \end{array} \right. \quad (3)$$

### Momentum Equations

The Navier-Stokes equation for an incompressible, homogeneous flow is

$$\frac{\partial u_i}{\partial t} + u_j \frac{\partial u_i}{\partial x_j} = -\frac{1}{\rho} \frac{\partial p}{\partial x_i} + g_i + \nu \nabla^2 u_i \quad (4)$$

where

$t$  = time

$p$  = instantaneous pressure

$g_i$  = component in the  $i$ th direction of the gravitational acceleration

$\nu$  = fluid kinematic viscosity

The resulting momentum equation under Scheme I is found by following the usual way of first replacing  $u_i = \langle u_i \rangle + u_i''$  and  $p = \langle p \rangle + p''$ , and then averaging spatially using the aforementioned rules, yielding (Raupach and Shaw 1982):

$$\begin{aligned} & \frac{\partial \langle u_i \rangle}{\partial t} + \langle u_j \rangle \frac{\partial \langle u_i \rangle}{\partial x_j} + \frac{\partial}{\partial x_j} \langle u_i'' u_j'' \rangle = \\ & -\frac{1}{\rho} \frac{\partial \langle p \rangle}{\partial x_i} - \frac{1}{\rho} \left\langle \frac{\partial p''}{\partial x_i} \right\rangle + g_i + \nu \nabla^2 \langle u_i \rangle + \nu \langle \nabla^2 u_i'' \rangle \end{aligned} \quad (5)$$

Note that since  $p''$  is not constant at the fluid-element interface, then  $\langle \partial p'' / \partial x_i \rangle$  is not equal to  $\partial \langle p'' \rangle / \partial x_i$  (which by definition is zero).

To obtain the averaged equation under Scheme II, first time-average the equation in the usual way, then substitute  $\bar{u}_i = \langle \bar{u}_i \rangle + \bar{u}_i''$  and  $\bar{p} = \langle \bar{p} \rangle + \bar{p}''$ , and finally a spatial average is performed yielding:

$$\begin{aligned} & \frac{\partial \langle \bar{u}_i \rangle}{\partial t} + \langle \bar{u}_j \rangle \frac{\partial \langle \bar{u}_i \rangle}{\partial x_j} + \frac{\partial}{\partial x_j} \langle \bar{u}_i'' \bar{u}_j'' \rangle + \frac{\partial}{\partial x_j} \langle \bar{u}_i' \bar{u}_j' \rangle = \\ & -\frac{1}{\rho} \frac{\partial \langle \bar{p} \rangle}{\partial x_i} - \frac{1}{\rho} \left\langle \frac{\partial \bar{p}''}{\partial x_i} \right\rangle + g_i + \nu \nabla^2 \langle \bar{u}_i \rangle + \nu \langle \nabla^2 \bar{u}_i'' \rangle \end{aligned} \quad (6)$$

It is easily observed that Equations 5 and 6 are identical, provided that the averaging plane under Scheme I is large enough to assure that  $\langle u_i \rangle = \langle \bar{u}_i \rangle$  and  $\langle p \rangle = \langle \bar{p} \rangle$ , with the only exception being in the form of the Reynolds stress term. Thus the one-dimensional momentum equation for flow through obstacles accounts not only for a Reynolds stress due to turbulent momentum transfer,  $\langle \bar{u}_i' u_j' \rangle$ , but also for stresses that arise due to spatial variations of the mean flow field,  $\langle \bar{u}_i'' \bar{u}_j'' \rangle$ . Hence the total resulting stress becomes:

$$\langle u_i'' u_j'' \rangle = \langle \bar{u}_i'' \bar{u}_j'' \rangle + \langle \bar{u}_i' u_j' \rangle \quad (7)$$

Unfortunately the dispersive fluxes (first term on the right) have so far eluded direct measurements either in open channels or atmospheric boundary layers, so that their relative effect upon the total stress, albeit believed to be small, still remains unknown. From a mathematical/physical point of view it becomes however clear that the simple addition of drag-related body forces in the momentum equation is essentially incorrect since the dispersive fluxes are not included. The problem becomes even more relevant when higher-order moments of velocity are considered.

### Energy (Second-Order Moment) Equations

The usual procedure for obtaining the equations for the mean flow as well as for the turbulent kinetic energy (e.g., Hinze 1975) will be followed. Thus, the total kinetic energy under Scheme I yields:

$$\frac{1}{2} \langle u_i u_i \rangle = \frac{1}{2} \langle u_i \rangle \langle u_i \rangle + \frac{1}{2} \langle u_i'' u_i'' \rangle \quad (8)$$

With due regard to the commutative properties mentioned in the previous section, the equation for the mean kinetic energy is (Raupach and Shaw 1982):

$$\begin{aligned} \left( \frac{\partial}{\partial t} + \langle u_j \rangle \frac{\partial}{\partial x_j} \right) \frac{\langle u_i \rangle \langle u_i \rangle}{2} &= \langle u_i'' u_j'' \rangle \frac{\partial \langle u_i \rangle}{\partial x_j} \\ &- \frac{\partial}{\partial x_j} \left( \langle u_i \rangle \langle u_i'' u_j'' \rangle + \frac{\langle p \rangle \langle u_j \rangle}{\rho} \right) \\ &+ \nu \langle u_i \rangle \langle \nabla^2 u_i'' \rangle - \frac{1}{\rho} \langle u_i \rangle \left\langle \frac{\partial p''}{\partial x_i} \right\rangle \end{aligned} \quad (9)$$

and likewise the budget of turbulent kinetic energy under such scheme gives (Raupach and Shaw 1982):

$$\begin{aligned}
\left( \frac{\partial}{\partial t} + \langle u_j \rangle \frac{\partial}{\partial x_j} \right) \frac{\langle u_i'' u_i'' \rangle}{2} &= - \langle u_i'' u_j'' \rangle \frac{\partial \langle u_i \rangle}{\partial x_j} \\
- \frac{\partial}{\partial x_j} \left( \frac{\langle u_i'' u_i'' u_j'' \rangle}{2} + \frac{\langle p'' u_j'' \rangle}{\rho} \right) &+ \nu \langle u_i'' \nabla^2 u_i'' \rangle \\
+ \frac{1}{\rho} \langle u_i \rangle \left\langle \frac{\partial p''}{\partial x_i} \right\rangle &
\end{aligned} \tag{10}$$

The right-hand side of each equation contains four terms: (a) a shear-production term, a source term in Equation 10 but a sink term in the budget of mean flow energy, which converts mean kinetic energy to large-scale turbulent kinetic energy; (b) a turbulent transport term with the usual inertial and pressure components; (c) a viscous term; and (d) a wake-production term, a source term in Equation 10 but a sink in Equation 9, representing the rate of work of the mean flow against the force exerted by the obstacles. The viscous term accounts for molecular diffusion, molecular transport, and viscous dissipation of turbulent kinetic energy (Townsend 1976). The fourth term in Equation 10 accounts for the conversion of both mean and large-scale turbulent kinetic energy toward smaller scale turbulent kinetic energy in the wakes of the elements, which is sometimes referred to as "short-circuited cascade" (Raupach and Thom 1981). This wake-generated turbulent kinetic energy has therefore a scale proportional to the dimensions of the elements in the canopy, i.e., much smaller than the typical length scales of shear-generated eddies (Raupach and Thom 1981; Raupach and Shaw 1982).

Under averaging Scheme II, the decomposition of the total kinetic energy is a little more complicated, yielding:

$$\begin{aligned}
\frac{1}{2} \langle \overline{u_i u_i} \rangle &= \frac{1}{2} \langle \overline{u_i} \overline{u_i} \rangle + \frac{1}{2} \langle \overline{u_i' u_i'} \rangle \\
&= \frac{1}{2} \langle \overline{u_i} \rangle \langle \overline{u_i} \rangle + \frac{1}{2} \langle \overline{u_i'' u_i''} \rangle + \frac{1}{2} \langle \overline{u_i' u_i'} \rangle
\end{aligned} \tag{11}$$

where the last two terms on the right-hand side represent different components of the turbulent kinetic energy under this scheme.

Budgets for each of the last two terms on the right in Equation 11 are readily obtained (Raupach and Shaw 1982):

$$\left(\frac{\partial}{\partial t} + \langle \bar{u}_j \rangle \frac{\partial}{\partial x_j}\right) \frac{\langle \bar{u}_i' u_i' \rangle}{2} = - \langle \bar{u}_i' u_j' \rangle \frac{\partial \langle \bar{u}_i \rangle}{\partial x_j} - \frac{\partial}{\partial x_j} \left( \frac{\langle \bar{u}_i' u_i' u_j' \rangle}{2} + \frac{\langle \bar{u}_i' u_i'' \bar{u}_j'' \rangle}{2} + \frac{\langle \bar{p}' u_j' \rangle}{\rho} \right) \quad (12)$$

$$+ \nu \langle \bar{u}_i' \nabla^2 \bar{u}_i' \rangle - \left\langle \bar{u}_i' u_j'' \frac{\partial \bar{u}_i''}{\partial x_j} \right\rangle$$

and

$$\left(\frac{\partial}{\partial t} + \langle \bar{u}_j \rangle \frac{\partial}{\partial x_j}\right) \frac{\langle \bar{u}_i'' \bar{u}_i'' \rangle}{2} = - \langle \bar{u}_i'' \bar{u}_j'' \rangle \frac{\partial \langle \bar{u}_i \rangle}{\partial x_j} + \left\langle \bar{u}_i' u_j'' \frac{\partial \bar{u}_i''}{\partial x_j} \right\rangle \quad (13)$$

$$- \frac{\partial}{\partial x_j} \left[ \frac{\langle \bar{u}_i' u_i' u_j' \rangle}{2} + \frac{\langle \bar{u}_i' u_i'' \bar{u}_j'' \rangle}{2} + \frac{\langle \bar{p}' u_j' \rangle}{\rho} \right]$$

$$+ \nu \langle \bar{u}_i'' \nabla^2 \bar{u}_i'' \rangle + \frac{1}{\rho} \langle u_i \rangle \left\langle \frac{\partial p''}{\partial x_i} \right\rangle$$

The four terms on the right-hand side of Equation 12 have similar meanings to the ones in Equation 10, except that the wake-production term appears here as a horizontal average of the product of local deviations of Reynolds stresses and velocity gradients from their spatial-averaged values. On a smaller scale, this last term produces turbulent kinetic energy in the same way as does the shear-production term. More attention has to be given to the five terms on the right in Equation 13: (a) a production term; (b) the wake-production term of Equation 12, here a sink term; (c) a turbulent transport term involving the role of dispersive fluxes of energy; (d) a viscous term; and (e) a wake-production (source) term, similar to the fourth term in Equation 10.

Careful analysis of the preceding expressions allows for better insight into the turbulence structure and its generation mechanisms in flows through vegetation. Basically it can be observed that, irrespective of the averaging scheme, the budget of turbulent kinetic energy is composed of sources, sinks, and transport terms. Two characteristic processes act as turbulent kinetic energy generators, i.e., transferring energy from larger scales (either mean flow or larger eddies) toward turbulent fluctuations in space or time at smaller scales: (a) the work of Reynolds and dispersive stresses against mean velocity gradients; and (b) the work of mean flow or large eddies against pressure differences due to the obstacles. Looking at Equation 7 and at the first term on the right of Equation

10, we can see that the action of mechanism (a) may in turn be subdivided as

$$\langle \overline{u_i' u_i'} \rangle > \frac{\partial \langle \overline{u_i} \rangle}{\partial x_j}$$

which is the same as the first term on the right of Equation 12, and therefore contributes to the generation of fluctuations in time, and

$$\langle \overline{u_i'' u_i''} \rangle > \frac{\partial \langle \overline{u_i} \rangle}{\partial x_j}$$

which is equal to the first term on the right of Equation 13, and thus generates spatial perturbations of time-averaged values. On the other hand, the work of the mean flow against pressure differences in space (i.e., mechanism b) is a source term for the budget of spatial fluctuations of time-averaged velocities, where a shear-generation-like term appears as a sink, thus transferring energy from space fluctuations toward small-scale fluctuations in time.

Regarding transport processes, the second term on the right in Equation 12 is identical to the corresponding term in the turbulent kinetic energy budget of shear flows without obstacles, with the exception being the appearance of a dispersive flux of turbulent kinetic energy,  $\langle \overline{u_i' u_i'' u_j''} \rangle$ .

In the turbulent kinetic energy budgets there are two viscous-related sink terms, accounting for the direct conversion of mechanical energy into heat. The one in Equation 12 is related to the spatial average of the typical viscous

$$\text{dissipation of turbulent kinetic energy, } \varepsilon = \nu \overline{\frac{\partial u_i'}{\partial x_j} \left( \frac{\partial u_i'}{\partial x_j} + \frac{\partial u_j'}{\partial x_i} \right)}$$

This relation can be shown as follows (Townsend 1976; Hinze 1975):

$$\overline{\nu u_i' \frac{\partial^2 u_i'}{\partial x_j^2}} = \nu \left[ \frac{\partial^2}{\partial x_j^2} \left( \frac{1}{2} \overline{u_i'^2} \right) + \frac{\partial^2 \overline{u_i' u_j'}}{\partial x_i \partial x_j} \right] - \varepsilon \quad (14)$$

so that at high enough Reynolds numbers the viscous term in Equation 12 is equivalent to the rate of dissipation of turbulent kinetic energy into heat, hence determining the viscous cutoff of turbulent fluctuations in time. The other viscous term, the fourth term in Equation 13, accounts for the direct dissipation into heat of spatial fluctuations of time-averaged mean velocities.

There are two limiting cases worth being analyzed. The first one is considered in the work of Raupach and Shaw (1982) and concerns the case when the length scale of the canopy elements (and of their wakes, or in other words the scale of the wake-generated turbulence) is much larger than the Kolmogorov microscale,  $\eta$ , so that the viscous term in Equation 13 becomes negligible. In this situation, if all the dispersive fluxes are considered to be of lower order of

magnitude, then for steady advection-free conditions:

$$- \left\langle \overline{u_i' u_j'} \frac{\partial \overline{u_i'}}{\partial x_j} \right\rangle \approx \frac{1}{\rho} \langle u_i \rangle \left\langle \frac{\partial p''}{\partial x_i} \right\rangle \quad (15)$$

In other words, the work of the mean flow against pressure differences becomes equal to the wake-production term for the turbulent fluctuations in time.

The other limiting case is when the length scale of the canopy elements (and of their wakes, i.e. the scale of the wake-generated turbulence) is much smaller than (or even of the order of) the Kolmogorov microscale. In this situation almost all the energy arising from the work of the mean flow against pressure forces is spent in the generation of spatial fluctuations, and is therefore directly dissipated into heat. In steady advection-free conditions, it follows that:

$$- \nu \langle \overline{u_i''} \nabla^2 \overline{u_i''} \rangle = \frac{1}{\rho} \langle u_i \rangle \left\langle \frac{\partial p''}{\partial x_i} \right\rangle \quad (16)$$

So that

$$- \left\langle \overline{u_i' u_j'} \frac{\partial \overline{u_i'}}{\partial x_j} \right\rangle \approx 0$$

and hence there is a negligible contribution from the wakes to the spatial average of the turbulent fluctuations in time. The first of these two situations seems to be common to atmospheric flows, whereas the second situation is more common to water flows with relatively low plant concentrations. This is reasonable, considering that the Kolmogorov microscale is smaller in air than in water. In addition, the characteristic length scales of canopy elements in atmospheric flows can be expected to be in general much larger than those found in water flows.

The discussion in the previous paragraphs clarifies the problem mentioned in the literature review concerning the different coefficients assigned to the wake-production terms in different turbulence models. It becomes therefore obvious that if one is trying to numerically simulate the spatial average of the local, time-averaged turbulent kinetic energy (or any  $\langle \overline{u_i'^2} \rangle$  for that matter) in a flow with elements of the order of the Kolmogorov microscale, then the wake-related source term in the energy equation would be almost zero. In other words, in this case the drag-related weighting factors in the turbulent kinetic energy and in the dissipation equations would be very close to zero. However, for the numerical computation of the total turbulent kinetic energy (i.e.

$(\langle \overline{u_i''} \overline{u_i''} \rangle + \langle \overline{u_i'} \overline{u_i'} \rangle)/2$ ), these coefficients are expected to be close to

1.0 and 1.33, respectively (see "Turbulence Modeling by a First-Level Two-Equation Closure Scheme").

In the computation of flow through vegetation using a two-equation model, a question arises about which turbulent kinetic energy will be simulated: the one governed by Equation 10 or 12? Moreover, since in two-equation models the transport equation for turbulent kinetic energy provides a velocity scale for estimating the turbulent eddy viscosity, which one of the two will provide a better approach for this purpose? The answer to this question will also determine the type of transport equation used for estimating the viscous dissipation rate of turbulent kinetic energy. In other words, which will be simulated

$\nu < \overline{u_i' \nabla^2 u_i'} >$  or  $\nu < u_i'' \nabla^2 u_i'' >$ ? But before these questions are answered, i.e., before addressing the point on the modeling of the former expressions, some considerations concerning the parameterization of drag forces will be presented.

## Modeling of Form-Drag Forces in Open-Channel Flows

The previous section discussed how drag-related terms can be introduced in the conservation equations without arbitrarily introducing body forces. The present section will deal with the modeling of such forces. As mentioned before, the term  $\frac{1}{\varrho} \langle \partial p'' / \partial x_i \rangle$  represents the so-called drag force per unit volume. To demonstrate this assertion Figure 3.2 shows a schematic of the pressure field for an isolated two-dimensional object. By definition the pressure force (per unit length in  $z$ ),  $f_x$ , on the perimeter,  $s$ , of the cylinder acting in the  $x$ -direction is (e.g. Pantom 1984):

$$f_x = \int n_x p ds \quad (17)$$

where

$n$  = vector normal to the perimeter of the object

$n_x$  =  $x$ -component of vector  $n$

It is readily seen that at a fixed spanwise location, the longitudinal gradient in  $p''$  times  $\Delta x$  is equal to  $(n_{xu} p + n_{xd} p)$ , where  $n_{xu}$  and  $n_{xd}$  represent the vector  $n_x$  in the upstream and downstream faces of the object, respectively, and  $\Delta x$  the distance between these two points in the  $x$ -direction.

In fluid mechanics, the drag force is usually parameterized as:

$$\frac{1}{\varrho} \left\langle \frac{\partial p''}{\partial x_i} \right\rangle = \frac{1}{2} C_D a < u_i >^2 \quad (18)$$

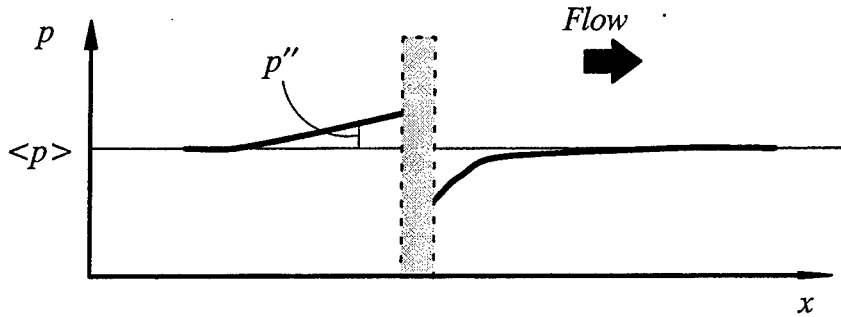


Figure 3.2 Schematic of pressure field

where  $a$  is the ratio between the sum of the differential frontal areas of the obstacles divided by the differential volume of fluid (Figure 3.3) and thus has dimensions of  $L^{-1}$ , and  $C_D$  is the so-called drag coefficient which physically is proportional to the momentum thickness of the wake behind the object.

Although the determination of  $C_D$  is a key factor in the modeling of flow through obstacles, very few experimental observations exist concerning the determination of this coefficient in the particular case of open-channel flows. Realizing this problem, during the completion of the present work a set of experiments was conducted at the Hydrosystems Laboratory, University of Illinois at Urbana-Champaign, in order to specify values of  $C_D$  for free-surface flows through simulated vegetation (Dunn 1996). Rigid as well as flexible cylinders were used in the study. Using a new methodology developed to evaluate the drag coefficient based on vertical profiles of spatial and temporal mean velocity and Reynolds stresses, results showed that  $C_D = 1.13 \pm 15$  percent, for the range of dimensionless parameters employed in the work.

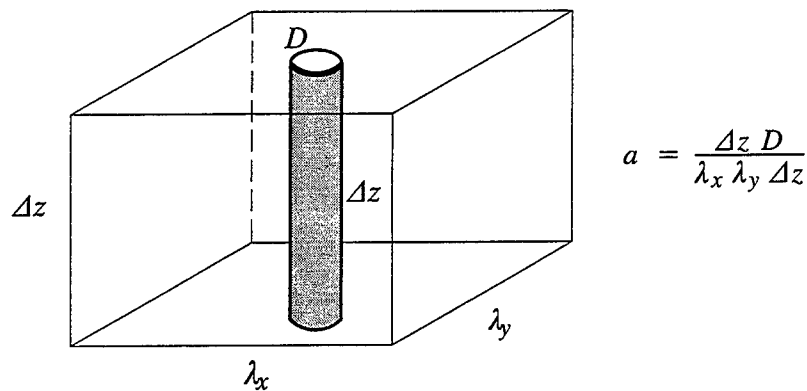


Figure 3.3 Definition diagram for cylinder density

Experimental data from this study will be compared herein with results from the numerical simulations.

## **Turbulence Modeling by a First-Level, Two-Equation Closure Scheme**

As can be observed from previous expressions, transport equations for velocity moments of any order involve knowledge of higher order moments, in a way that produces a mathematical problem with more unknowns than equations. This is the so-called closure problem in turbulence.

In general three different alternatives are available today for the numerical computation of turbulent flows:

- a.* Direct numerical simulation using the full set of Navier-Stokes equations, hence simulating all eddy sizes (e.g., Kim, Moin and Moser 1987).
- b.* Explicit simulation of only the large, energy-containing eddies, which have length scales determined by each particular problem (resolved scales), with the flux of energy towards the smaller eddies in the spectrum (subgrid scales) modeled by introducing an effective viscosity, which increases the molecular viscosity of the fluid (e.g. Piomelli 1994).
- c.* Use of the Reynolds-averaged form of the Navier-Stokes equations (or similar equations for higher order moments) plus some assumptions that allow solving the closure problem of having more unknowns than equations (Rodi 1984).

The closure problem at the first-order level, that is in the turbulence-averaged form of the Navier-Stokes equations, has been traditionally solved by means of different numbers of equations having as a common framework an eddy viscosity model. Thus this approach inevitably breaks down where the concepts underlying the eddy viscosity hypothesis are in violation of the physical processes (see section in this Chapter "Limitations of Turbulence Models Based on Flux-Gradient Approximations). Since the late seventies, models have also been developed in engineering practice for higher order closures. Second-order models, for example, are based on the full equations for the Reynolds stress tensor, and of course third-order moments are being modeled (Wilson and Shaw 1977).

According to the number of transport equations being used for closing the problem of the Reynolds stresses, the models have been called zero-, one- and

two-equation models. Since all these models rely on the concept of an eddy viscosity, and its determination requires the knowledge of one velocity and one length scale, the problem reduces to the estimation of these two variables in the turbulence field. The simplest prescription of the Reynolds stress in the level of zero equation (or algebraic models) is the well known mixing-length model, obtained by applying the methods of gas kinetic theory to turbulent, macroscopic motions of fluid continuum (e.g., McComb 1990). Although successfully applied in many situations, its major drawback is in its lack of universality: i.e., the prescription of the mixing-length varies from one type of flow to another. The next order of difficulty is the one-equation model, which makes use of a transport equation for the turbulent kinetic energy (assumed proportional to the square of the characteristic velocity) together with some assumptions to prescribe the production, diffusion, and dissipation terms. In this case a length scale still needs to be specified by means of some empirical relation.

The next level of complication is the introduction of a second transport equation with the help of which the required length scale can be computed. The basis for these kinds of models seems to have been given some fifty years ago almost simultaneously by Kolmogorov (1942) and Prandtl (1945). According to Kolmogorov (Barenblatt 1995) at any point of a turbulent flow the statistical dimensionless properties of the vortex dissipative structures are similar, and only their time and length scales are different. Both scales may be estimated by different sets of two transport equations, either for  $(k, \epsilon)$ ,  $(k, l)$ ,  $(k, \omega)$ , etc. ( $k, \epsilon, l, \omega$  representing the turbulent kinetic energy, dissipation rate, length scale and dissipation per unit turbulent kinetic energy, respectively). The first of the former set, the  $k$ - $\epsilon$  model, is probably the most commonly used model in engineering practice, and has proved to be a reliable tool in a wide variety of problems in hydraulic and environmental engineering (Rodi 1984).

In the  $k$ - $\epsilon$  model the Reynolds stresses are estimated using the eddy viscosity concept as follows:

$$-\overline{u_i' u_j'} = \nu_T \left( \frac{\partial \overline{u_i}}{\partial x_j} + \frac{\partial \overline{u_j}}{\partial x_i} \right) - \frac{2}{3} \delta_{ij} k \quad \nu_T = C_\mu \frac{k^2}{\epsilon} \quad (19)$$

where

$\nu_T$  = kinematic eddy viscosity

$C_\mu$  = parameter with standard value of 0.09

$\delta_{ij}$  = Kronecker delta

A similar approach will be followed herein, namely:

$$\begin{aligned}
- \langle u_i'' u_j'' \rangle &= - \langle \overline{u_i'' u_j''} \rangle - \langle \overline{u_i' u_j'} \rangle \\
&= \nu_T \left( \frac{\partial \langle u_i \rangle}{\partial x_j} + \frac{\partial \langle u_j \rangle}{\partial x_i} \right) - \frac{2}{3} \delta_{ij} k
\end{aligned} \tag{20}$$

The question then concerns the turbulent kinetic energy to be modeled (i.e.,  $k = \langle \overline{u_i' u_i'} \rangle / 2$  or  $k = \langle u_i'' u_i'' \rangle / 2$ ).

The answer to this question can be obtained by contracting Equation 20, i.e., making  $i=j$ , yielding:

$$- \langle \overline{u_i'' u_i''} \rangle - \langle \overline{u_i' u_i'} \rangle = 2 \nu_T \frac{\partial \langle u_i \rangle}{\partial x_i} - \frac{6}{3} k \tag{21}$$

From continuity (Equation 3) the first term on the right vanishes, so that Equation 21 reduces to:

$$k = \frac{\langle \overline{u_i'' u_i''} \rangle + \langle \overline{u_i' u_i'} \rangle}{2} \tag{22}$$

This finding clarifies which rate of turbulent dissipation has to be modeled. Since by definition the characteristic velocity scale is considered proportional to the turbulent kinetic energy defined in Equation 22, then the dissipation rate defined in Equation 10 has to be used accordingly for defining the associated length scale, namely  $\varepsilon = \nu \langle u_i'' \nabla^2 u_i'' \rangle$ .

One last consideration is needed in order to model Equation 10. The exact form of the inertial and pressure transport terms is of no practical use since it involves unknown correlations of higher order. To obtain a closed set of equations, assumptions similar to those used in the standard k- $\varepsilon$  model are made, namely that the total (inertial and pressure) diffusive flux of  $k$  can be assumed proportional to its gradient:

$$\frac{\langle u_i'' u_i'' u_j'' \rangle}{2} + \frac{\langle p'' u_j'' \rangle}{2} = \frac{\nu_T}{\sigma_k} \frac{\partial \langle u_i'' u_i'' \rangle}{\partial x_j} / 2 \tag{23}$$

Now the set of partial differential equations that will be numerically modeled for simulating the turbulence structure of uniform, two-dimensional open-channel flow through vegetation can be written down as follows:

a. Continuity Equation:

$$\frac{\partial \langle u_1 \rangle}{\partial x} = 0 \tag{24}$$

b. *x-Momentum Equation:*

$$\frac{\partial \langle u_1 \rangle}{\partial t} = gS_o + \frac{\partial}{\partial z} \left[ (v_T + \nu) \left( \frac{\partial \langle u_1 \rangle}{\partial z} \right) \right] - f_x \quad (25)$$

where

$g$  = gravitational acceleration

$S_o$  = bed slope

c. *Turbulent Kinetic Energy Equation:*

$$\frac{\partial k}{\partial t} = \frac{\partial}{\partial z} \left[ \left( \frac{\nu_T}{\sigma_k} + \nu \right) \frac{\partial k}{\partial z} \right] + P_k - \varepsilon + C_{fk} f_x \langle u_1 \rangle \quad (26)$$

d. *Dissipation Rate Equation:*

$$\begin{aligned} \frac{\partial \varepsilon}{\partial t} &= \frac{\partial}{\partial z} \left[ \left( \frac{\nu_T}{\sigma_\varepsilon} + \nu \right) \frac{\partial \varepsilon}{\partial z} \right] \\ &+ \frac{\varepsilon}{k} \left[ C_1 (P_k + C_{f\varepsilon} f_x \langle u_1 \rangle) - C_2 \varepsilon \right] \end{aligned} \quad (27)$$

where:

$$\begin{aligned} P_k &= \nu_T \left( \frac{\partial \langle u_1 \rangle}{\partial z} \right)^2 \\ f_x &= \frac{1}{2} C_D a \langle u_1 \rangle \sqrt{\langle u_1 \rangle^2} \\ \nu_T &= C_\mu \frac{k^2}{\varepsilon} \end{aligned}$$

and the set of standard constants takes the following values:  $C_\mu = 0.09$ ,  $C_1 = 1.44$ ,  $C_2 = 1.92$ ,  $\sigma_k = 1.0$  and  $\sigma_\varepsilon = 1.30$ . The parameters  $C_{fk}$  and  $C_{f\varepsilon}$  have to be modeled and are sometimes considered results of the model calibration (Tsujiimoto, Kitamura and Okada, 1991<sup>b</sup>). The unsteady terms in the previous equations are retained only for computational purposes, so that a steady solution is reached as an asymptotic state (see the section in this Chapter, "Numerical Algorithm").

However, comparing Equations 10 and 26, one expects the value of the coefficient  $C_{fk}$  to be equal (or very close) to one. Moreover, it can be shown (Burke 1982) that for the  $\varepsilon$ -equation to be in balance, the value of the coefficient  $C_{f\varepsilon}$  has to be dependent upon the value of  $C_{fk}$ . To clarify this, consider a steady, horizontal flow through vertical, infinite long cylinders, where all derivatives in the vertical direction vanish. Then, from the k-equation  $\varepsilon = C_{fk} f_x \langle u_1 \rangle$ , and from the  $\varepsilon$ -equation  $C_1 C_{f\varepsilon} f_x \langle u_1 \rangle = C_2 \varepsilon$  so that,  $C_{f\varepsilon} = C_2 / C_1 C_{fk}$ .

In order to solve the system of partial differential equations, appropriate boundary conditions for each variable have to be specified. This issue is addressed in the next section.

## Boundary Conditions and Constants for Open-Channel Flow Through Vegetation

One of the biggest limitations of the set of partial differential equations given in the previous section is that viscous effects have been neglected, and thus the model is not able to resolve flow regions too close to solid boundaries. In other words, the model is expected to yield acceptable results only in local, high-Reynolds-numbers conditions. In the standard version of a high-Reynolds-number  $k$ - $\epsilon$  model, values of velocity, turbulent kinetic energy, and dissipation are specified at a point near the wall, located in the so-called equilibrium region, where the flow exhibits such large local rates of energy production and dissipation that both terms are approximately in local equilibrium. Basically this assumption yields values for velocity,  $k$  and  $\epsilon$  related to the existence of a semi-logarithmic mean velocity profile. On the other hand, the free surface region is sometimes treated as a symmetry plane (i.e., the fluxes of all variables are zero, which is known as “rigid lid assumption”), but more accurate results are obtained when turbulence damping effects are considered by specifying values of the dissipation rate as a function of  $k$  and the flow depth  $H$  (Celik and Rodi 1984, 1988). This latter approach is in line with experimental observations that show  $\epsilon$  to be proportional to the ratio  $u_{rms}^3/L_x$ , where  $u_{rms}$  is the root-mean-square value of the streamwise velocity fluctuations and  $L_x$  is their macro-length scale (approximately constant and equal to 70 percent of the flow depth in the free-surface region, Nezu and Nakagawa 1993). This latter approach will be followed in the present work, so that the boundary conditions to be used are:

*a. At the bed:*

$$U_o = \frac{u_*}{\kappa} \text{Ln}\left(E \frac{z_o u_*}{\nu}\right) \quad k_o = \frac{u_*^2}{\sqrt{C_\mu}} \quad \epsilon_o = \frac{u_*^3}{\kappa z_o} \quad (28)$$

*b. At the free surface:*

$$\frac{dU}{dz} = \frac{dk}{dz} = 0 \quad \epsilon = \frac{k^{3/2}}{b_\epsilon H} \quad (29)$$

where

$b_\varepsilon$  = model coefficient

$z_o$  = first grid point away from the wall

$E$  = roughness parameter, approximately equal to 9 for hydraulically smooth conditions and to  $30\nu/u_*'/k_s$  for fully-rough beds.

$k_s$  = equivalent sandgrain roughness

It is worth mentioning that Equation 29 is only valid under non-emergent conditions. García (1992) showed how these boundary conditions can be modified to account for buoyancy effects induced by sediment in suspension.

Concerning the value of the constant  $C_\mu$ , different approaches exist in the literature. Celik and Rodi (1984) reported that values of  $C_\mu = 0.05$  result in predictions of near-bed values of streamwise velocity and kinetic energy in good agreement with experimental observations. Rodi (1976) proposed an algebraic expression for estimating Reynolds stresses, from which a formula for  $C_\mu$  can be obtained, which shows this value to be a function of the ratio between production and dissipation of turbulent kinetic energy. In modifying this expression to account for wake-generated turbulence, a new expression for  $C_\mu$  will be obtained in the next section.

## Estimation of Reynolds Stress Tensor Components

As mentioned in the preceding section, Rodi (1976) proposed an algebraic expression for estimating the different components of the Reynolds stress tensor. His approach is slightly modified in what follows to account for wake-generated turbulence. Consider the transport equation of  $k$ :

$$\frac{Dk}{Dt} = Dif(k) + P - \varepsilon + P_w \quad (30)$$

where

$Dif(k)$  = the diffusive transport of  $k$

$D(.) / Dt$  = total derivative

$P_w$  = wake production term

A similar expression can be obtained for each Reynolds stress:

$$\frac{D \langle u_i'' u_j'' \rangle}{Dt} = Dif(\langle u_i'' u_j'' \rangle) + P_{ij} \quad (31)$$

$$- C_{1R} \frac{\varepsilon}{k} \left[ \langle u_i'' u_j'' \rangle - \delta_{ij} \frac{2}{3} k \right] - \gamma [P_{ij} - \delta_{ij} \frac{2}{3} P] - \frac{2}{3} \delta_{ij} \varepsilon + P_{w_{ij}}$$

where the third and fourth terms on the right account for pressure-strain effects

(Rodi 1976; see also Launder, Reece and Rodi 1975). As it can be observed, Equations 30 and 31 are differential equations due to their left-hand side and the first term on the right of each expression. Now, mathematically it can be written:

$$\frac{D \langle u_i'' u_j'' \rangle}{Dt} = \frac{\langle u_i'' u_j'' \rangle}{k} \frac{Dk}{Dt} + k \frac{D \langle u_i'' u_j'' \rangle / k}{Dt} \quad (32)$$

where a similar expression can be obtained for  $Dif(\langle u_i'' u_j'' \rangle)$ . If the ratio  $\langle u_i'' u_j'' \rangle / k$  can be assumed approximately constant in the computational domain (something that is in fairly good agreement with the authors' own experimental observations, as it will be shown later), it is therefore possible to write:

$$\frac{D \langle u_i'' u_j'' \rangle}{Dt} - Dif(\langle u_i'' u_j'' \rangle) \approx \frac{\overline{u_i u_j}}{k} \left[ \frac{Dk}{Dt} - Dif(k) \right] \quad (33)$$

and hence from Equation 30 it follows that:

$$\frac{D \langle u_i'' u_j'' \rangle}{Dt} - Dif(\langle u_i'' u_j'' \rangle) \approx \frac{\langle u_i'' u_j'' \rangle}{k} (P - \varepsilon + P_w) \quad (34)$$

Combining Equations 31 and 34 yields:

$$\frac{\langle u_i'' u_j'' \rangle}{k} (P - \varepsilon + P_w) = P_{ij} - C_{1R} \frac{\varepsilon}{k} \left( \langle u_i'' u_j'' \rangle - \delta_{ij} \frac{2}{3} k \right) \quad (35)$$

or:

$$\frac{\langle u_i'' u_j'' \rangle}{k} = \frac{\frac{2}{3} \delta_{ij} \left[ 1 + \frac{1}{C_{1R}} \left( \frac{P}{\varepsilon} - 1 \right) \right]}{M} + \frac{1 - \gamma}{C_{1R}} \frac{\frac{P_{ij}}{\varepsilon} - \frac{2}{3} \delta_{ij} \frac{P}{\varepsilon}}{M} + \frac{1}{C_{1R}} \frac{P_w}{M} \quad (36)$$

where

$$M = 1 + \frac{1}{C_{1R}} \left( \frac{P + P_w}{\varepsilon} - 1 \right) \quad (37)$$

Equation 36 is an algebraic expression for obtaining the Reynolds stresses, once  $P$ ,  $\varepsilon$ ,  $P_{ij}$ ,  $P_w$  and  $P_{w_{ij}}$  are known.

An important consequence of Equation 36 is that if the value of  $\langle u_1'' u_3'' \rangle$  is computed, and assumed to be equal to:

$$-\langle u_1''u_3'' \rangle = \nu_T \frac{\partial \langle u_1 \rangle}{\partial z} = C_\mu \frac{k^2}{\varepsilon} \frac{\partial \langle u_1 \rangle}{\partial z} \quad (38)$$

then it is easy to show that:

$$C_\mu = \frac{2}{3} \frac{1-\gamma}{C_{1R}} \frac{1 - \frac{1}{C_{1R}}(1-\gamma P/\varepsilon)}{M^2} \quad (39)$$

which clearly shows  $C_\mu$  to vary as a function of both ratios  $P/\varepsilon$  and  $Pw/\varepsilon$ .

Regarding the values of the coefficients  $\gamma$  and  $C_{1R}$  (see Launder, Reece and Rodi 1975), the former takes a value of 0.60 for isotropic turbulence, whereas the latter was originally found to be equal to 1.4 by Rotta (1951). However, Rotta (1962) later showed that a value about twice as large provided a better fit to Uberoi's (1957) data on the decay of highly anisotropic turbulence. Rodi (1976) suggests the use of  $\gamma=0.4$  and  $C_{1R}=2.5$ . Figure 3.4 illustrates the variation of  $C_\mu$  with the ratio between total production and dissipation, for the combination  $\gamma=0.6$  and  $C_{1R}=2.5$ . It can be observed that for  $P/\varepsilon=1.0$ , Equation 39 yields a value of  $C_\mu=0.091$ , hence in very good agreement with proposed values for this constant in flow regions under local turbulence equilibrium conditions.

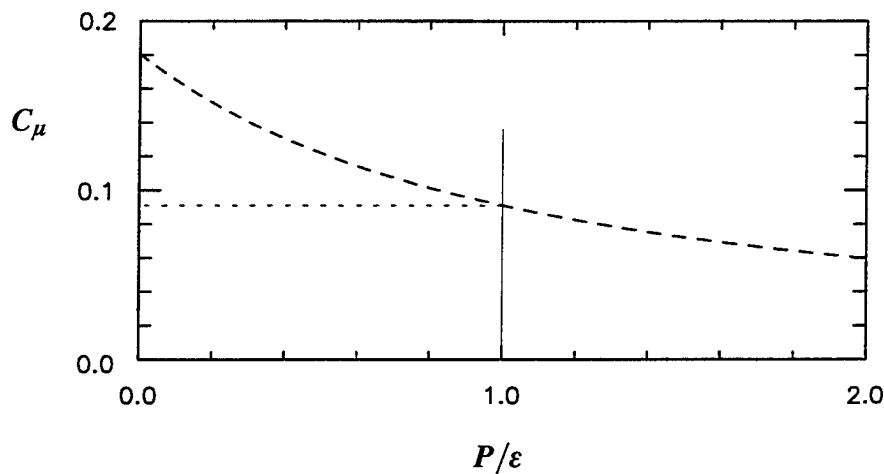


Figure 3.4 Variation of  $C_\mu$  with the ratio  $P/\varepsilon$

## Limitations of Turbulence Models Based on Flux-Gradient Approximations

As it can be observed from the expressions given in the preceding section, most of the assumptions made involve the use of flux gradient models. Over the years, there has been some criticism concerning the limitations of these models. In particular, Corrsin (1974) enumerates some of the necessary (but not sufficient) conditions for these assumptions to represent the actual processes in terms of homogeneity and stationarity of the mean field being transported and of the turbulence properties:

- a. The transport mechanism length-scale must be much smaller than the distance over which the curvature of the mean transported field gradient changes appreciably.
- b. The transport mechanism time scale must be much smaller than the time during which the mean transported field changes appreciably.
- c. The transport mechanism length scale must be essentially constant over a distance for which the mean transported field changes appreciably.
- d. The transport mechanism velocity must be appreciably more uniform than the length scale.

Defining the Lagrangian length scale for momentum transfer,  $L_s$ , as the product of the Eulerian (integral) time scale of the turbulent shear stress,  $T_s$ , and the root-mean-square of the bed-normal velocity fluctuations,  $w_{rms}$ , whereas the latter also is used as a velocity scale, Corrsin (1974) expressed the former requirements mathematically as:

$$a. \quad \left| \frac{\overline{U_{zzz}}}{\overline{U_z}} \right| \frac{L_s^2}{24} \ll 1 \quad (40)$$

$$b. \quad \left| \frac{\overline{U_{zt}}}{\overline{U_z}} \right| \frac{T_s}{2} \ll 1 \quad (41)$$

$$c. \text{ and } d. \quad \overline{U} \left| \frac{\partial \overline{U}}{\partial z} \right|^{-1} \left| \frac{1}{L_s} \frac{\partial L_s}{\partial z} \right| + \frac{1}{w_{rms}} \left| \frac{\partial w_{rms}}{\partial z} \right| \ll 1 \quad (42)$$

where symbols like  $\overline{U_{zt}}$  represent second derivatives of mean velocities with respect to the vertical coordinate and time. Evaluating the former expressions using boundary layer data from Blackwelder and Kovaszny (1972), Corrsin found that conditions a and b were satisfied, whereas condition c and d were

violated, namely those requiring cross-stream uniformity of the length scale and root-mean-square velocity fluctuations.

Despite the mentioned violations, gradient flux models have surprisingly yielded very good agreement with experimental observations for a wide variety of applications. As it will be shown later, results reported herein confirm this assertion.

## Numerical Algorithm

This section will discuss the algorithm used for the numerical study of steady, uniform open-channel flow through vegetation. Under these conditions all the differential equations used can formally be reduced to:

$$\frac{\partial \psi}{\partial t} = \frac{\partial}{\partial x_j} \left( \Gamma_\psi \frac{\partial \psi}{\partial x_j} \right) + S_\psi \quad (43)$$

where

$\psi$  = any dependent variable

$\Gamma_\psi$  = associated exchange coefficient defined as  $\Gamma_\psi = \mu_{eff}/(\rho\sigma_{eff})$

$\mu_{eff}$  = effective dynamic viscosity

$\sigma_{eff}$  = effective Prandtl/Schmidt number

$S_\psi$  = source or sink term

Thus by assuming spatial variations only in the vertical direction, the numerical solution of Equation 43 requires the discrete specification of  $\psi$  in the  $(z,t)$  space, and thus integration over the control volume as shown in Figure 3.5. The control volume method proposed by Patankar and Spalding (1970) will be used with an equation solver developed by Svensson (1986) called PROBE. A brief description of the numerical algorithm follows, but the reader interested in more details is referred to the aforementioned references.

If Equation 43 is integrated in space and time, it then may be written:

$$\int_{z(i-\frac{1}{2})}^{z(i+\frac{1}{2})} \int_U^B \frac{\partial \psi}{\partial t} dz dt \approx \Delta z(i) [\psi_B(i) - \psi_U(i)] \quad (44)$$

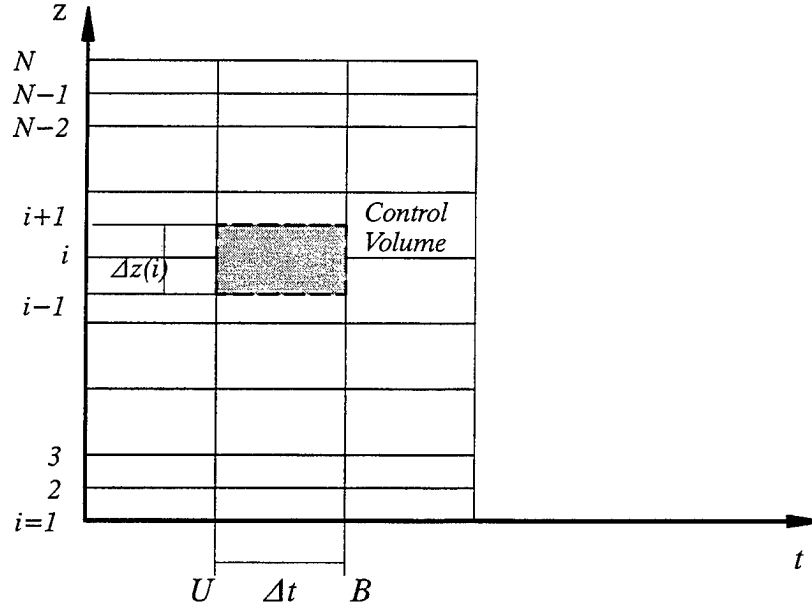


Figure 3.5 Definition of control volume

$$\int_{z(i-\frac{1}{2})}^{z(i+\frac{1}{2})} \int_U^B \frac{\partial}{\partial x_j} \left( \Gamma_\psi \frac{\partial \psi}{\partial x_j} \right) dz dt \approx \int_U^B \left[ \left( \Gamma_\psi \frac{\partial \psi}{\partial z} \right)_{i+\frac{1}{2}} - \left( \Gamma_\psi \frac{\partial \psi}{\partial z} \right)_{i-\frac{1}{2}} \right] dt \quad (45)$$

$$\approx \Delta t \left[ \left( \Gamma_\psi \frac{\partial \psi}{\partial z} \right)_{i+\frac{1}{2}, t^*} - \left( \Gamma_\psi \frac{\partial \psi}{\partial z} \right)_{i-\frac{1}{2}, t^*} \right]$$

where  $t^*$  is some time between  $U$  and  $B$ , usually set equal to  $B$  due to numerical stability reasons. Now, further decomposition of the terms in brackets in Equation 45 in finite difference form yields:

$$\int_{z(i-\frac{1}{2})}^{z(i+\frac{1}{2})} \int_U^B \frac{\partial}{\partial z} \left( \Gamma_\psi \frac{\partial \psi}{\partial z} \right) dz dt \quad (46)$$

$$\approx \Delta t \left[ \Gamma_{\psi(i+\frac{1}{2})} \frac{\psi_B(i+1) - \psi_B(i)}{\Delta z(i+\frac{1}{2})} - \Gamma_{\psi(i-\frac{1}{2})} \frac{\psi_B(i) - \psi_B(i-1)}{\Delta z(i-\frac{1}{2})} \right]$$

For simplicity Equation 46 can be rewritten as:

$$\int_{z(i-\frac{1}{2})}^{z(i+\frac{1}{2})} \int_U^B \frac{\partial}{\partial z} \left( \Gamma_\psi \frac{\partial \psi}{\partial z} \right) dz dt \quad (47)$$

$$\approx \Delta t \left\{ T_+ [\psi_B(i+1) - \psi_B(i)] - T_- [\psi_B(i) - \psi_B(i-1)] \right\}$$

where  $T_+ = \Gamma_{\psi(i+\frac{1}{2})} / \Delta z(i+\frac{1}{2})$  and  $T_- = \Gamma_{\psi(i-\frac{1}{2})} / \Delta z(i-\frac{1}{2})$ .

The source term may in turn be integrated as:

$$\int_{z(i-\frac{1}{2})}^{z(i+\frac{1}{2})} \int_U^B S_\psi dt dz \approx \Delta z(i) S_{\psi, r^*} \Delta t \quad (48)$$

Furthermore, it is common to subdivide the source term into two parts, one containing the variable itself, as:

$$S_{\psi, r^*} = S(i) + S'(i) \psi_B \quad (49)$$

so that Equation 48 becomes:

$$\int_{z(i-\frac{1}{2})}^{z(i+\frac{1}{2})} \int_U^B S_\psi \approx \Delta z(i) \Delta t [S(i) + S'(i) \psi_B] \quad (50)$$

Now, combining Equations 44, 47 and 50 yields:

$$\Delta z(i) [\psi_B(i) - \psi_U(i)] \approx \Delta t \left\{ T_+ [\psi_B(i+1) - \psi_B(i)] - T_- [\psi_B(i) - \psi_B(i-1)] \right\} \quad (51)$$

$$+ \Delta z(i) \Delta t [S(i) + S'(i) \psi_B]$$

which may be rearranged as:

$$A(i) \psi_B(i-1) + B(i) \psi_B(i) + C(i) \psi_B(i+1) = D(i) \quad (52)$$

where:

$$A(i) = T_-$$

$$B(i) = -A(i) - B(i) - \frac{\Delta z(i)}{\Delta t} + \Delta z(i) S'(i) \quad (53)$$

$$C(i) = T_+$$

$$D(i) = -\psi_{U(i)} \frac{\Delta z(i)}{\Delta t} - \Delta z(i) S(i)$$

It can be observed that Equation 52 is the compact expression for a tri-diagonal matrix, and thus, once the boundary conditions are prescribed, Equation 52 can be solved using for example the Thomas algorithm (Patankar and Spalding 1970).

Regarding the boundary conditions, basically two different cases may be distinguished: (a) the value of  $\psi$  is prescribed, or (b) the flux of  $\psi$  is given at the boundary. In case (a) consider only  $\psi(1) = \psi_{LB}$  and  $\psi(N) = \psi_{UB}$ , where  $\psi_{LB}$  and  $\psi_{UB}$  are the prescribed values of the variable at the lower and upper boundary, respectively. For case (b) with  $\gamma_{\psi, LB}$  and  $\gamma_{\psi, UB}$  representing the prescribed fluxes at the lower and upper boundary, respectively,

$$\gamma_{\psi, LB} = \frac{\Gamma_{\psi(1+\frac{1}{2})}}{\Delta z(1+\frac{1}{2})} (\psi_{D(2)} - \psi_{D(1)}) \quad (54)$$

$$\gamma_{\psi, UB} = \frac{\Gamma_{\psi(N-\frac{1}{2})}}{\Delta z(N-\frac{1}{2})} (\psi_{D(N-1)} - \psi_{D(N)}) \quad (55)$$

so that:

$$\psi_{D(1)} = -\gamma_{\psi, LB} \frac{\Delta z(1+\frac{1}{2})}{\Gamma_{\psi(1+\frac{1}{2})}} + \psi_{D(2)} \quad (56)$$

$$\psi_{D(N)} = -\gamma_{\psi, UB} \frac{\Delta z(N-\frac{1}{2})}{\Gamma_{\psi(N-\frac{1}{2})}} + \psi_{D(N-1)} \quad (57)$$

In the particular case of the k- $\epsilon$  model, accounting for sediment transport in suspension, there will then be a system of four partial differential equations in the variables  $U$ ,  $k$ ,  $\epsilon$  and  $C$ , representing the mean velocity, turbulent kinetic energy, rate of dissipation, and mean sediment concentration, respectively. Source terms and boundary conditions will be treated as described in the section "Turbulence Modeling by a First-Level Two-Equation Closure Scheme".

## 4 Turbulence Structure in Open-Channel Flows Without Vegetation

---

Before the algorithm presented in the previous section for simulating the turbulence structure and transport processes in vegetated waterways is employed, the capabilities of the model will be tested for the more often studied case of open channels without vegetation. This chapter deals with the verification of the model comparing numerical predictions of the turbulence structure in open-channel flow, under different roughness conditions, against experimental observations as well as semi-empirical expressions. Afterwards, the following chapter presents predictions of sediment transport processes in open channels without vegetation.

### Mean Flow

Mean velocity profiles corresponding to two different roughness conditions, hydraulically smooth and transitionally rough beds, were simulated numerically and the results compared with the authors' experimental observations. The experiments were conducted under uniform flow conditions at the Hydrosystems Laboratory, University of Illinois at Urbana-Champaign, in a 19.50-m-long, 0.91-m-wide and 0.61-m-deep tilting flume. Velocity measurements were taken with a Sontek acoustic Doppler velocimeter at a sampling frequency of 25 Hz. For the smooth-bed case the slope was set to approximately 0.0006 and the mean flow depth was 0.24 m, whereas for the transitionally rough case the slope was about 0.002 with a mean flow depth of 0.24 m. Figure 4.1 compares model predictions with the observations.

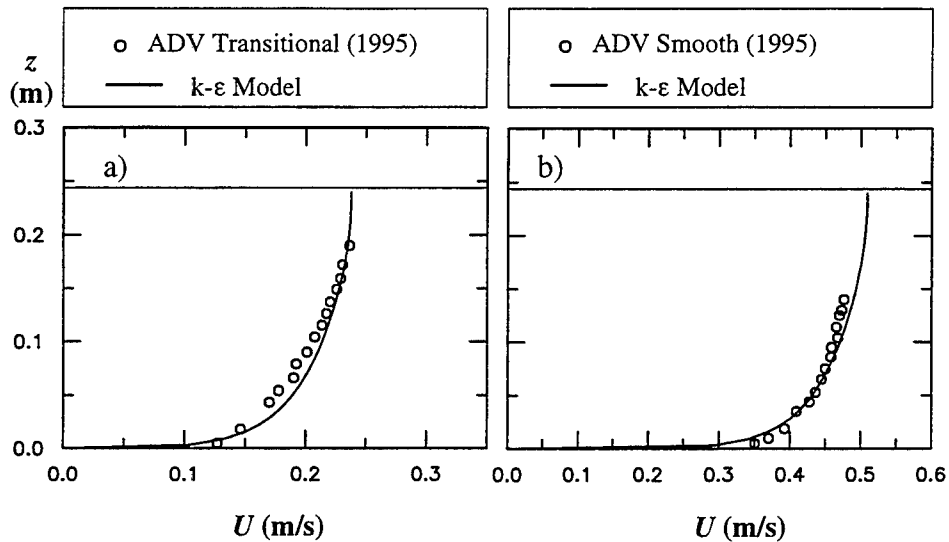


Figure 4.1 Observed and predicted vertical distributions of mean velocity for experiments on transitionally rough and hydraulically smooth bed conditions

## Second-order Moments

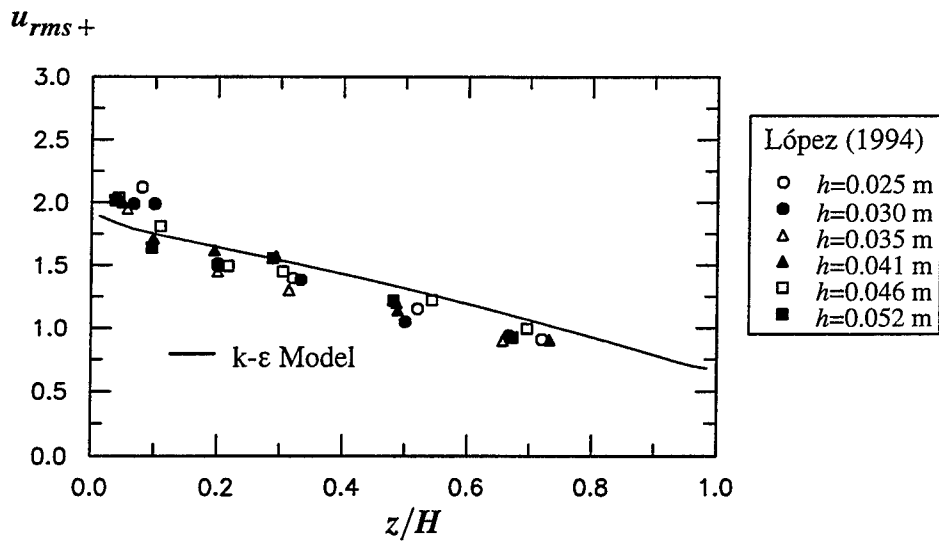
Dimensionless values of streamwise and vertical standard deviations of velocity were computed, and results were compared against some of the authors' measurements in smooth (López 1994) and transitionally rough (Niño 1995) beds as well as with experiments by Nezu (1977) for fully rough conditions (the subscript + indicates normalization using  $u_*$  as scaling velocity). Both the authors' observations and Nezu's velocity measurements were taken using hot-film anemometry. Results are shown in Figure 4.2 and Figure 4.3.

## Energy Budget Terms

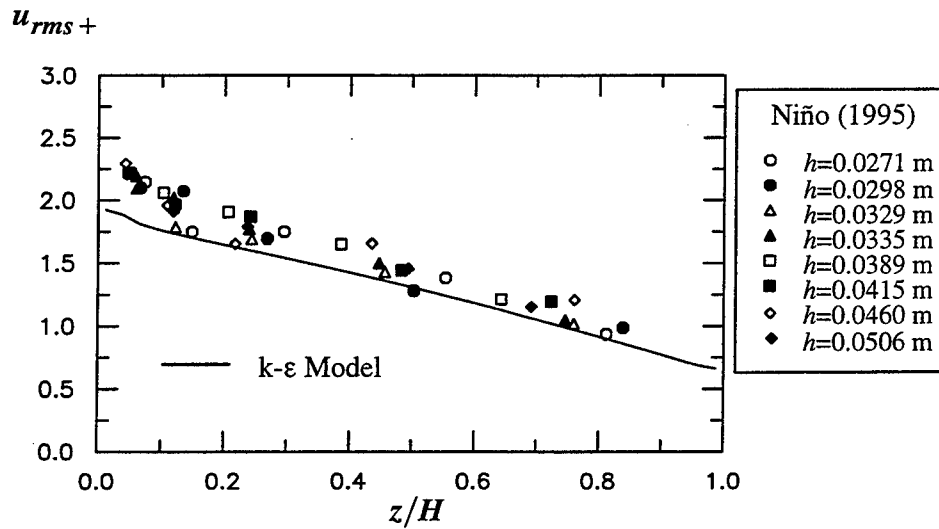
The capability of the model to simulate different terms in the energy budget was also checked by comparing experimental observations of turbulent production and dissipation rates with numerical results. Figure 4.4a illustrates the agreement for the dimensionless vertical profile of turbulent production rate in smooth-bed flows, where data were taken with the acoustic sensor. Figure 4.4b depicts comparisons for turbulence dissipation for smooth (López 1994) and transitionally rough (Niño 1995) beds, where the solid line represents a semiempirical expression proposed by Nezu and Nakagawa (1993).

## Eddy Viscosity and Mixing Length

As mentioned in the previous section, the boundary condition specifying  $\varepsilon$  as a function of  $k$  at the free surface allows for the turbulence damping at the

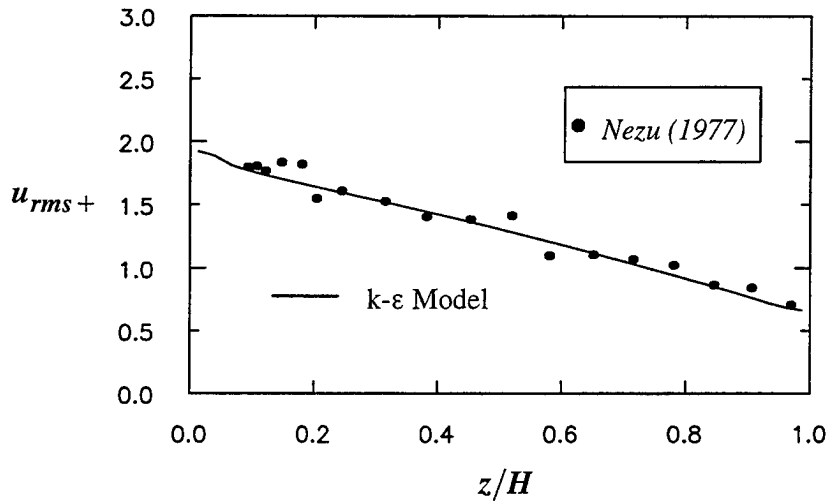


a. Hydraulically smooth condition



b. Transitionally rough condition

Figure 4.2 Observed and predicted vertical distribution of dimensionless rms value of streamwise velocity fluctuations (Continued)



c. Fully rough regime

Figure 4.2 (Concluded)

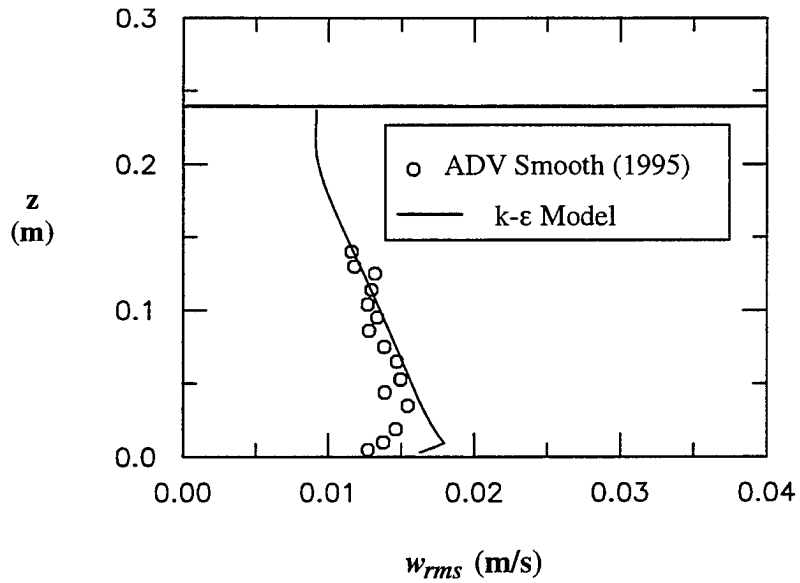
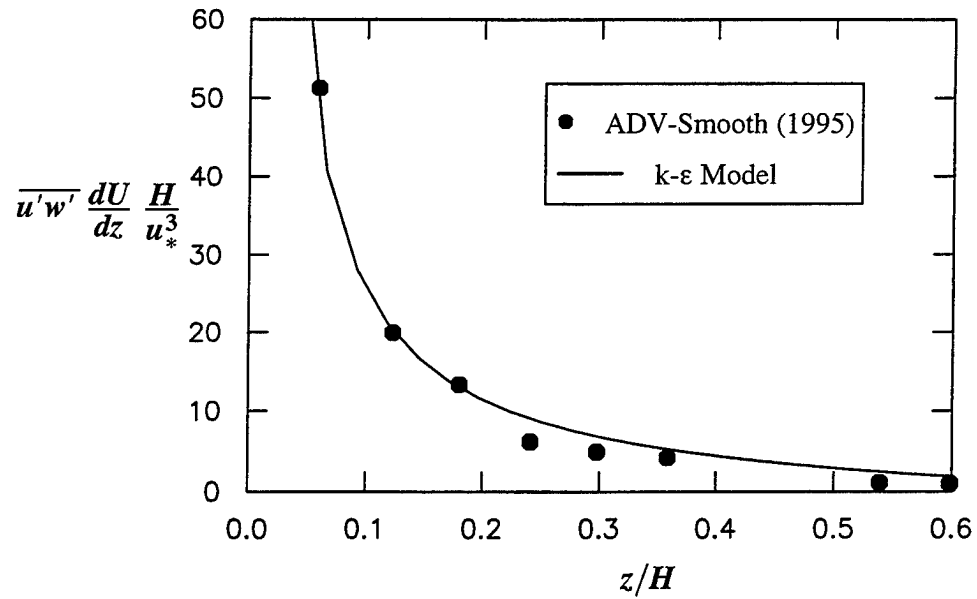
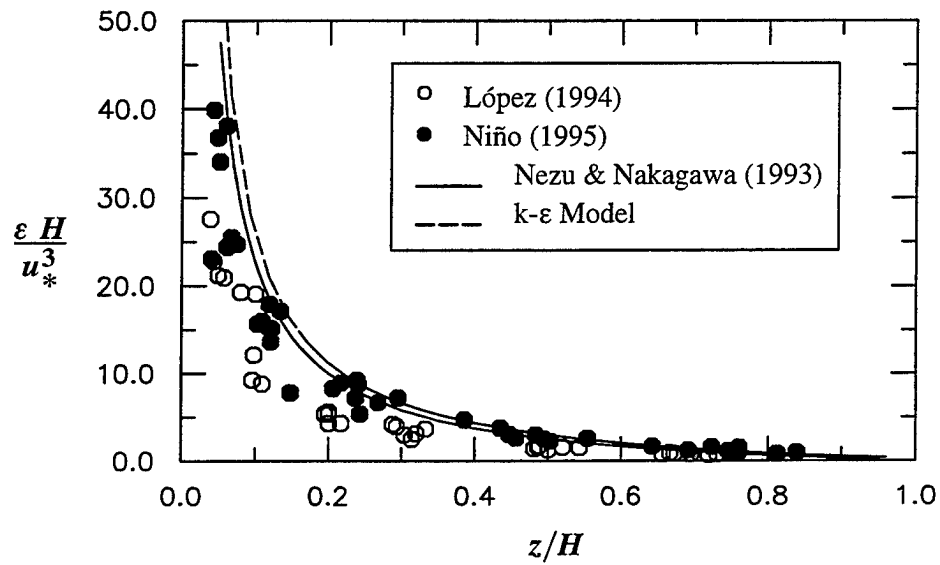


Figure 4.3 Observed and predicted vertical distribution of rms value of vertical velocity fluctuations, smooth-bed condition



a. Turbulence production, smooth-bed condition



b. Turbulence dissipation, smooth-bed (López 1994) and transitionally-rough regime (Niño 1995)

Figure 4.4 Observed and predicted vertical distribution of dimensionless energy budget terms

air-water interface, i.e., reproducing the typical parabolic profile of kinematic eddy viscosity observed in experiments. Figure 4.5a and b depict eddy viscosity and mixing length profiles in dimensionless form for different alternatives in the specification of the boundary condition, together with experimental observations in smooth bed conditions conducted with the acoustic sensor and semiempirical expressions proposed by Nezu and Rodi (1986).

## Turbulent Scales

Dimensionless vertical profiles of macro length scales,  $L_x$ , were computed as:

$$L_x = K \frac{u_{rms}^3}{\varepsilon} \quad (58)$$

where  $K$  is a function of Reynolds number (Nezu and Nakagawa 1993). Results are illustrated in Figure 4.6 together with experimental observations by López (1994) and Niño (1995).

Likewise dimensionless profiles of Taylor and Kolmogorov micro-length scales,  $\lambda$  and  $\eta$ , respectively, were estimated as:

$$\lambda = \sqrt{15\nu \frac{u_{rms}^2}{\varepsilon}} \quad (59)$$

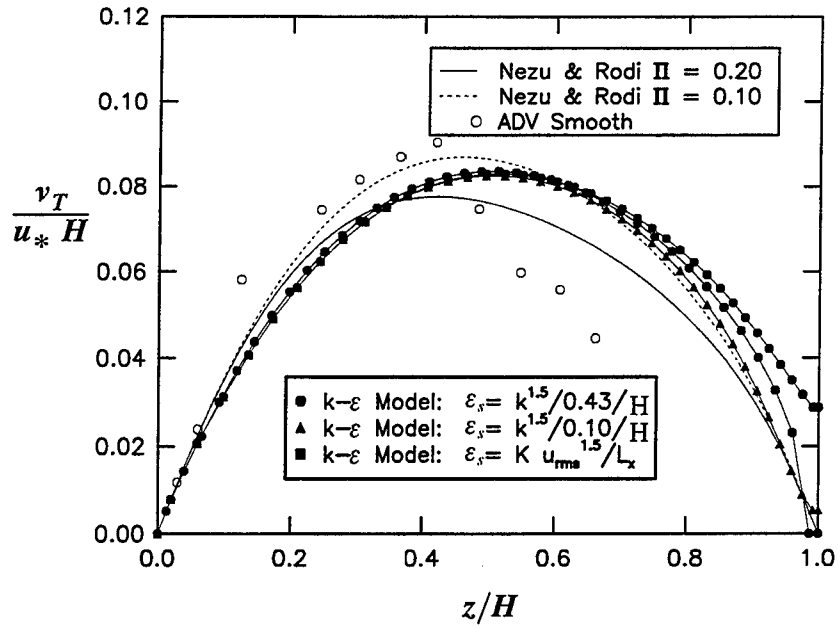
and

$$\eta = \left(\frac{\nu^3}{\varepsilon}\right)^{1/4} \quad (60)$$

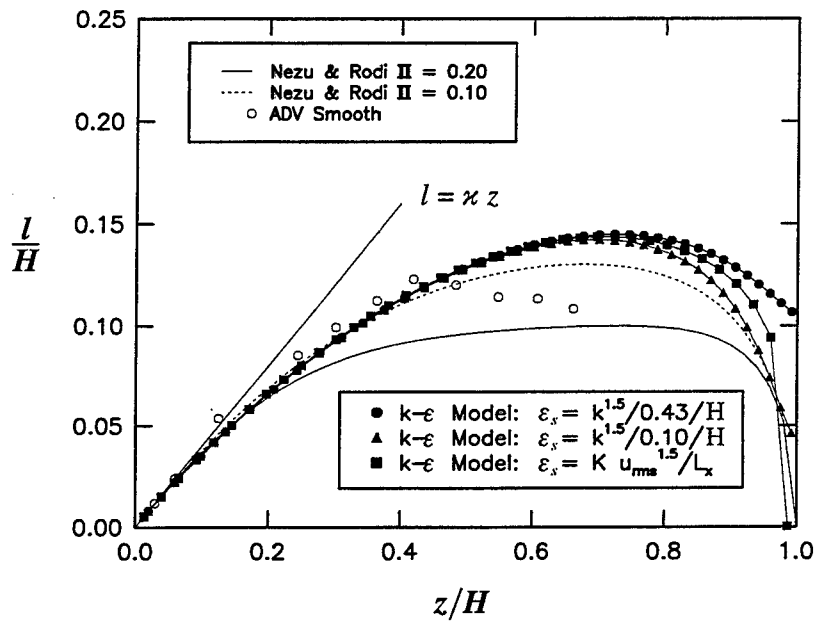
Figure 4.7a and b compare the numerical results for Taylor's micro-scale with experimental observations and semiempirical expressions by Nezu and Nakagawa (1993), whereas Figure 4.8a and b show similar values for the Kolmogorov micro-scale (therein  $Re_*$  stands for the flow shear Reynolds number defined as  $Re_* = u_* H/\nu$ ).

## Validity of Flux Gradient Assumptions

Following Corrsin (1974), data collected with the acoustic sensor were used to check the validity of the underlying assumptions involving the use of flux gradient models in wall-bounded shear flows. The criteria represented by Equations 40 and 42 have been evaluated in Figure 4.9. As was also observed by Corrsin (1974) for the case of turbulent boundary layers, it was found that of



a. Kinematic eddy viscosity



b. Mixing length

Figure 4.5 Observed and predicted vertical distribution of dimensionless kinematic eddy viscosity and mixing length, smooth-bed condition.

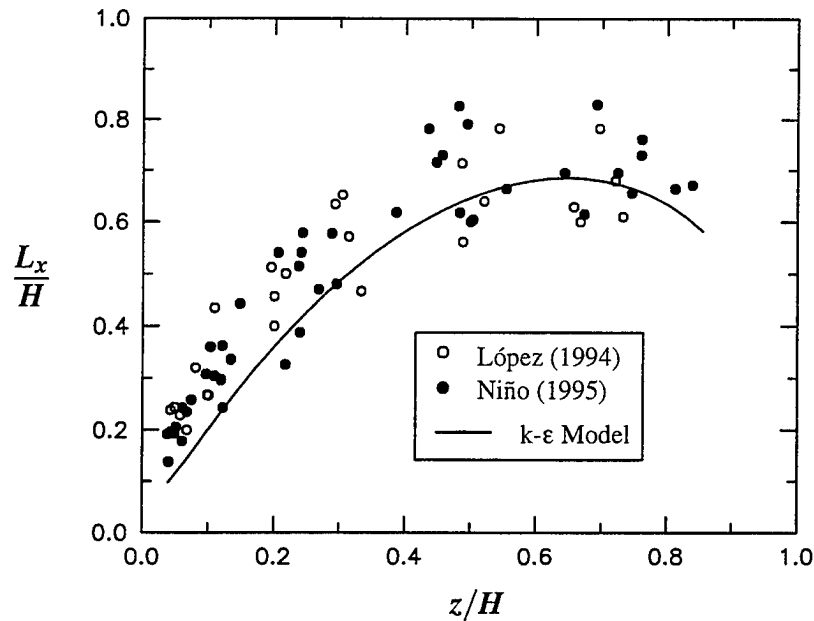
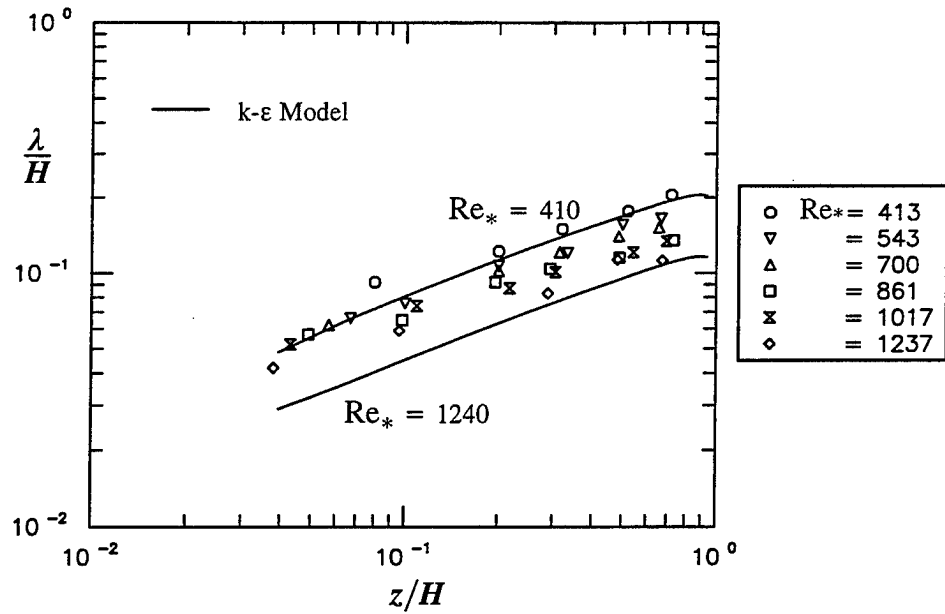
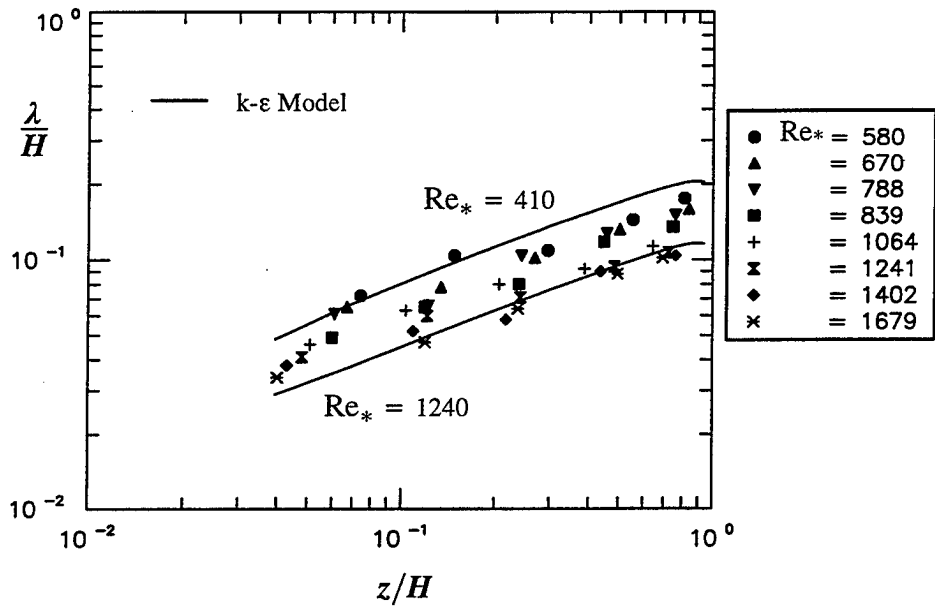


Figure 4.6 Observed and predicted vertical distribution of dimensionless streamwise macro-length scale, smooth and transitionally rough bed conditions

all the homogeneity and stationary conditions required for the applicability of gradient transport models in turbulence, the one requiring cross-stream uniformity of the length scale and root-mean-square velocity fluctuations, i.e. Equation 42, is the most seriously violated. However, as reflected by the good agreement between model predictions and experimental data in Figures 4.1 to 4.8, the violation of such requirement does not seem to significantly affect the turbulence simulation with the model, at least for the mean flow and relatively low-order turbulence statistics commonly used in engineering research (i.e. univariate and joint second-order moments of velocity fluctuations).

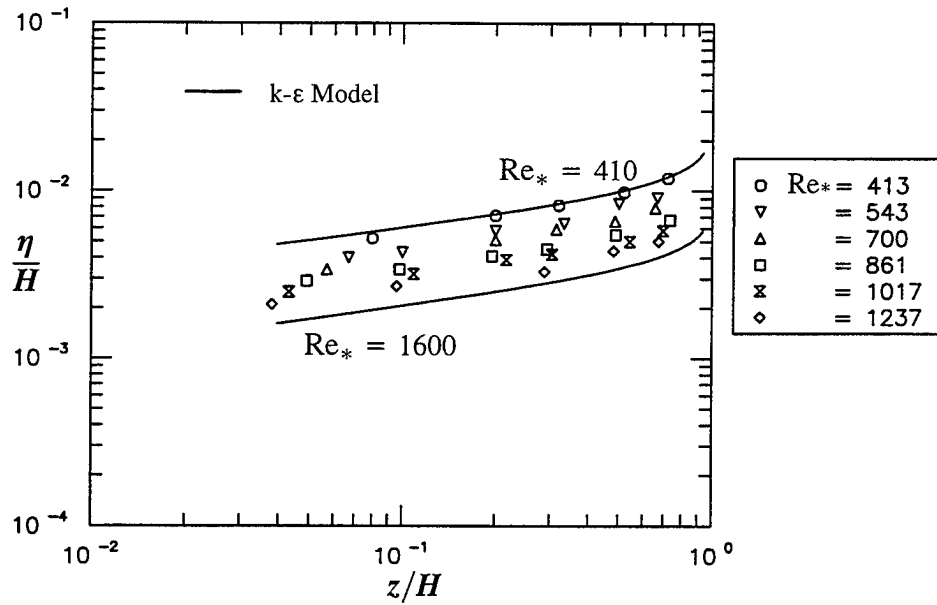


a. Smooth bed condition (López 1994)

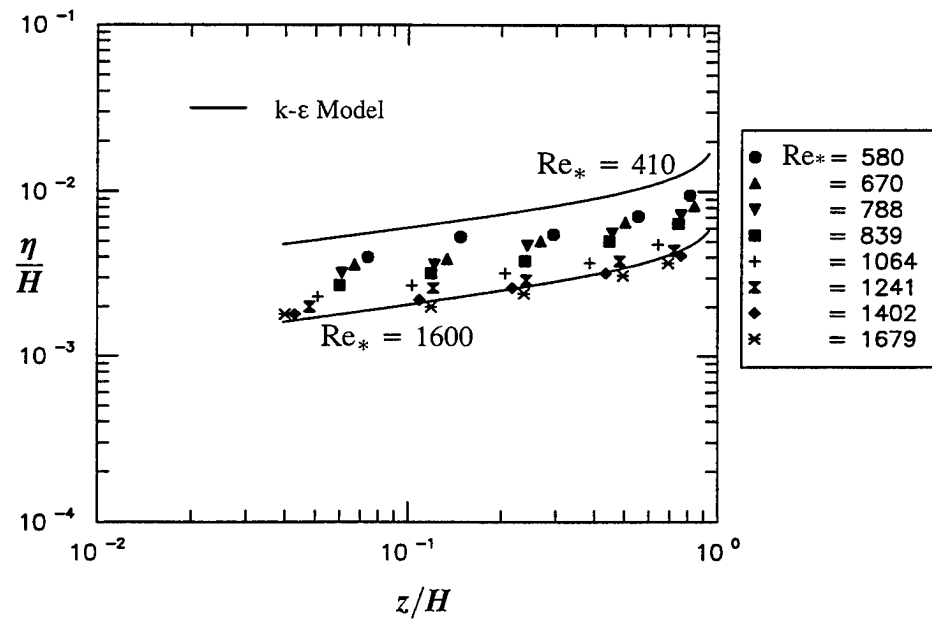


b. Transitionally rough regime (Niño 1995)

Figure 4.7 Observed and predicted vertical distribution of dimensionless Taylor's micro-scale



a. Smooth bed condition (López 1994)



b. Transitionally rough regime (Niño 1995)

Figure 4.8 Observed and predicted vertical distribution of dimensionless Kolmogorov micro-scale

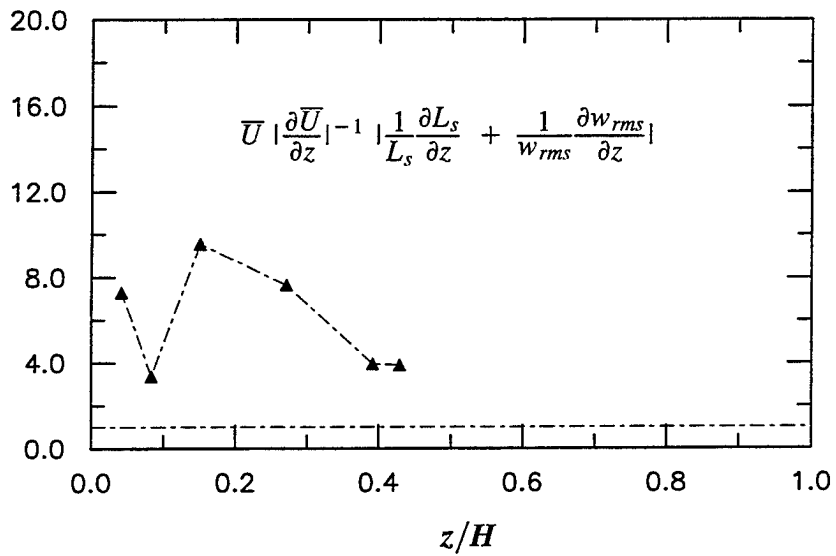
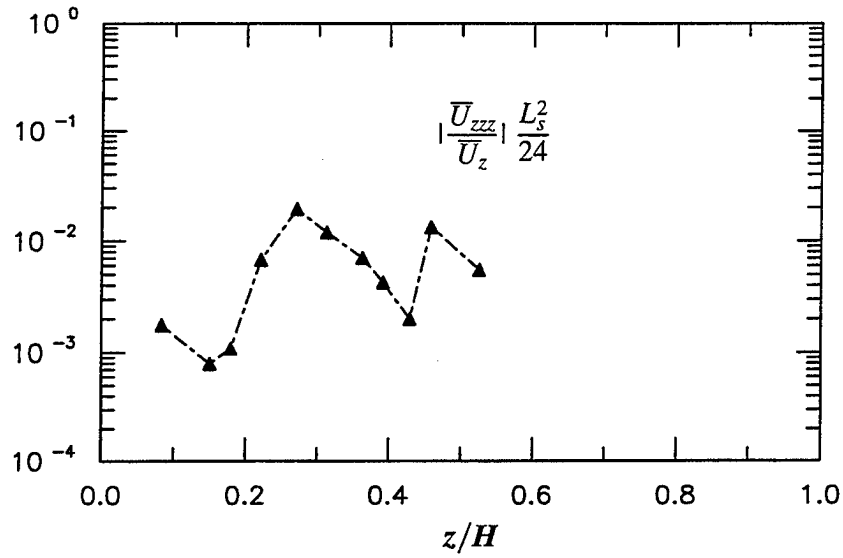


Figure 4.9 Evaluation of Corrsin's criteria according to equations 40 and 42

# 5 Suspended Sediment Transport in Open-Channel Flows Without Vegetation

---

The capability of the model for simulating (non-cohesive) suspended sediment transport in open channels will be tested herein. The equation for the vertical diffusion of sediment is solved together with the momentum,  $k$ - and  $\varepsilon$ -transport equations, forming thus a system of four nonlinear partial differential equations. This system of equations becomes eventually coupled if the influence of the sediment mixture on the flow structure is accounted for by buoyancy terms in the equations for turbulent kinetic energy and dissipation rates, or if the density of the two-phase mixture becomes significantly greater than the density of clear water.

## Equation for Vertical Sediment Diffusion

Vertical profiles of suspended sediment concentrations were computed by solving the equation for the vertical diffusion of sediment, which for uniform flow conditions reads:

$$\frac{\partial \langle \bar{C} \rangle}{\partial t} = \frac{\partial}{\partial z} (w_s \langle \bar{C} \rangle - \langle \bar{C}' w' \rangle) \quad (61)$$

where

$\langle \bar{C} \rangle$ ,  $C'$  = spatial/temporal mean and temporal fluctuating suspended sediment concentrations, respectively

$w_s$  = terminal fall velocity of sediment particle

$w'$  = bed-normal temporal velocity fluctuation

The first term on the right was approximated again using a gradient flux model,  $\langle \overline{C' w'} \rangle = -\nu_T/\sigma_c \partial \langle \overline{C} \rangle / \partial z$ , thus yielding:

$$\frac{\partial \langle \overline{C} \rangle}{\partial t} = \frac{\partial}{\partial z} \left[ \frac{\nu_T}{\sigma_c} \frac{\partial \langle \overline{C} \rangle}{\partial z} + w_s \langle \overline{C} \rangle \right] \quad (62)$$

where  $\sigma_c$  is the Prandtl-Schmidt number for sediment particles. As it will be shown later, depending on the assumptions made, this equation can be solved either coupled or uncoupled with the set of partial differential equations defining the k- $\epsilon$  model. For a given sediment particle size the terminal fall velocity was estimated as:

$$\frac{w_s}{\sqrt{gRD_s}} = \left[ \frac{4}{3} \frac{1}{C_{D_s}} \right]^{1/2} \quad (63)$$

where

$R$  = submerged specific gravity of sediment

$D_s$  = mean sediment diameter

$C_{D_s}$  = drag coefficient of sediment particles

The drag coefficient for the sediment particle was computed with a relation for spheres:

$$C_{D_s} = \frac{24}{R_p} \left[ 1 + 0.152 R_p^{1/2} + 0.0151 R_p \right] \quad (64)$$

with  $R_p = w_s D_s/\nu$ .

## Buoyancy Effects upon Suspended Sediment Transport Capacity

The effect of suspended sediment (and its vertically variable concentration profile) upon the transport properties of a stream is evidenced in three different ways:

- a. By affecting the turbulence intensity of the carrier flow due to the energy spent in keeping the sediment suspended. This effect is commonly accounted for by adding a buoyancy-related sink term in the turbulent kinetic energy budget and a source term in the equation for the dissipation rate (Rodi 1984). Barenblatt (1953, 1979) demonstrated that (for relatively low concentrations) under similar flow conditions (i.e. the

same friction velocity) a water flow carrying sediment in suspension accelerates under the action of particles in comparison with the clear fluid flow. This action is mainly explained by a decrease in turbulent kinetic energy, which ultimately causes a drag reduction (Barenblatt and Golitsyn 1974). More recently, García (1992) showed how buoyancy may also be taken into consideration in the boundary conditions for two-equation models, as:

$$\left(\frac{dU}{dz}\right)_o = \frac{u_*}{\kappa z} \phi_u(K_o, \beta) \quad (65)$$

$$k_o = \frac{u_*}{\sqrt{C_\mu}} \phi_k(K_o) \quad (66)$$

$$\varepsilon_o = \frac{u_*^3}{\kappa z} \phi_\varepsilon(K_o, \beta) \quad (67)$$

where

$$K_o = \frac{gRw_s^2C_o z_o}{u_*^4}$$

$$\beta = \text{constant with a value close to 5}$$

and, as before, the subindex  $o$  stands for the value of the variable at the first grid point away from the bed, which also has to be located within the equilibrium layer. It can be shown (López 1997) that the former two approaches yield identical results, with:

$$\phi_u(K_o, \beta) = \frac{\kappa u_*}{w_s} \quad (68)$$

$$\phi_k(K_o) = \sqrt{1 - K_o} \quad (69)$$

$$\phi_\varepsilon(K_o, \beta) = \frac{\kappa u_*}{w_s} (1 - K_o) \quad (70)$$

and

$$\beta = \frac{\kappa u_*/w_s - 1}{K_o} \quad (71)$$

It would be of interest to test if the value of  $\beta$ , as prescribed by equation 71, is indeed constant as suggested by observations of atmospheric boundary-layer flows.

b. By changing the density of the mixture,  $\rho_m$ :

$$\rho_m = \rho_w (1 + R C) \quad (72)$$

with  $\rho_w$  representing the density of clear water. Or by changing the viscosity of the mixture,  $\nu_m$ , where according to Einstein (Graf 1971):

$$\nu_m = \nu_w (1 + k_e C) \quad (73)$$

with  $\nu_w$  denoting the viscosity of clear water. Happel and Brenner (1965) found the Einstein viscosity constant,  $k_e$ , to be  $k_e = 2.5$ .

c. By changing the Prandtl-Schmidt number,  $\sigma_c$  (Lauder, Reece and Rodi 1975), in the sediment diffusion equation.

$$\sigma_c = \sigma_{co} \frac{1 + \Phi_c'(C_c' - \Phi_c) B}{1 + \Phi_c \Phi_c B} \quad (74)$$

where

$\sigma_{co}$  = the Prandtl/Schmidt number under nonstratified conditions

$\phi_c, \phi_c', C_c'$  = model parameters, that for the case of temperature-induced stratification are equal to 0.31, 0.16 and 1.60, respectively

$B$  = dimensionless buoyancy parameter defined as  $-gR \frac{k^2}{\varepsilon^2} \frac{\partial C}{\partial z}$

The influence of each of these factors depends upon the particular problem under consideration. Several experimental (Vanoni 1946; Einstein and Chien 1955; Coleman 1981) and theoretical (Barenblatt and Golitsyn 1974) works have shown how the velocity of the flow increases with the mean sediment concentration. However the interaction of suspended matter and the turbulence structure of the flow is to date not fully understood. In the present work seven different combinations of the factors discussed in the preceding paragraph were numerically analyzed in order to determine the effects on the suspended sediment transport capacity of the flow and finally decide which model to use in the presence of vegetation. Combination 1 corresponded to a decoupled solution of the vertical diffusion equation, therefore neglecting all the factors mentioned. Combination 2 dealt with the inclusion of the buoyancy-related terms in the transport equations for  $k$  and  $\varepsilon$ , but maintaining the standard wall functions and keeping constant both the density of the mixture and  $\sigma_c$ . In combination 3, buoyancy was considered and the density of the mixture was allowed to vary vertically with the concentration. Combination 4 corresponded to the inclusion of buoyant terms plus variations in density and  $\sigma_c$ . In the fifth combination, density and  $\sigma_c$  were kept constant while considering both buoyant-related terms and modified wall functions. Combination 6 is similar to the former except that density was also allow to vary with concentration. And lastly, the seventh combination considered both variations in density of the mixture and  $\sigma_c$  while also introducing the buoyancy-related terms and the modified wall functions.

Basically two different outputs were considered, vertical profiles of suspended sediment concentration and total transport capacity, obtained by vertically integrating the product of mean velocity and local sediment concentration. Results of vertical concentration profiles were compared against

the Rousean distribution:

$$\frac{C}{C_b} = \left[ \frac{(H-z)}{z} \frac{(H-b)}{b} \right]^{\frac{w_s}{\kappa u_*}} \quad (75)$$

where

$$b = 0.05 H$$

$$C_b = \text{near-bed sediment concentration}$$

The sediment concentration near the bed was estimated using the expression of García and Parker (1991):

$$C_b = \frac{A Z_u^5}{\left(1 + \frac{A}{0.30} Z_u^5\right)} \quad (76)$$

with  $Z_u = u_*/w_s \text{ Rep}^{0.6}$  and  $A = 1.30 \times 10^{-7}$ . Equation 76 provides a mean of estimating the bed sediment concentration under equilibrium conditions at  $z/H = 0.05$ , and was derived using data covering the following ranges of the variables:

$$2.0 \cdot 10^{-4} < C_b < 6.0 \cdot 10^{-2};$$

$$0.70 < u_*/w_s < 7.50;$$

$$240 < H/D_s < 2,400;$$

$$3.50 < \text{Rep} < 37.0.$$

The computed suspended transport capacity,  $q_{ss}$ , was compared against predictions from the formula due to Einstein (1950):

$$q_{ss} = 11.57 C_b u_* b \left[ I_1 \text{Ln} \left( \frac{30 H}{k_c} \right) + I_2 \right] \quad (77)$$

where  $k_c$  represents a measure of the roughness, and  $I_1$  and  $I_2$  are numerically evaluated integrals (see also Graf 1971).

It must be said that a particular limitation arises when trying to solve all the equations as a coupled system. This limitation is based on the fact that the wall functions have to be evaluated at a grid point,  $z_o$ , located between 30 and 100 wall units from the bed, whereas the proposed expression for estimating the near-bed concentration gives the value of  $C_b$  at  $z_o = 0.05H$ . Therefore, for a

smooth-bed two-dimensional open channel:

$$30 \leq \frac{0.05H \sqrt{g S_o H}}{\nu} \leq 100 \quad (78)$$

where  $S_o$  = bed slope. Equation 78 constitutes an important constraint that specifies the required range of  $H$  for a given slope and water temperature.

Suspended sediment transport capacity was computed for a two-dimensional open channel with  $S_o = 0.001$  and  $H = 0.07$  m for different sediment sizes using the seven aforementioned combinations. Results are depicted in Figure 5.1 in dimensionless form together with predictions from the Einstein's (1950) formula. In order to appreciate the effects of buoyancy on water discharge, Figure 5.2 illustrates the ratio  $q_w/q_{w0}$  corresponding to the same conditions as Figure 5.1, where  $q_w$  is the computed water discharge for each combination and  $q_{w0}$  is the computed water discharge for combination 1, thus without considering any sediment-turbulence interaction.

These graphs show that, while water discharge increases as much as 56 percent depending upon the sediment concentration and calculation procedure, suspended sediment transport capacity is relatively well predicted by neglecting sediment-turbulence interactions, especially for low concentrations. Based on these results and the fact that the sediment-laden flows considered herein have relatively low sediment concentrations, the results shown in the next two paragraphs were computed neglecting buoyancy effects.

## Vertical Profile of Suspended Sediment Concentration

Figure 5.3 shows computed dimensionless vertical profile of suspended sediment concentration together with predictions by the Rousean model for three different sediment sizes, namely 40, 100 and 150  $\mu\text{m}$  ( $Re_p = 1.87, 4.02$  and 11.38, respectively).

## Suspended Sediment Transport Capacity

Figure 5.4 shows results of the variation in suspended sediment transport capacity,  $q_{ss}$ , for a two-dimensional channel ( $S_o = 0.0036$  and  $H = 0.35$  m) for seven different sediment sizes, whereas Figure 5.5 depicts this capacity as a function of flow depth for given values of  $S_o$  and  $D_s$ . Results of the numerical model are compared in both figures to predictions with the formula by Einstein (1950).

	Buoy	$\rho$	$\sigma_c$	BC
○	N	c	c	N
●	Y	c	c	N
□	Y	v	c	N
■	Y	v	v	N
△	Y	c	c	Y
▲	Y	v	c	Y
▽	Y	v	v	Y

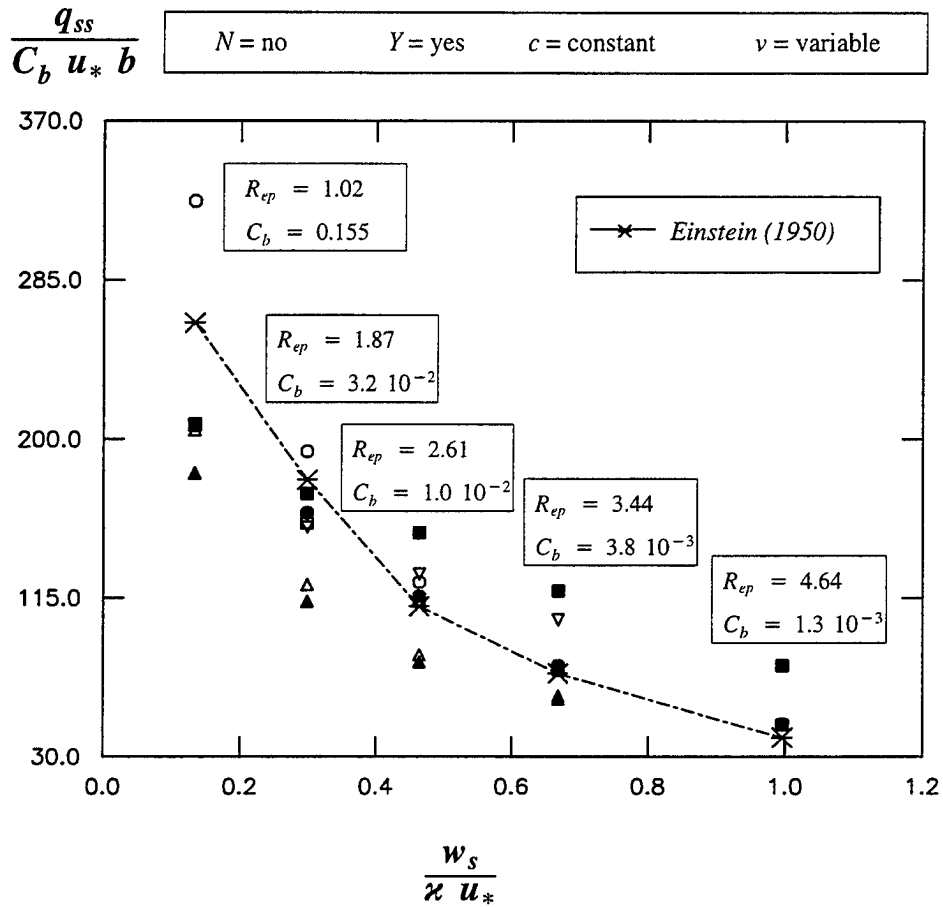


Figure 5.1 Suspended sediment transport capacity as function of Rouse number and different buoyancy effects together with predictions by Einstein's (1950) formula

	Buoy	$Q$	$\sigma_c$	BC
○	N	c	c	N
●	Y	c	c	N
□	Y	v	c	N
■	Y	v	v	N
△	Y	c	c	Y
▲	Y	v	c	Y
▽	Y	v	v	Y

$\frac{q_w}{q_{w0}}$  N = no      Y = yes      c = constant      v = variable

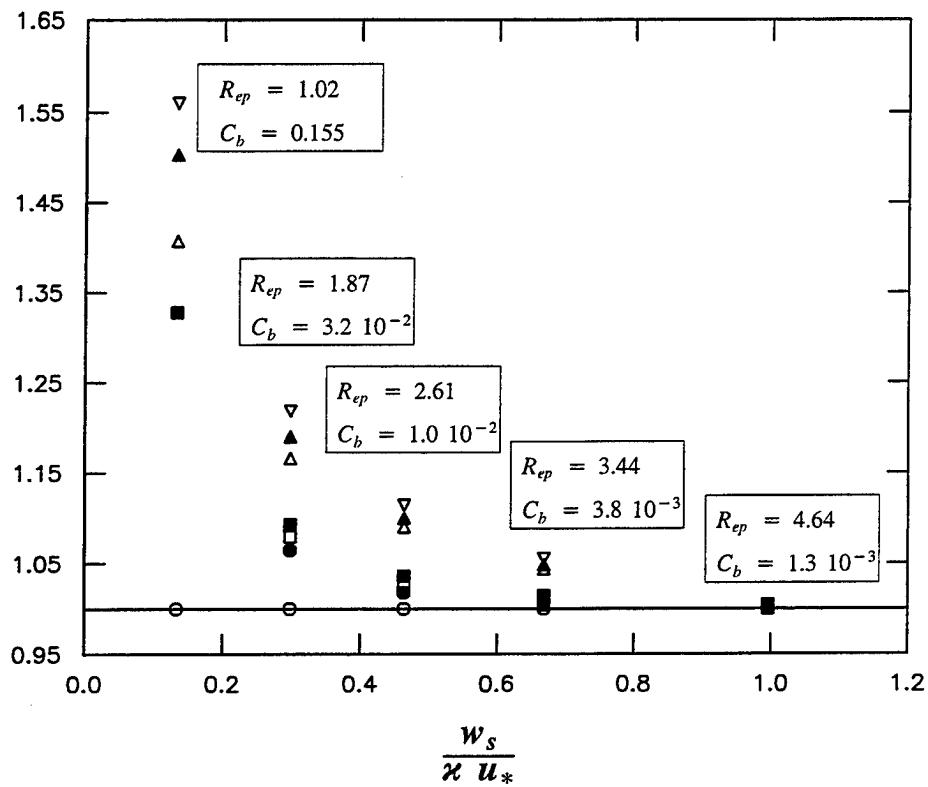


Figure 5.2 Relative water discharge as function of Rouse number and different buoyancy effects

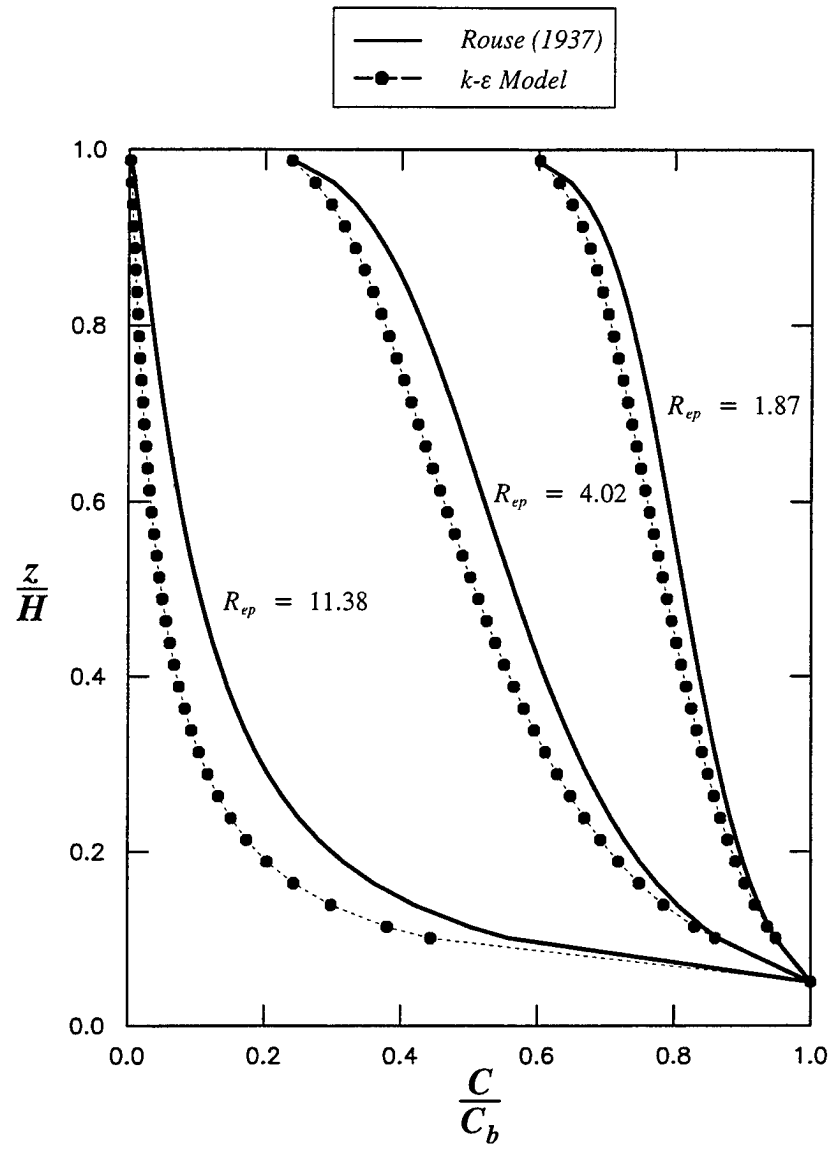


Figure 5.3 Dimensionless vertical profile of suspended sediment concentration for different mean diameters

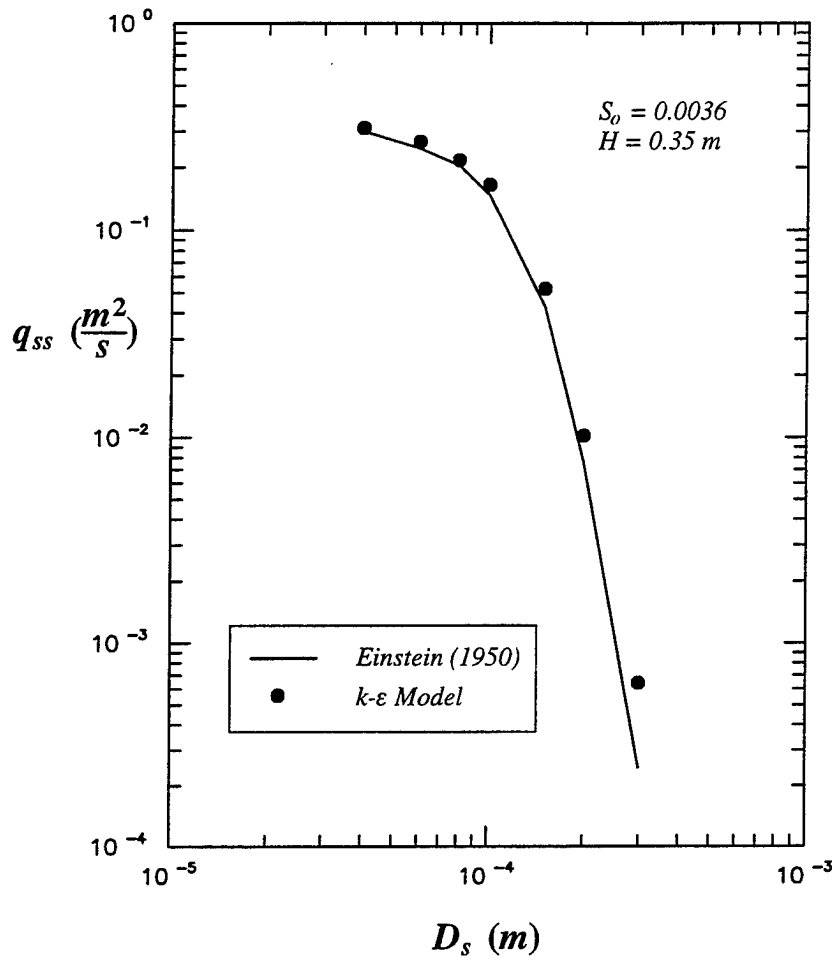


Figure 5.4 Estimated suspended sediment transport capacity for different mean diameters

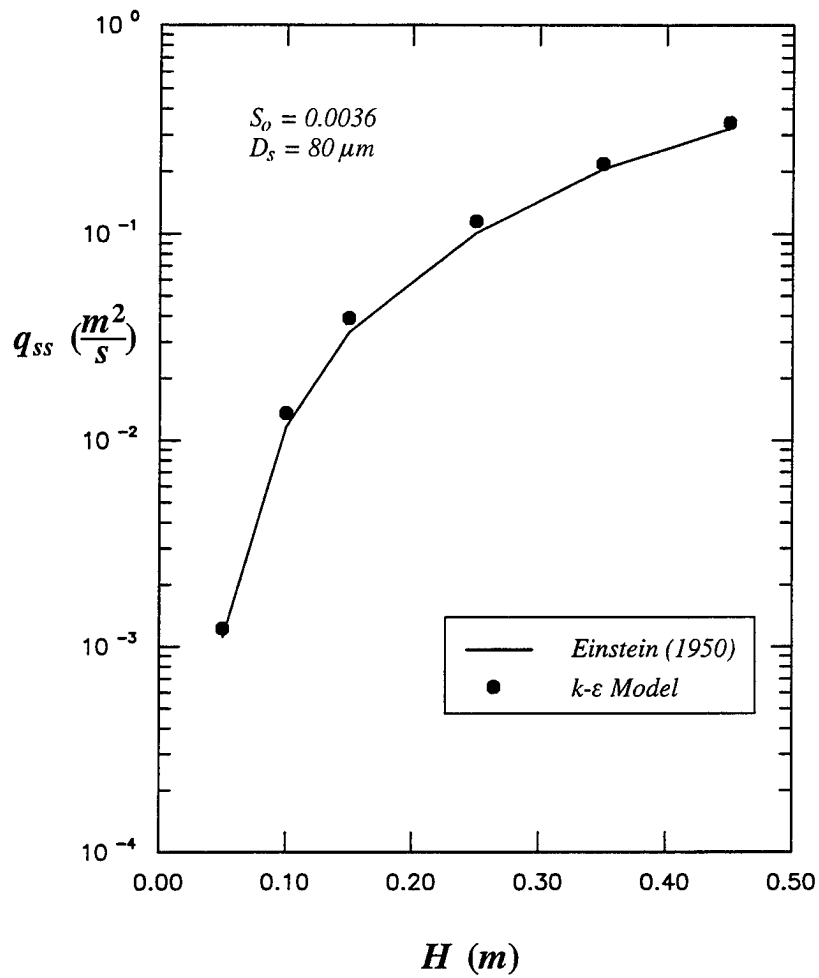


Figure 5.5 Estimated suspended sediment transport capacity for different mean flow depths

# 6 Turbulence Structure in Vegetated Open-Channel Flows

---

In this chapter experimental results for open-channel flows in the presence of both rigid and flexible simulated vegetation will be used to check the validity of the assumptions made previously. First, the experimental conditions will be summarized. Then, computed vertical profiles of mean flow as well as turbulence characteristics will be compared against experimental results. Lastly, the impact of using wall functions different from the usual ones in the standard model will be briefly explored and Corrsin's criteria for the applicability of gradient-flux models in the presence of vegetation will be evaluated.

## Experiments in Open-Channel Flows with Simulated Vegetation

As mentioned in Chapter 3, a series of experiments was conducted at the Hydrosystems Laboratory with the goal of characterizing the drag coefficient in the particular case of free-surface, turbulent flows and of providing information for the verification of the  $k-\epsilon$  model. Regarding the second reason, it was considered crucial for the authors to conduct their own observations because most of the data available lacked a detailed description of the experiments; in particular, no clear specification of the measuring location and the spatial averaging procedure are given. From the discussions in Chapter 3, the importance of the averaging procedure employed to determine one-dimensional parameters becomes clear.

The experiments were conducted under uniform flow conditions in a 19.50-m-long, 0.91-m-wide and 0.61-m-deep tilting flume (Dunn, López and

García 1996). Velocity measurements were taken with a Sontek acoustic Doppler velocimeter at a sampling frequency of 25 Hz, at four different plan-locations with 10 measuring points in each vertical. Cylindrical wooden dowels and commercial drinking straws were used to simulate rigid and flexible vegetation, respectively. Table 6.1 provides a summary of the experimental conditions, where  $a$  represents plant density,  $S_o$  is the averaged bed (water-surface) slope,  $Q$  is the discharge,  $H$  represents the normal flow depth,  $\alpha$  is the averaged deflection angle of the simulated plants,  $Re$  is the Reynolds number and  $Fr$  is the Froude number.

**TABLE 6.1 Experimental Conditions**

Exp #	$a$ (1/m)	$S_o$	$Q$ (m <sup>3</sup> /s)	$H$ (m)	$\alpha$ (°)	$Re$	$Fr$	
Rigid Vegetation	Exp. 1	1.09	0.0036	0.179	0.335	0.00	224,000	0.33
	Exp. 2	1.09	0.0036	0.088	0.229	0.00	113,000	0.29
	Exp. 3	1.09	0.0036	0.046	0.164	0.00	57,000	0.24
	Exp. 4	1.09	0.0076	0.178	0.276	0.00	191,000	0.36
	Exp. 5	1.09	0.0076	0.098	0.203	0.00	125,000	0.37
	Exp. 6	0.27	0.0036	0.178	0.267	0.00	196,000	0.39
	Exp. 7	0.27	0.0036	0.095	0.183	0.00	120,000	0.42
	Exp. 8	2.46	0.0036	0.180	0.391	0.00	258,000	0.29
	Exp. 9	2.46	0.0036	0.058	0.214	0.00	69,700	0.19
	Exp. 10	2.46	0.0161	0.180	0.265	0.00	203,000	0.40
	Exp. 11	0.62	0.0036	0.177	0.311	0.00	222,000	0.35
	Exp. 12	0.62	0.0110	0.181	0.233	0.00	238,000	0.58
Flexible Vegetation	Exp. 13	1.09	0.0036	0.179	0.368	35.0	228,000	0.28
	Exp. 14	1.09	0.0101	0.180	0.232	51.0	257,000	0.62
	Exp. 15	1.09	0.0036	0.093	0.257	34.0	112,000	0.23
	Exp. 16	0.27	0.0036	0.179	0.230	65.0	227,000	0.56
	Exp. 17	2.46	0.0036	0.078	0.279	12.0	94,900	0.18
	Exp. 18	2.46	0.0101	0.179	0.284	45.0	250,000	0.45

## Mean Flow Characteristics

Model predictions regarding mean (spatial and temporal averaged) velocities were compared against the experimental observations. The modeled turbulent

kinetic energy in the two-equation turbulence model corresponded to Equation 10; hence values of  $C_{fk} = 1.0$  and  $C_{f\varepsilon} = 1.33$  were used in the computations. Figure 6.1 compares numerical simulations and experimental observations for two of the rigid-vegetation tests in Table 6.1, whereas Figure 6.2 shows predictions corresponding to the flexible conditions. As will be also observed in the Reynolds stress computations, the existence of secondary currents seems to play an important role above the simulated vegetation, both in retarding the flow and decreasing the turbulent momentum transfer in the vertical. Hence, since these computations simulate two-dimensional flows, computed mean velocities above the plant canopy are slightly larger than the measured ones.

Figure 6.3 depicts the vertical mean velocity profile of two experiments (rigid and flexible conditions) in semilog scale, showing the agreement between both numerical and experimental results with the logarithmic law. The differences in slope between the model predictions and the measured profile may be explained by the different values of the predicted and observed turbulent momentum transfer close to the top of the simulated canopy (see "Reynolds stresses" in next section). Indeed, the vertical slope of the velocity profile in the equilibrium layer of wall-bounded flows becomes  $dU/dz = u_*/\kappa z$ , which clearly explains that a larger value of the shear velocity yields larger slopes at the same distance from the bed. Note also how the numerical model predicts the existence of a region immediately above the simulated plants, where the velocity is not logarithmically distributed, in agreement with reported results on velocity distributions in the roughness sublayer (López 1997).

## Second-order Moments

This section shows the capability of the numerical model to simulate the vertical structure of second-order moments, i.e. Reynolds stresses and turbulence intensities.

### Reynolds stresses

Computed vertical profiles of spatially averaged Reynolds stresses are depicted in Figure 6.4 and 6.5 for rigid and flexible conditions, respectively, together with experimental observations, for the same experiments as Figure 6.1. As mentioned previously, a very good agreement between experimental values and model predictions is observed for flow within the simulated vegetation, whereas the measured Reynolds stresses above the simulated canopy were consistently smaller than the theoretical ones for two-dimensional open-channel

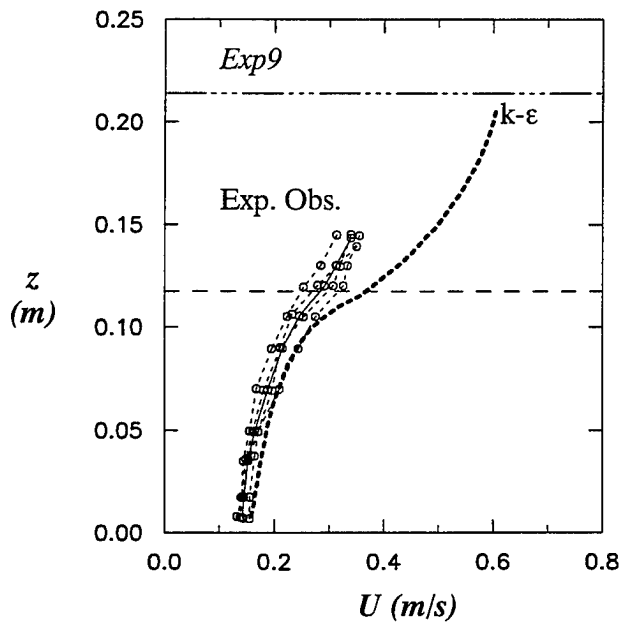
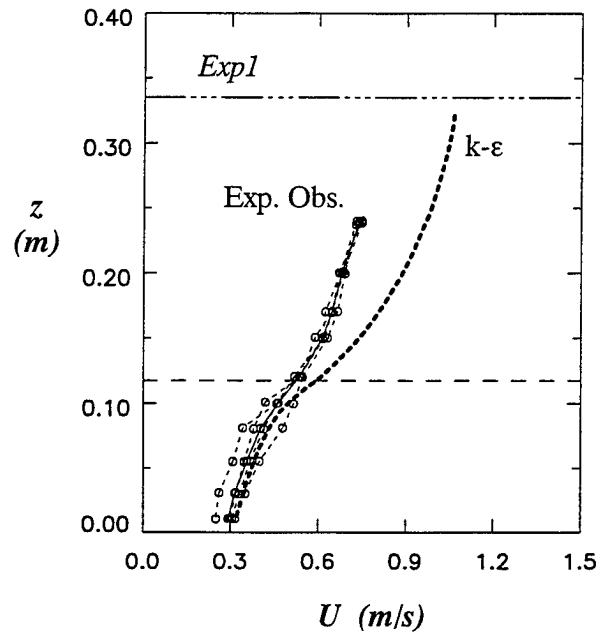


Figure 6.1 Observed and predicted vertical distribution of mean velocity, rigid conditions

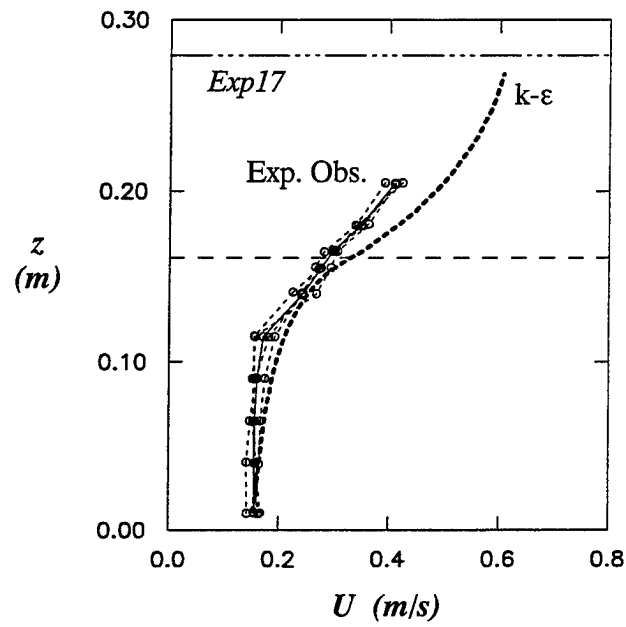
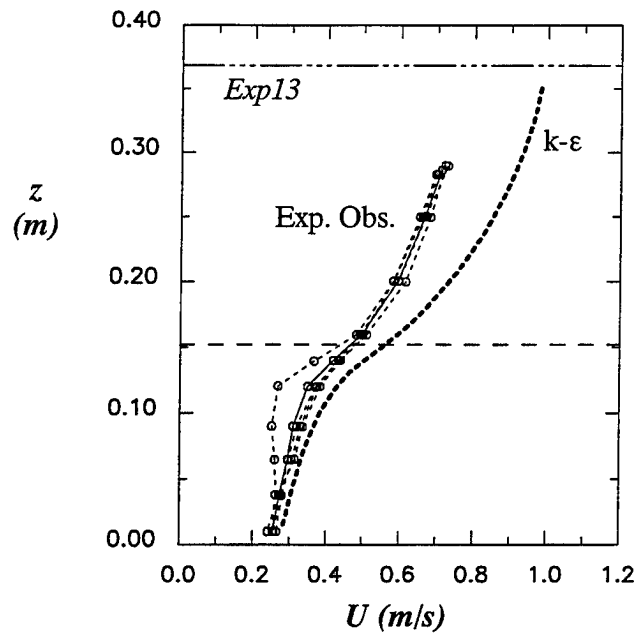
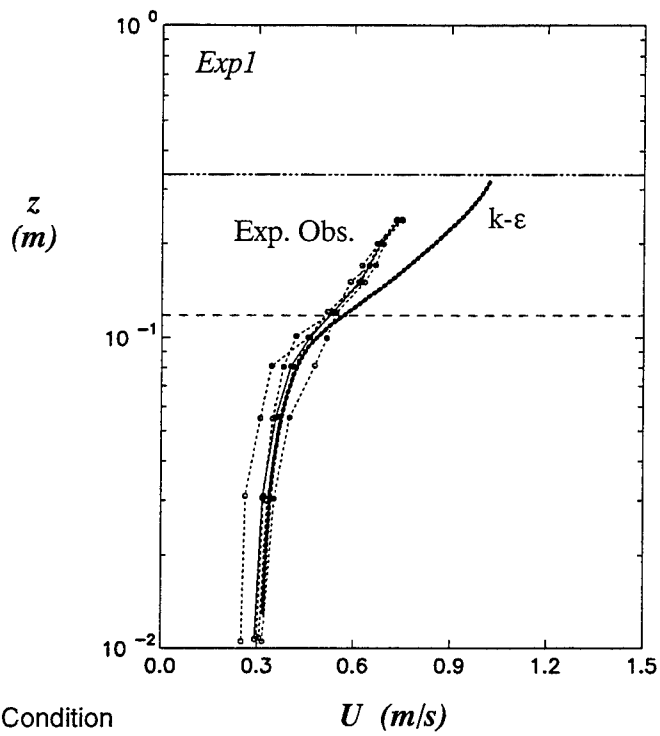
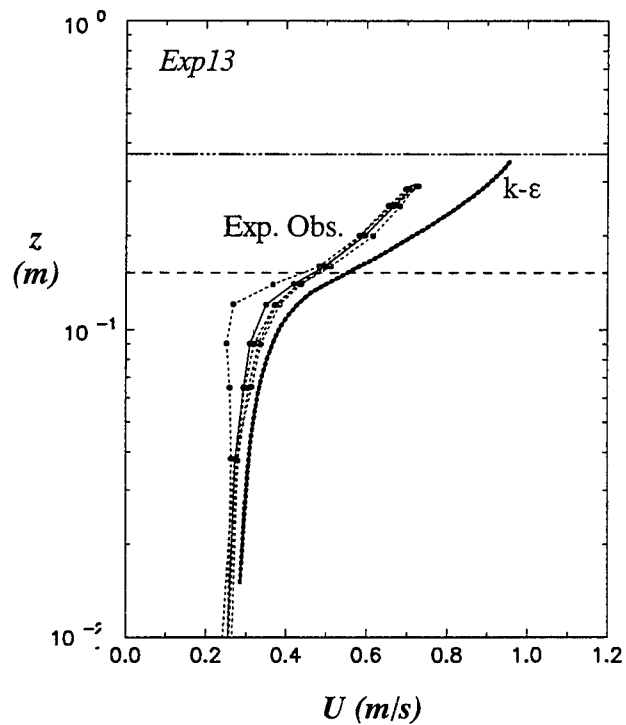


Figure 6.2 Observed and predicted vertical distribution of mean velocity, flexible conditions



a. Rigid Condition



b. Flexible condition

Figure 6.3 Observed and predicted vertical distribution of mean velocity in semilog scale

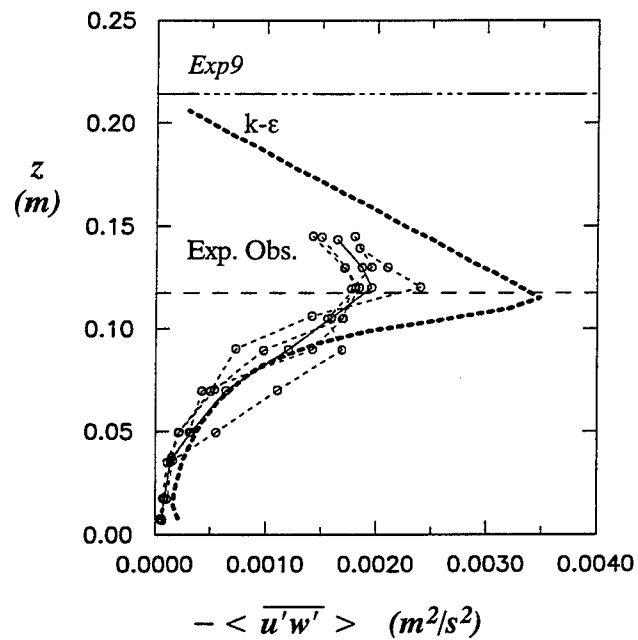
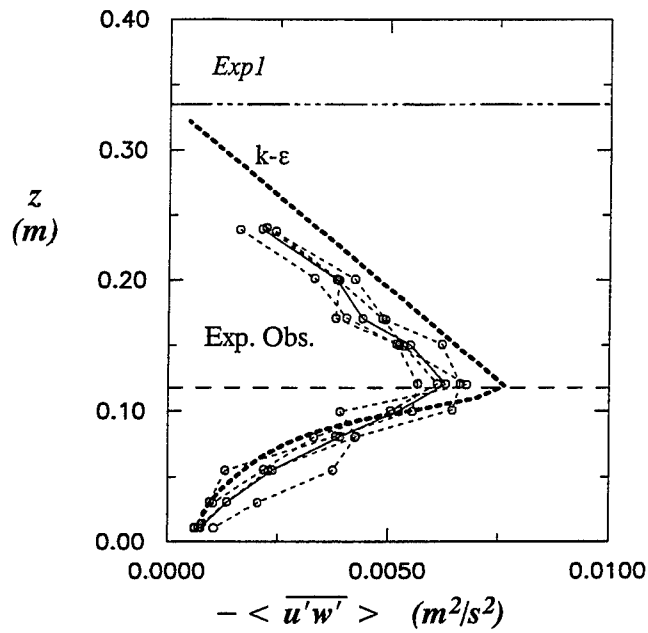


Figure 6.4 Observed and predicted vertical distribution of Reynolds stresses, rigid conditions

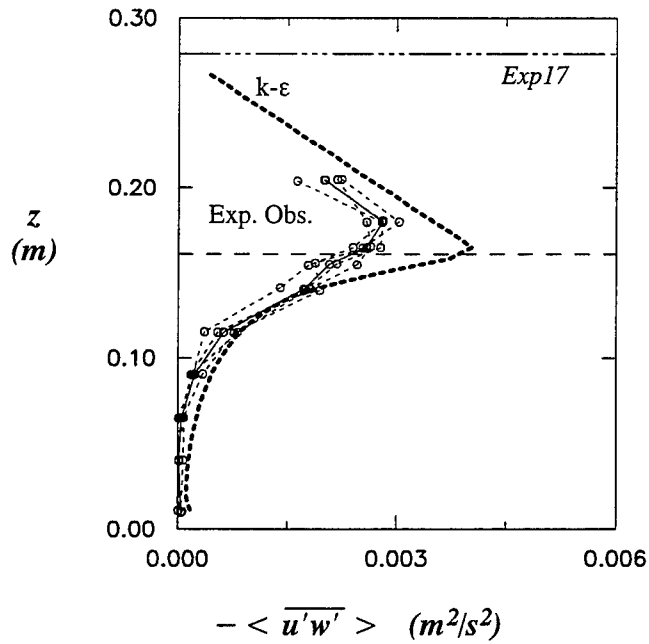
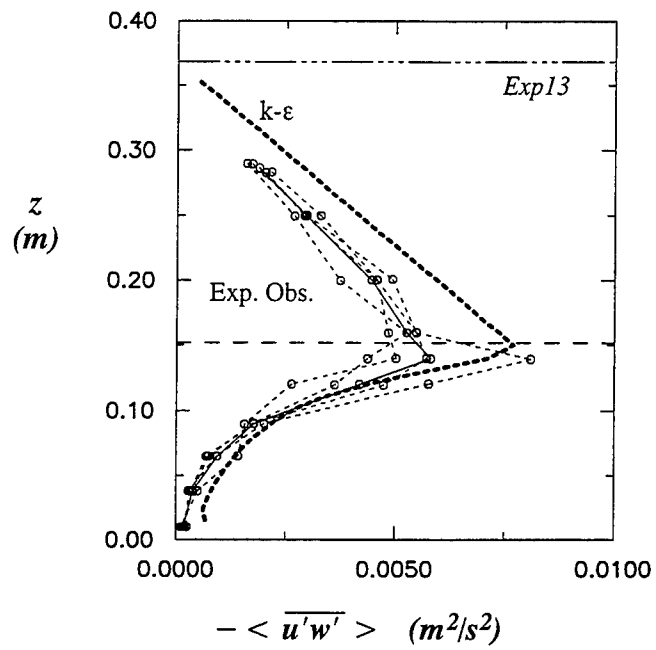


Figure 6.5 Observed and predicted vertical distribution of Reynolds stresses, flexible conditions

flows. However, this phenomenon is typical for free-surface flows (Nezu and Nakagawa 1993), the deviation being explained by the action of secondary currents as well as other components of the Reynolds stress tensor, the magnitude of this effect being a function of the width-to-depth ratio (aspect ratio).

### **Turbulent kinetic energy and turbulence intensities**

Computations of experimental values of total turbulent kinetic energy and turbulence intensities,  $\langle u_i'' u_i'' \rangle$ , are very difficult to obtain, especially due to the large number of measuring locations needed to obtain representative values of  $\langle \overline{u_i' u_i'} \rangle$ . It is worth noting again that for  $i \neq j$  (i.e. off-diagonal components of the total turbulent stress tensor) the contribution of the wake-related production term is negligible (Raupach et al. 1986). Hence, in order to compare numerical results with experimental observations of  $\langle \overline{u_i' u_i'} \rangle$ , the model was run with  $C_{fk} = 0.0$  and  $C_{f\epsilon} = 0.0$ . Figures 6.6 and 6.7 depict the results obtained for the streamwise turbulence intensities together with the experimental data. In order to better visualize the difference between  $\langle \overline{u_i' u_i'} \rangle$  and  $\langle u_i'' u_i'' \rangle$ , Figure 6.8 illustrates the computed values of the total streamwise intensities obtained when the model was run using  $C_{fk} = 1.0$  and  $C_{f\epsilon} = 1.33$ .

In light of these results and the discussion in chapter 3, it becomes clear why very small weighting coefficients in the drag-related source terms for the  $k$  and  $\epsilon$  equations yield very good predictions of the observed values of turbulence intensities in water flows.

## **Energy Budget Terms**

To further investigate the performance of the model, different terms in the turbulent kinetic energy budget were computed, and when possible compared against the experimental observations.

### **Spatially averaged time-mean values**

As mentioned in the previous section, only accurate measurements of spatially averaged time-mean values could be obtained from the experiments, and those are the results that are simulated herein. Figure 6.9 and 6.10 illustrate vertical profiles of the different terms in the energy budget made dimensionless using  $U_{*hp}$  and  $h_p$  as scaling velocity and length scales, respectively.  $U_{*hp}$  is the

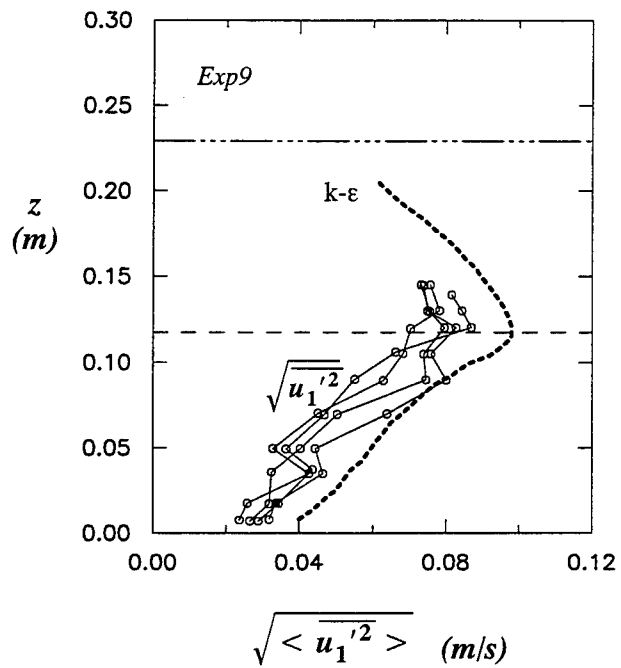
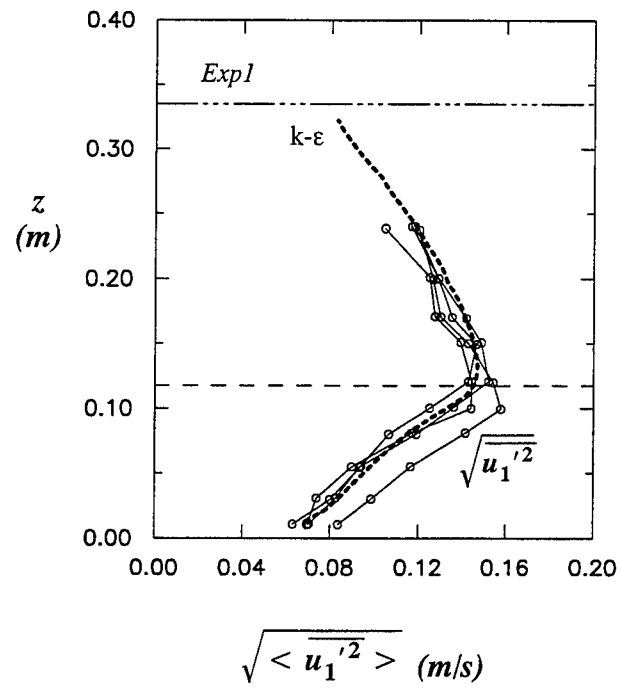


Figure 6.6 Observed and predicted vertical distribution of streamwise turbulence intensity, rigid condition

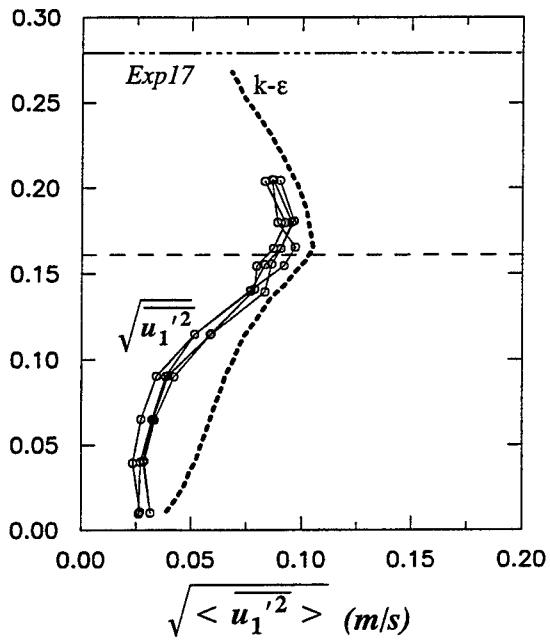
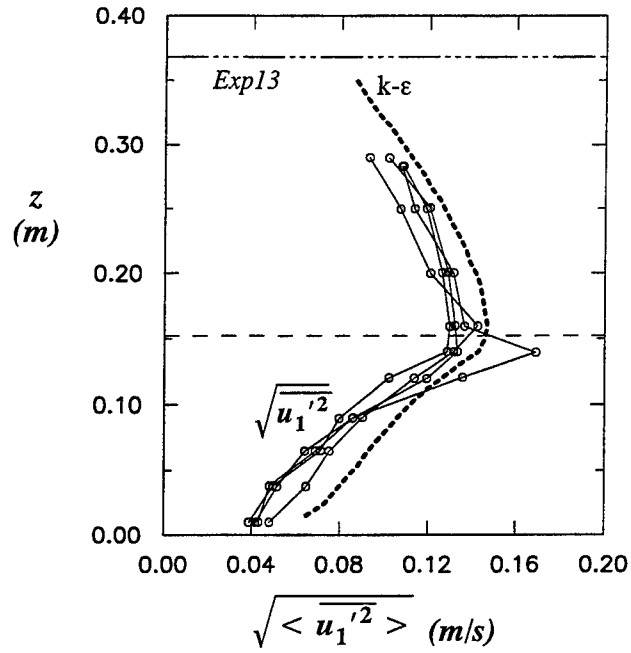
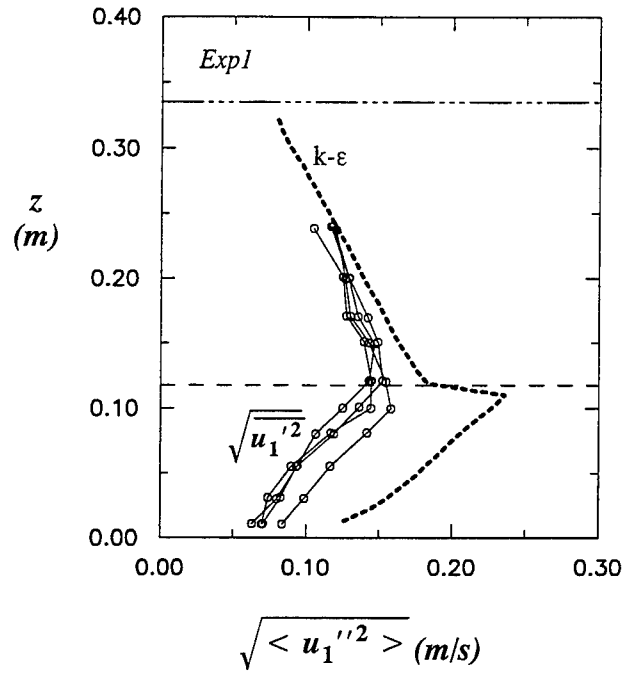
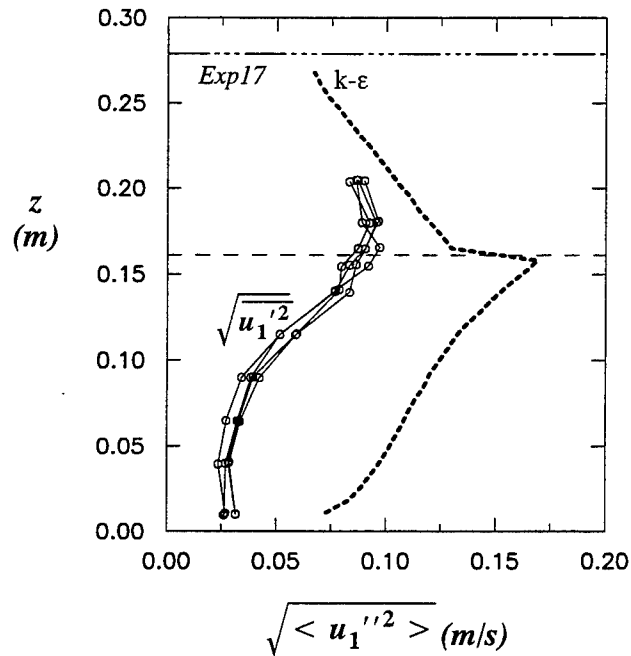


Figure 6.7 Observed and predicted vertical distribution of streamwise turbulence intensity, flexible condition



a. Rigid vegetation



b. Flexible vegetation

Figure 6.8 Observed and predicted vertical distribution of total streamwise turbulence intensity

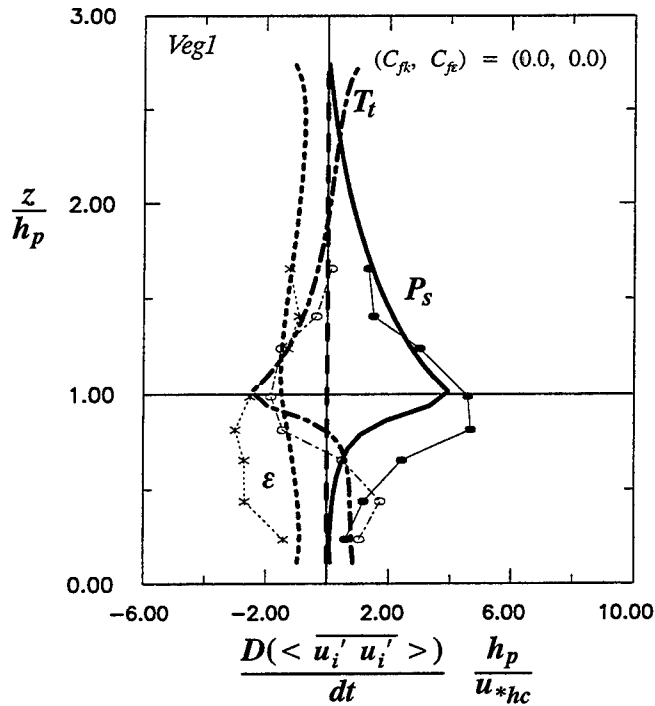
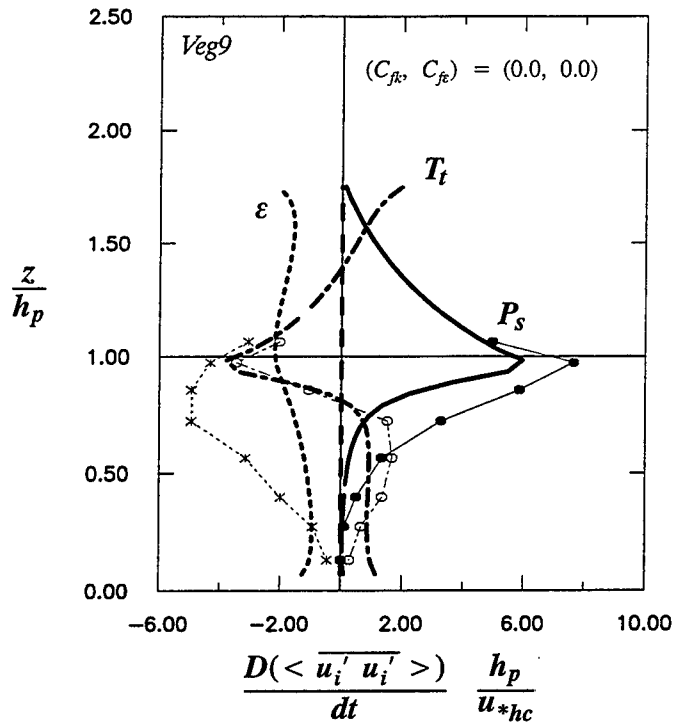


Figure 6.9 Observed and predicted vertical distribution of different terms in the spatially averaged, temporal-mean, turbulent kinetic energy budget for  $(C_{fk}, C_{fe}) = (0.0, 0.0)$ . Lines represent model predictions and symbols are observed values.

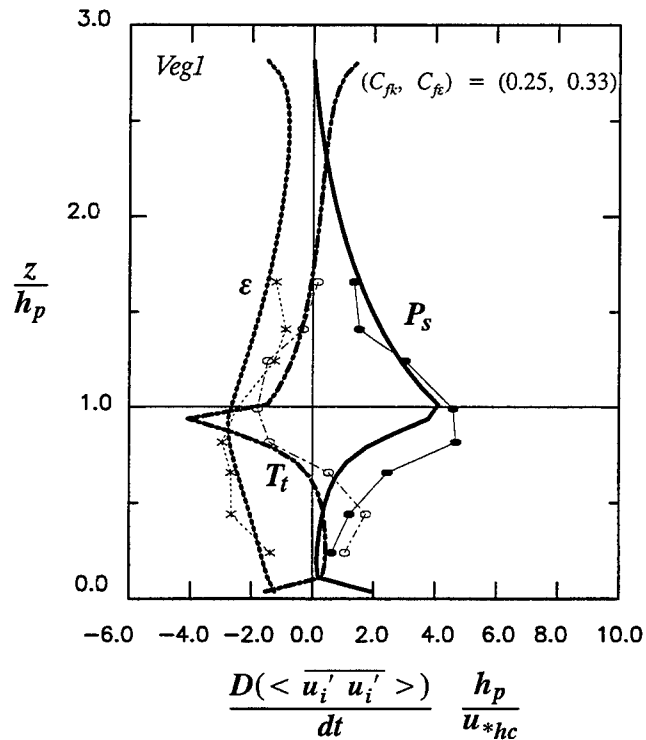
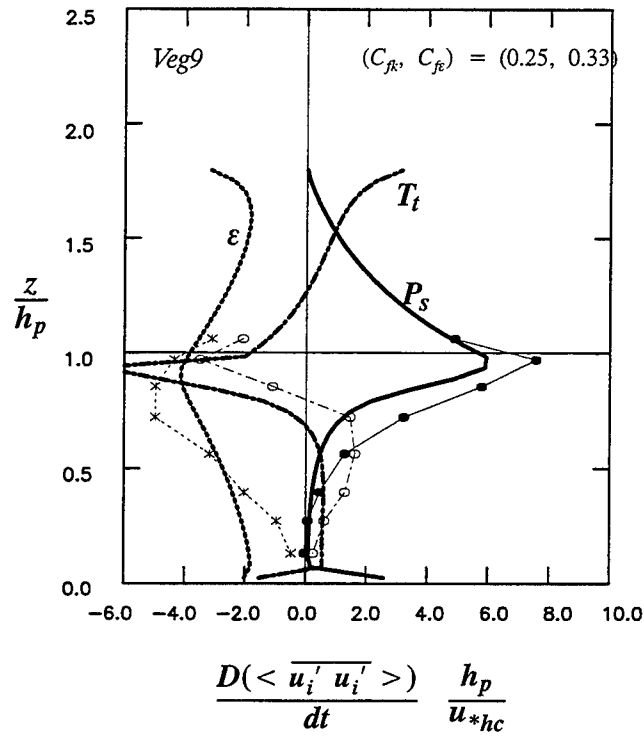


Figure 6.10 Observed and predicted vertical distribution of different terms in the spatially averaged, temporal-mean, turbulent kinetic energy budget for  $(C_{fk}, C_{fe}) = (0.25, 0.33)$ . Lines represent model predictions and symbols are observed values.

square root of the Reynolds stress at the top of the simulated canopy and  $h_p$  represents the average plant height.

### **Budget of total turbulent kinetic energy**

Although no experimental observations were available for comparison, dimensionless vertical profiles of the total turbulent kinetic energy were computed (i.e.,  $C_{fk} = 1.0$  and  $C_{f\varepsilon} = 1.33$ ). Figure 6.11 depicts the results obtained for the same experiments as in Figure 6.1.

### **Eddy Viscosity and Mixing Length**

Again, only reliable values of spatially averaged time-mean values of eddy viscosity and mixing length could be obtained from the experimental measurements. Figures 6.12 to 6.14 compare experimental observations with numerical results using three different sets of values for the weighting factors of the drag-related terms, namely  $(C_{fk}, C_{f\varepsilon}) = (0.0, 0.0)$ ,  $(C_{fk}, C_{f\varepsilon}) = (0.8, 1.04)$ , and  $(C_{fk}, C_{f\varepsilon}) = (1.00, 1.33)$ .

### **Turbulent Length Scales**

Dimensionless vertical profiles of macro- and micro-length scales were computed using Equations 58, 59 and 60. Numerical results corresponding to the conditions of Exp1 are plotted against experimental observations in Figure 6.15.

### **Momentum Transfer to the Bed**

In the evaluation of suspended sediment transport processes in open channels, the accurate estimation of the momentum transfer to the bed plays a crucial role, since this value is typically used to evaluate the ability of the flow to entrain sediment from the bed. Figure 6.16 illustrates the variation of the shear velocity, defined as the square root of the bed-shear stress per unit density, as a function of normalized plant density. Note that in this graph the shear velocity has been standardized using the total streamwise momentum due to gravity, i.e.  $\sqrt{g H S_o}$ .

### **Manning's Resistance Coefficient**

In order to evaluate the effect of vegetation upon flow resistance, values of Manning's resistance coefficients were computed as:

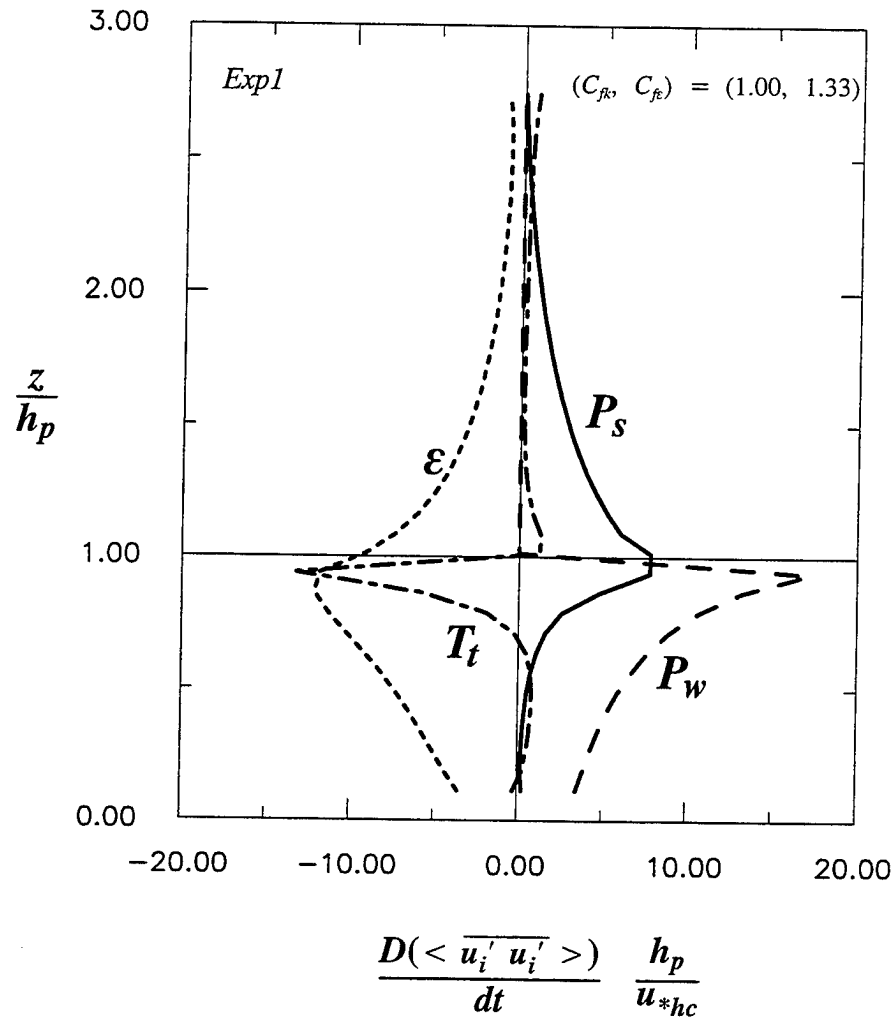


Figure 6.11 Observed and predicted vertical distribution of different terms in the total turbulent kinetic energy budget

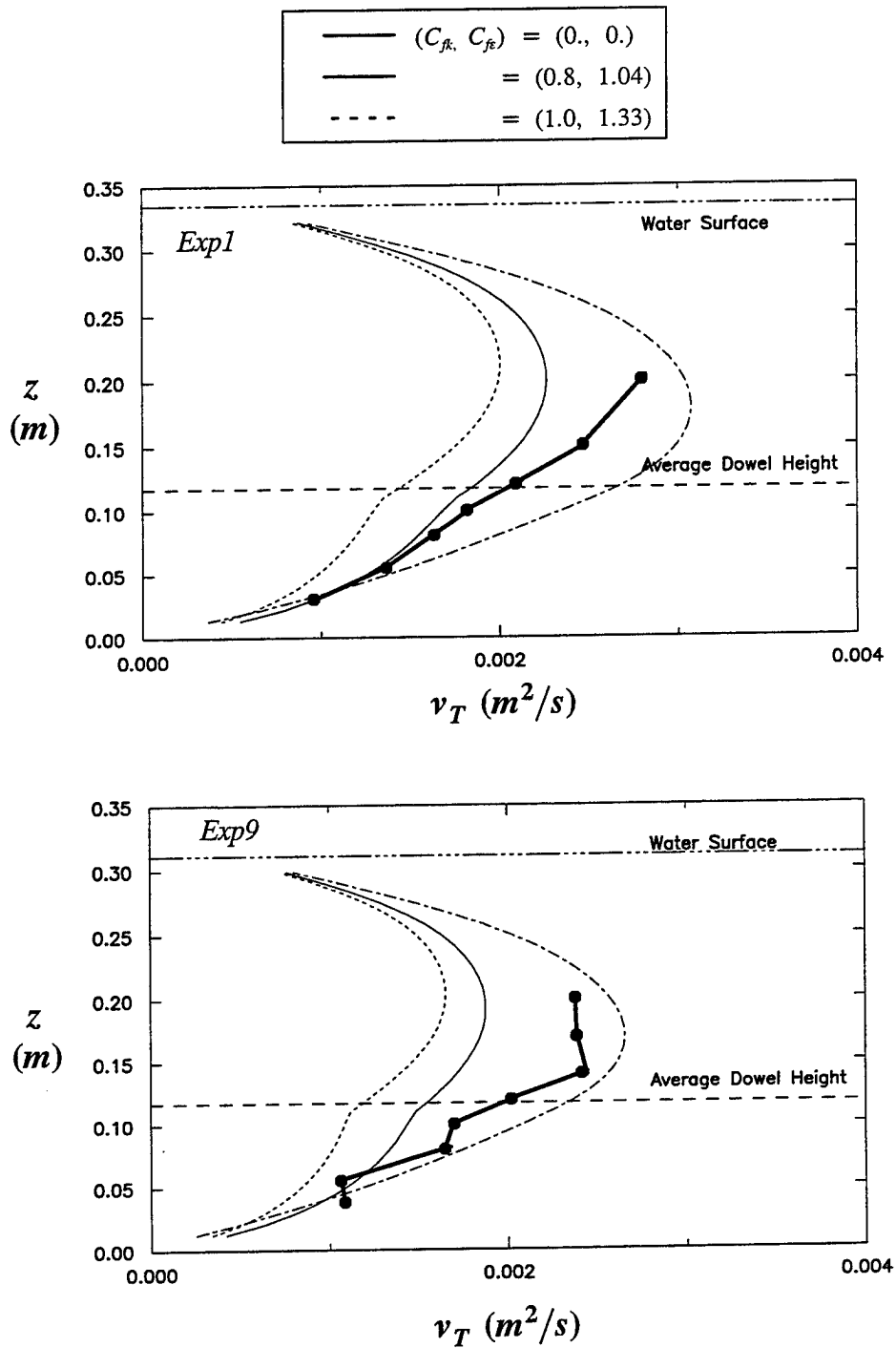


Figure 6.12 Observed and predicted vertical distribution of eddy viscosity, rigid condition

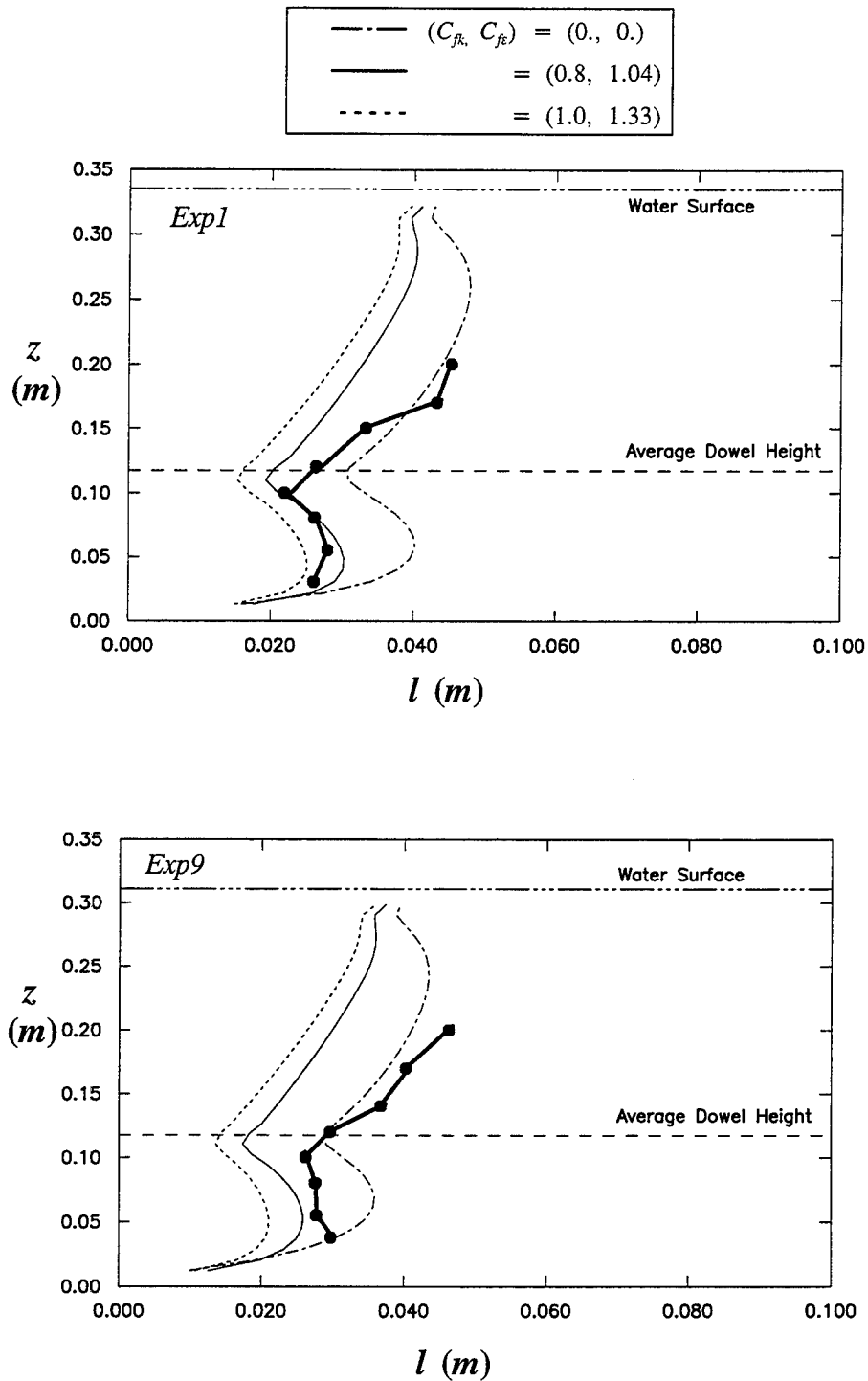
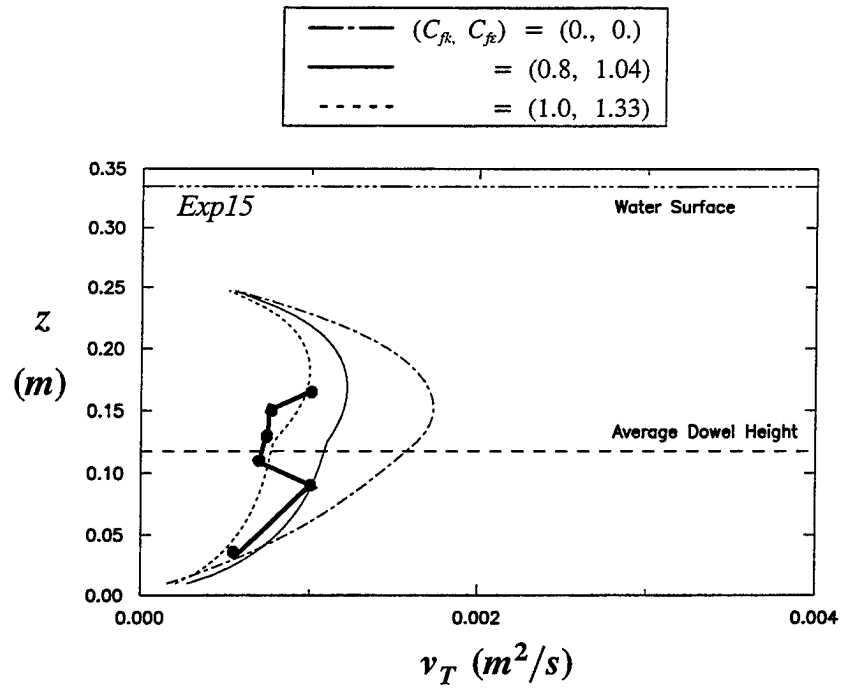
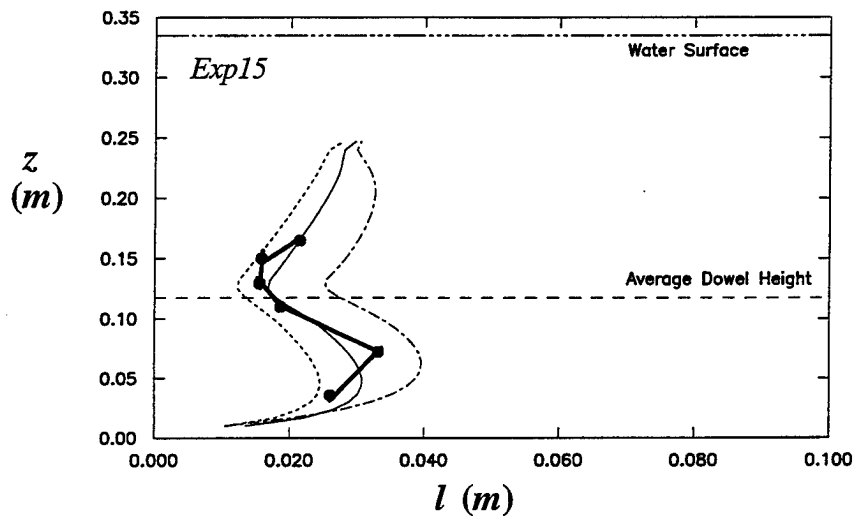


Figure 6.13 Observed and predicted vertical distribution of mixing length, rigid condition



a. Eddy viscosity



b. Mixing length

Figure 6.14 Observed and predicted vertical distribution of eddy viscosity and mixing length, flexible vegetation

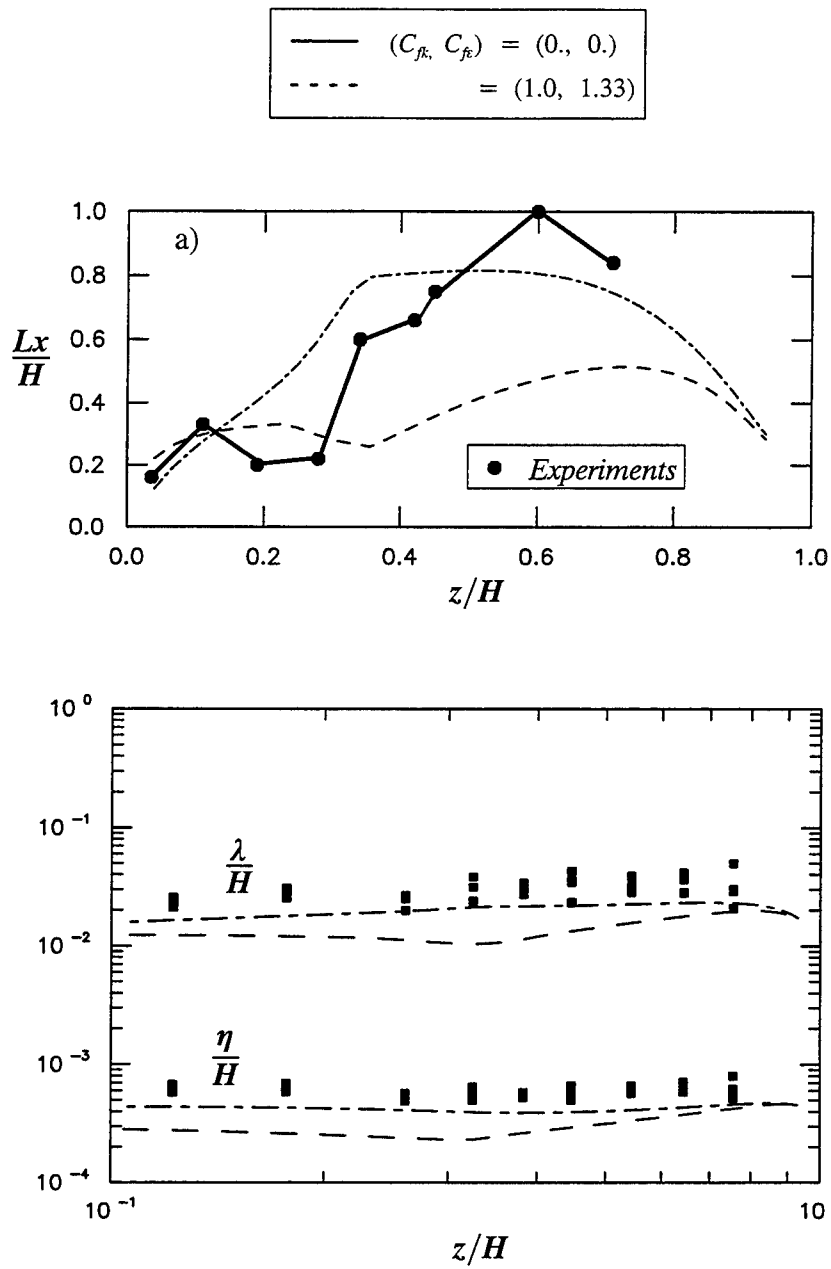


Figure 6.15 Observed (symbols) and predicted (thin lines) vertical distribution of dimensionless length scales for Exp1

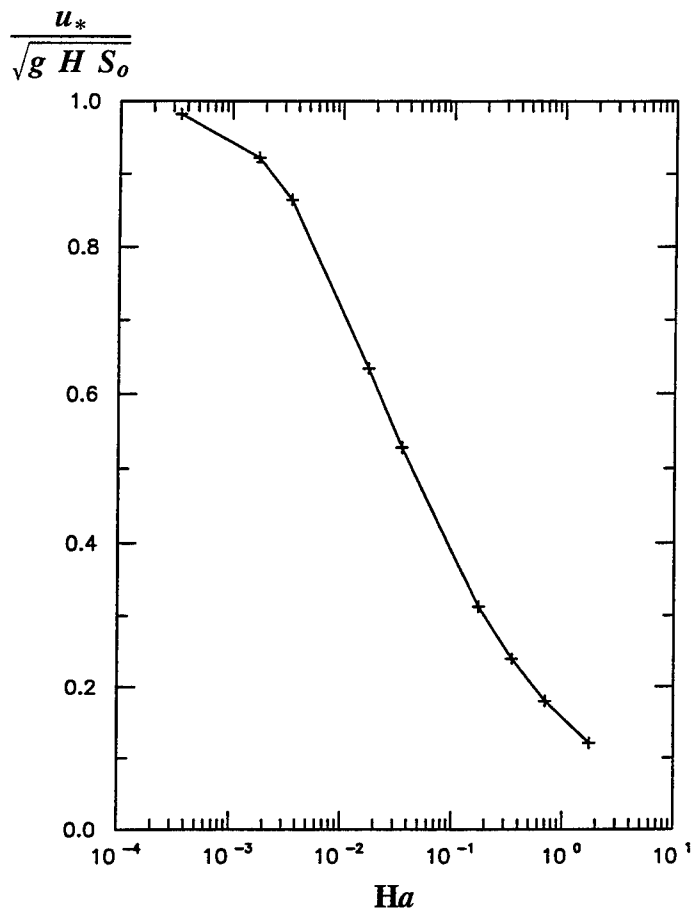


Figure 6.16 Momentum transfer towards the bed vs. dimensionless plant density

$$n = \frac{H^{5/3} S_o^{1/2}}{q_w} \quad (79)$$

where

$q_w$  = specific water discharge

Figure 6.17 shows the variation of  $n$  with plant density,  $a$ , for given values of water discharge,  $q_w = 1.12 \text{ m}^3/\text{m/s}$ , channel slope,  $S_o = 0.0036$ , and plant height,  $h_p = 0.10 \text{ m}$ . Since in engineering practice it is more common to measure density as number of plants/stems per square meter,  $\lambda_d$ , Figure 6.18 depicts the variation of both Manning's  $n$  and flow depth with  $\lambda_d$  for  $D = 6.4 \text{ mm}$  (diameter of cylinders used in authors' experiments). As can be observed, the resistance coefficient remains almost constant for low densities and it shows a sharp

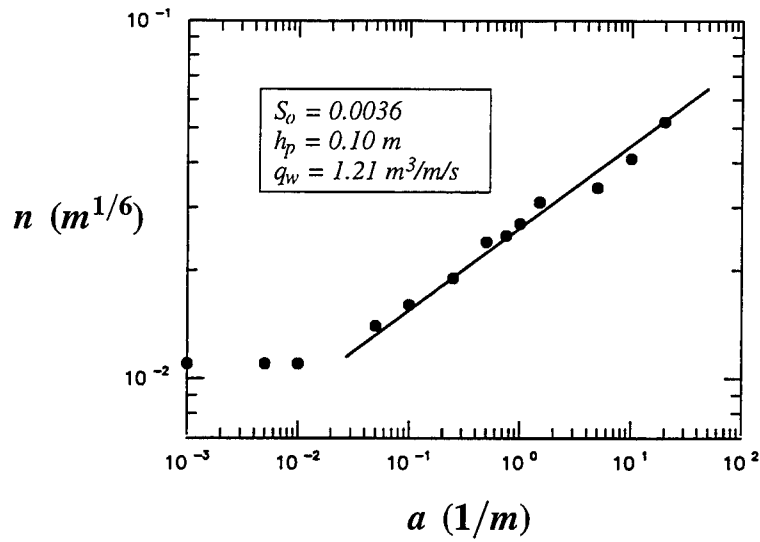


Figure 6.17 Computed values of Manning's resistance coefficient as a function of plant density

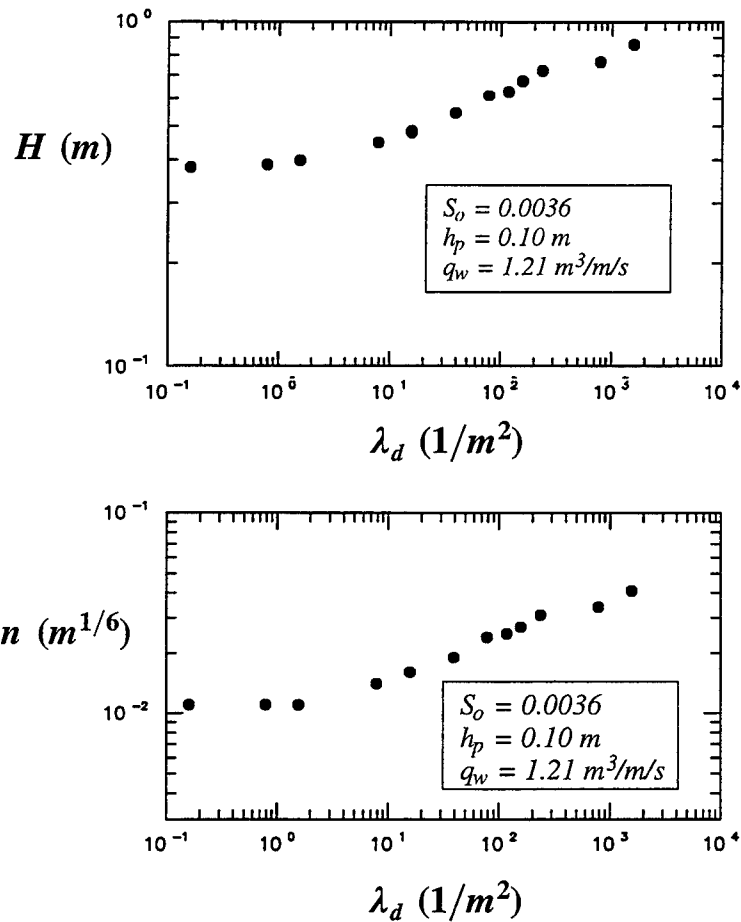


Figure 6.18 Computed values of flow depth and Manning's resistance coefficient as a function of density measured as number of plants per square meter

increase after a critical density value has been reached, increasing linearly afterwards. As mentioned in Chapter 2, this linear increase has also been observed in the field (Freeman, Hall and Abraham 1994).

## Impact of Wall Functions

As mentioned in Chapter 2, the wall functions used as bottom boundary conditions in the standard k- $\epsilon$  model implicitly assume the existence of an equilibrium layer (match or overlap region), where the logarithmic law describes the vertical distribution of mean velocities. As can be clearly observed from the budgets of turbulent kinetic energy this does not hold for the one-dimensional description of flow through vegetation. However, it was observed that the exact form of the wall functions was of little relevance for the computations, and that the drag-related source terms were of more critical importance for the flow structure. As an example, Figure 6.19 shows two different computations corresponding to Exp1, where the wall functions at the bed were modified as follows:

$$U_o = C_{vel} \frac{u_*}{\kappa} \text{Ln}\left(E \frac{z_o u_*}{\nu}\right) \quad (80)$$

$$k_o = C_k \frac{u_*^2}{\sqrt{C_\mu}} \quad (81)$$

$$\epsilon_o = C_\epsilon \frac{u_*^3}{\kappa z_o} \quad (82)$$

Indeed, specified values of mean velocities and shear stress using these expressions are so small that the simulated turbulence structure adjusts itself to a common profile, with results almost insensitive to the exact value of the boundary conditions at the bed. In view of these results, the standard wall functions have been used throughout the present work, i.e.,  $C_{vel} = 1.0$ ,  $C_k = 1.0$  and  $C_\epsilon = 1.0$ .

## Validity of Gradient-Flux Assumptions for Flow through Vegetation

Following the same ideas as in Chapter 4, data collected with the acoustic sensor were used to check the validity of the underlying assumptions involving the use of flux gradient models in vegetated, free-surface, wall-bounded shear flows. The criteria represented by Equations 40 and 42 have been evaluated in Figure 6.20, where results corresponding to flow without vegetation are also presented for comparison. Again, it may be clearly observed that from all the

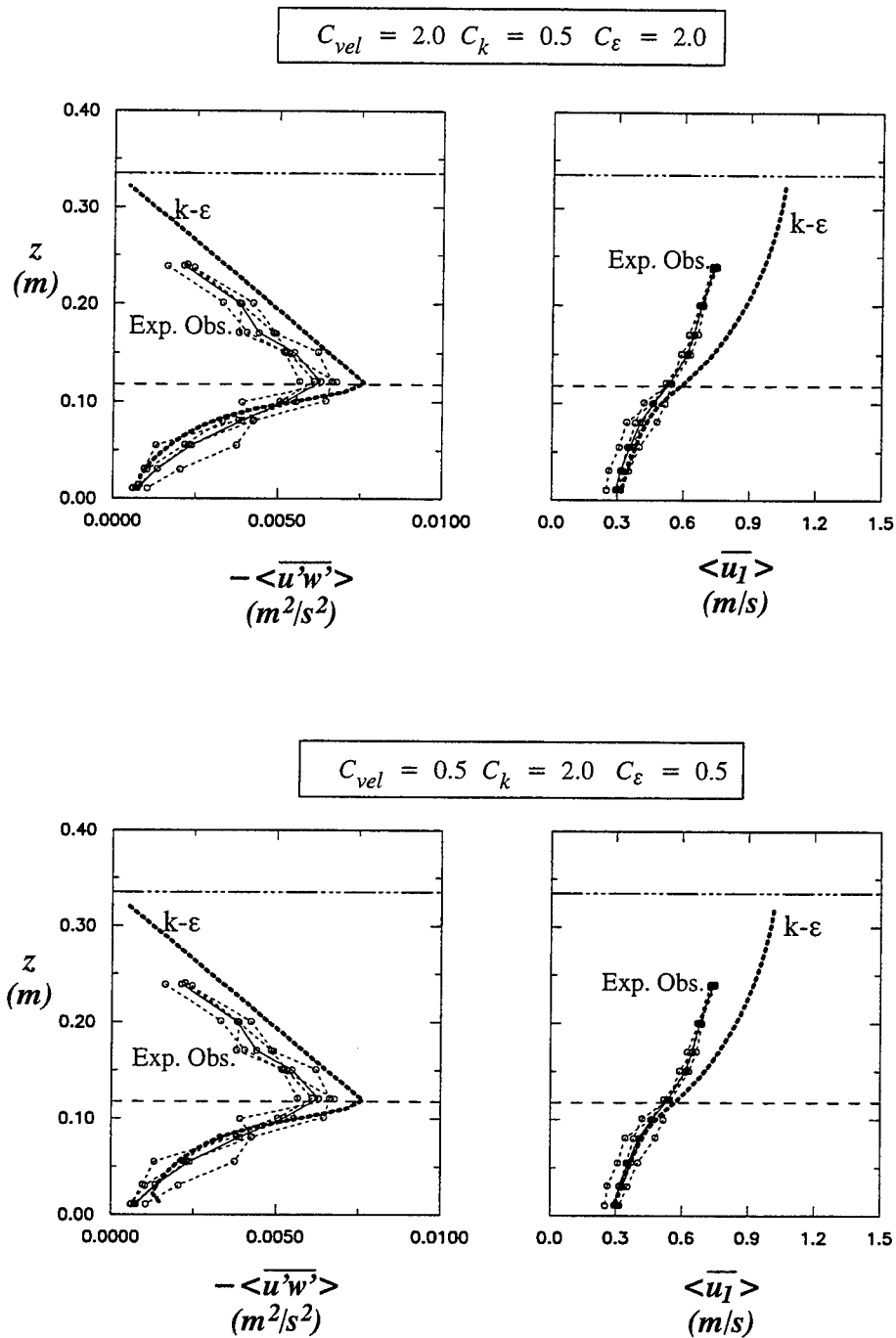


Figure 6.19 Impact of different wall functions

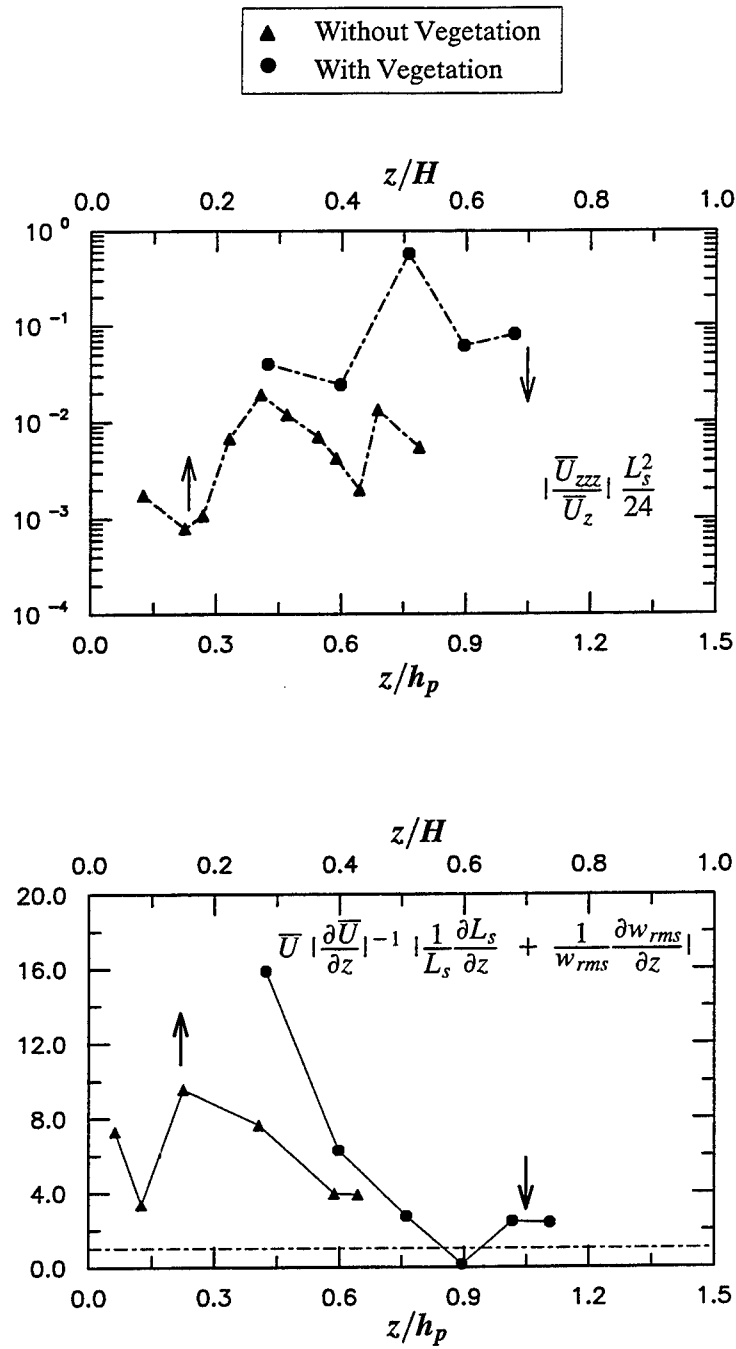


Figure 6.20 Evaluation of Corrsin's criteria for flow through vegetation

required conditions, the one requiring cross-stream uniformity of the length scale and root-mean-square velocity fluctuations, i.e., Equation 42, is the most seriously violated. As evidenced in previous figures, however, the violation of this requirement does not seem to significantly affect the turbulence simulations of the model, at least for the statistics commonly used in engineering research.

## Final Remarks

The graphs presented above demonstrate the overall ability of the numerical model to simulate not only the most commonly used flow statistics, like mean velocity, turbulence intensities and Reynolds stress, but also different terms in the budget of turbulent kinetic energy as well as mixing properties and turbulence macro and micro length scales for flow through vegetation. As mentioned before, observed profiles of temporal mean variables averaged over space are being best represented using negligible values for the drag-related weighting coefficients. Differences between numerical results using values of  $(C_{fk}, C_{f\varepsilon}) = (0.0, 0.0)$  and  $(C_{fk}, C_{f\varepsilon}) = (1.00, 1.33)$  are found to be larger at the top of the simulated plants, and to decrease towards the free surface. If real, these differences would imply the existence of streamwise turbulence heterogeneities in flow regions above the plants. More research is however needed to particularly address the influence of flow and vegetation properties upon the ratio between turbulent micro-length scales and element wakes, i.e. the relationship between these properties and the values of the weighting coefficients in the drag-related terms. Hereafter all the one-dimensional (thus involving the use of spatial and temporal averaged conservation laws) numerical simulations of turbulence processes will be performed with values for these coefficients of  $(C_{fk}, C_{f\varepsilon}) = (1.00, 1.33)$ , i.e. using Equation 10 for the turbulent kinetic energy balance and therefore  $k = (\overline{u_i'' u_i''} + \overline{u_i' u_i'})/2$ .

# 7 Suspended Sediment Transport in Vegetated Open Channels

---

In previous chapters two-equation turbulence model predictions have been verified against experimental observations both in open channels and vegetated free-surface flows, and the capability of the algorithm for simulating the turbulence structure has been checked. The last stage of the investigation will be then to apply the numerical code to estimate the suspended sediment transport capacity of flows in vegetated waterways. The present section begins with the introduction of dimensional analysis, which allows for the identification of the dimensionless parameters that govern the problem. Afterwards, the data set by Tollner, Barfield and Hayes (1982) will be employed to check the outcome of the numerical experiments. Further results include comparisons between simulated vertical distributions of sediment concentration and predicted profiles using the Rousean distribution, estimations of transport capacity as function of different dimensionless parameters, and computations of relative transport capacity between vegetated and nonvegetated open channels under similar hydraulic conditions, as a function of plant density, sediment diameter, etc.

## Dimensional Analysis of Sediment Transport in Vegetated Open Channels

The investigation of sediment transport processes in vegetated channels involves the consideration of so many variables characterizing the sediment, flow and plants properties, that the problem might seem almost intractable. Dimensional analysis constitutes a valuable tool in these situations. Any

variable,  $\chi$ , characterizing sediment transport processes in vegetated waterways may be expressed as a function of the same variables that govern the phenomenon in open channels without vegetation, plus some new variables that characterize the plant properties:

$$\chi = f\left[u_*, H, g, \mu, \varrho, (\varrho_s - \varrho), D_s, D, a, h_p, \alpha\right] \quad (83)$$

with  $\alpha$  representing a dimensionless parameter defining the flexibility of the vegetation. It is worth noting that in the previous expression  $u_*$  is the bed-shear velocity associated with the average streamwise momentum transfer to the bed.

If  $u_*$ ,  $\varrho$  and  $D_s$  are selected as the basic quantities for performing the standard dimensional analysis (see for example Yalin 1977), then:

$$\hat{\chi} = \hat{f}\left(\frac{u_* D_s}{\nu}, \frac{u_*^2}{g R D_s}, \frac{H}{D_s}, R, \frac{D}{D_s}, D_s a, \frac{h_p}{D_s}, \alpha\right) \quad (84)$$

where  $\hat{\chi}$  is the dimensionless form of the transport property and  $R = (\varrho_s - \varrho)/\varrho$ . It may be further observed that:

$$\frac{u_* D_s}{\nu} = \frac{u_*}{\sqrt{g R D_s}} \frac{D_s \sqrt{g R D_s}}{\nu} = \frac{u_*}{\sqrt{g R D_s}} R_{ep} \quad (85)$$

and

$$\frac{u_*^2}{g R D_s} = \frac{w_s^2}{g R D_s} \frac{u_*^2}{w_s^2} \quad (86)$$

Moreover, it can be shown that for grains of a given shape, the dimensionless parameter  $w_s^2/(gRD_s)$  can be represented solely as a function of  $R_{ep}$  (Parker 1978; Dietrich 1982). With all these considerations plus some additional combinations of dimensionless parameters, Equation 84 may be rewritten as:

$$\hat{\chi} = \hat{f}\left(R_{ep}, \frac{u_*}{w_s}, \frac{H}{D_s}, R, \frac{D}{D_s}, H a, \frac{h_p}{H}, \alpha\right) \quad (87)$$

Generally, calculations will be based on constant values of  $R = 1.65$  and very large values of the ratio  $H/D_s$  and  $D/D_s$ ; therefore Equation 87 may be further simplified into:

$$\hat{\chi} = \hat{f}\left(R_{ep}, \frac{u_*}{w_s}, H a, \frac{h_p}{H}, \alpha\right) \quad (88)$$

## Experiments by Tollner, Barfield and Hayes (1982)

As mentioned in the introduction, there are not many reliable data sets available with suspended sediment information for vegetated open channels. The complexity of the problem led some investigators to study sediment transport processes in the laboratory by simulating vegetation with different elements. In this section the predictions of the  $k-\varepsilon$  model will be compared with the experimental observations by Tollner, Barfield and Hayes (1982). These investigators used a relatively narrow and short laboratory flume (0.13-m-wide,

0.10-m-deep and 2.10-m-long) with 16d finish nails (Tollner, private communication) simulating rigid vegetation in a staggered pattern. They simulated sediment using glass beads of five different mean diameters. They found that their experimental results for suspended sediment transport could be well described using a modified version of Graf's parameters,  $\Phi_s^G$ , as:

$$\Psi = 0.52 (\Phi_s^G)^{-0.153} \quad (89)$$

where:

$$\Phi_s^G = \frac{C_o R_s \langle u_1 \rangle}{\sqrt{R g D_s^3}} \quad (90)$$

and

$$\Psi = \frac{R D_s}{R_s S_o} \quad (91)$$

where

$C_o$  = the volumetric suspended load concentration

$R_s$  = an "equivalent hydraulic radius" defined as:

$$R_s = \frac{b_p H}{b_p + 2 H} \quad (92)$$

with  $b_p$  representing the plant spacing.

It is worth mentioning that Equation 89 does not contain all the dimensionless parameters specified in Equation 88, in particular the parameters  $Ha$  and  $H/h_p$  are missing. The absence of the latter is justified because the authors seemed to have reported only values corresponding to emergent vegetation. The absence of the parameter  $Ha$  may also be justified by the fact that flow depth and nail spacing varied over a narrow range (the latter in the range 0.945-1.583 cm).

In order to compare numerical results with experimental observations the four hydraulic conditions given in Tollner (1974) were selected, where some turbulence measurements were conducted as well using hot-film anemometry. Figure 7.1 illustrates the results of the k- $\epsilon$  model compared to predictions by Equation 89. As can be observed, experimental results corresponding to the higher slope are very well predicted by the numerical model, while computed sediment transport capacity for the smallest slope is higher than the observed values. The observed disagreement may be attributed to the small dimensions of the experimental facilities, which may have precluded the establishment of equilibrium conditions. The shallow flow depths used in the experiments, ranging from about 1.3 to 5.0 cm, suggest also that the flows might not have had large enough Reynolds numbers, while the numerical model developed in the present work applies only to high-Reynolds-number flows.

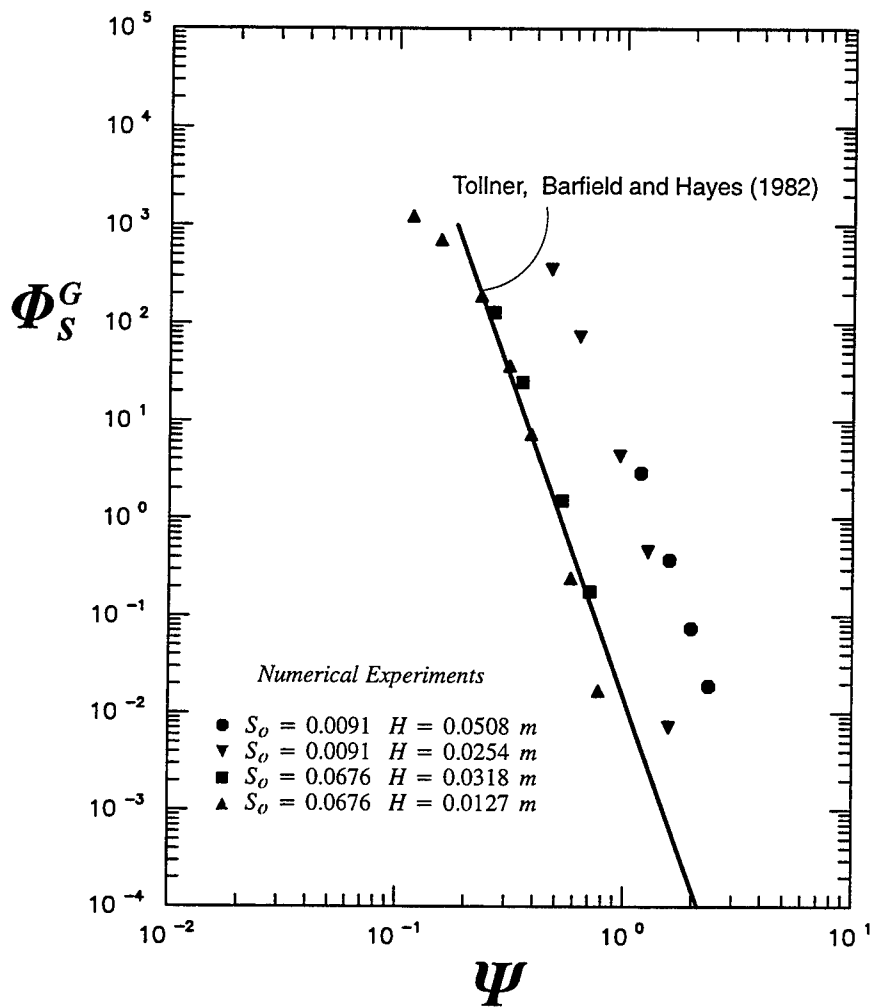


Figure 7.1 Numerical simulation of experimental observations by Tollner, Barfield and Hayes (1982)

## Vertical Profiles of Suspended Sediment Concentration

After the overall performance of the numerical code was checked, vertical profiles of suspended sediment concentrations were computed. It was found that, due to the particular shape of the vertical eddy viscosity profile, simulated relative distributions of suspended sediment concentrations differ only slightly from the classical profile in open channels (i.e. Rousean distribution). Figure 7.2 and 7.3 illustrate comparisons between simulated dimensionless profiles of suspended sediment concentration and predictions by the Rousean model for several sediment sizes, and two different conditions of bed slope and plant density. It is worth noticing that relative suspended sediment concentrations are larger than the ones predicted by the Rousean formula. It would seem that the effect of the vegetation is to promote a more uniform distribution of the suspended sediment, particularly within the plants.

## Suspended Sediment Transport Capacity

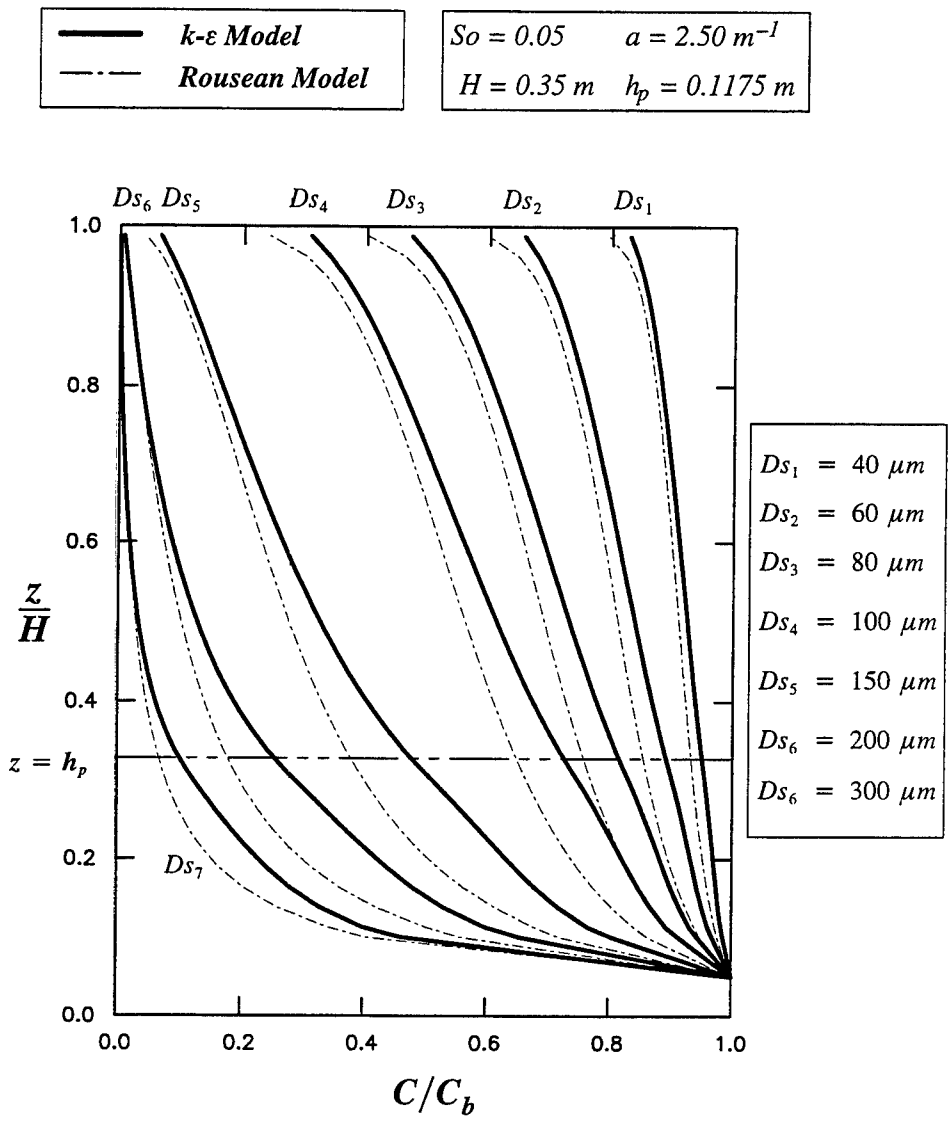
Dimensional analysis has shown that the suspended sediment transport capacity of vegetated channels depends upon several flow, sediment and plant parameters. This information is herein used to design a set of numerical experiments aiming at characterizing the particular effects of each of these parameters on the transport capacity. Such exercise provides also a means of testing the reliability of the numerical results, since the transport capacity should remain the same when dimensional variables are changed for identical values of the dimensionless parameters. Finally, the possibility of collapsing the information on transport capacity for different conditions is also investigated.

### Suspended Sediment Transport Capacity as function of $H/h_p$

In order to investigate the effects of the ratio  $H/h_p$  upon the suspended sediment transport capacity, the numerical model was used with constant values of mean flow depth and plant density ( $H = 0.35$  m and  $a = 2.0$  m<sup>-1</sup>) while three different values of plant height were used, namely  $h_p = 0.05, 0.10$  and  $0.25$  m in conjunction with varying sediment sizes and channel slopes. Figure 7.4 depicts the results obtained. The suspended transport capacity has been scaled using  $u_* D_s$  (see Yalin 1977); however any other scaling may be easily obtained combining the dimensionless parameters. For example Einstein's dimensionless version becomes:

$$\frac{q_{ss}}{\sqrt{g R D_s^3}} = \frac{q_{ss}}{u_* D_s} \frac{u_*}{\sqrt{g R D_s}} \quad (93)$$

with  $u_*/\sqrt{g R D_s}$  being the square-root of the Shields' stress.



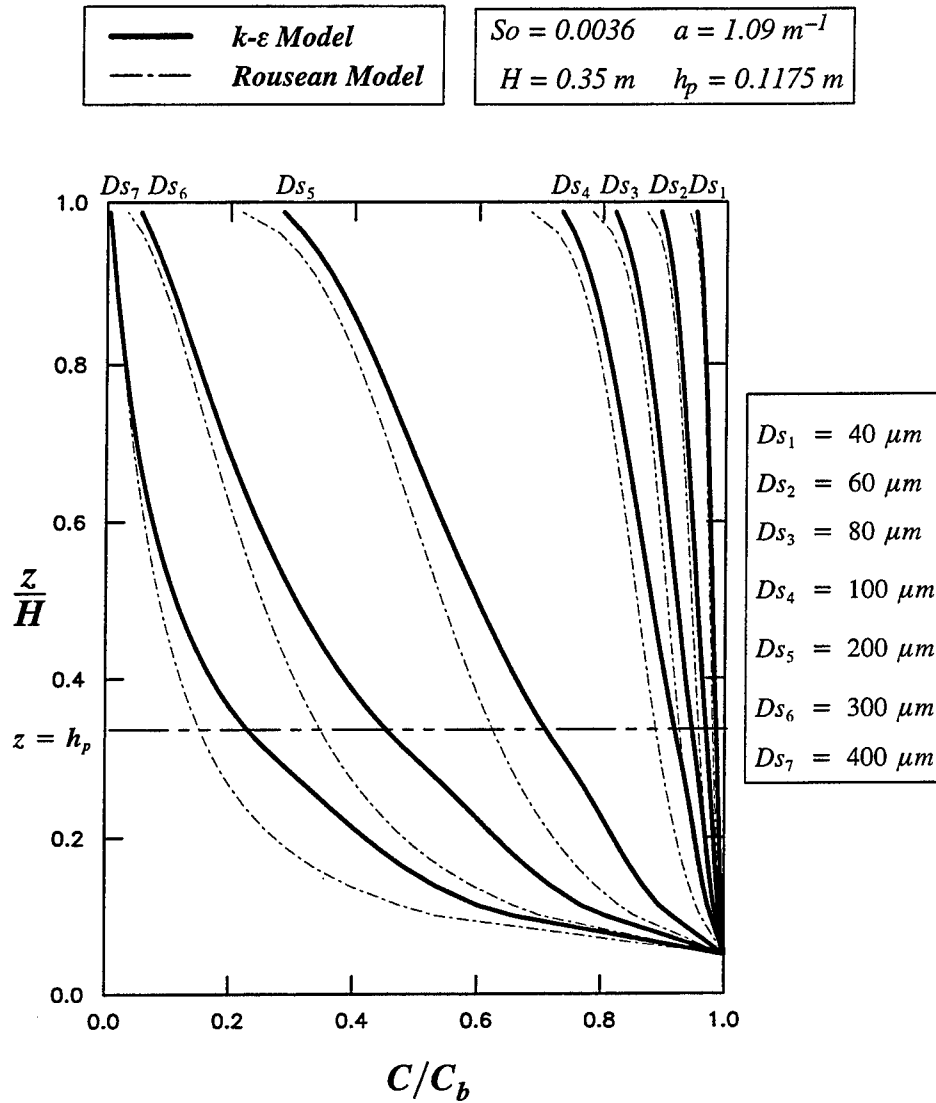


Figure 7.3 Observed and predicted vertical distribution of dimensionless suspended sediment concentration, condition II

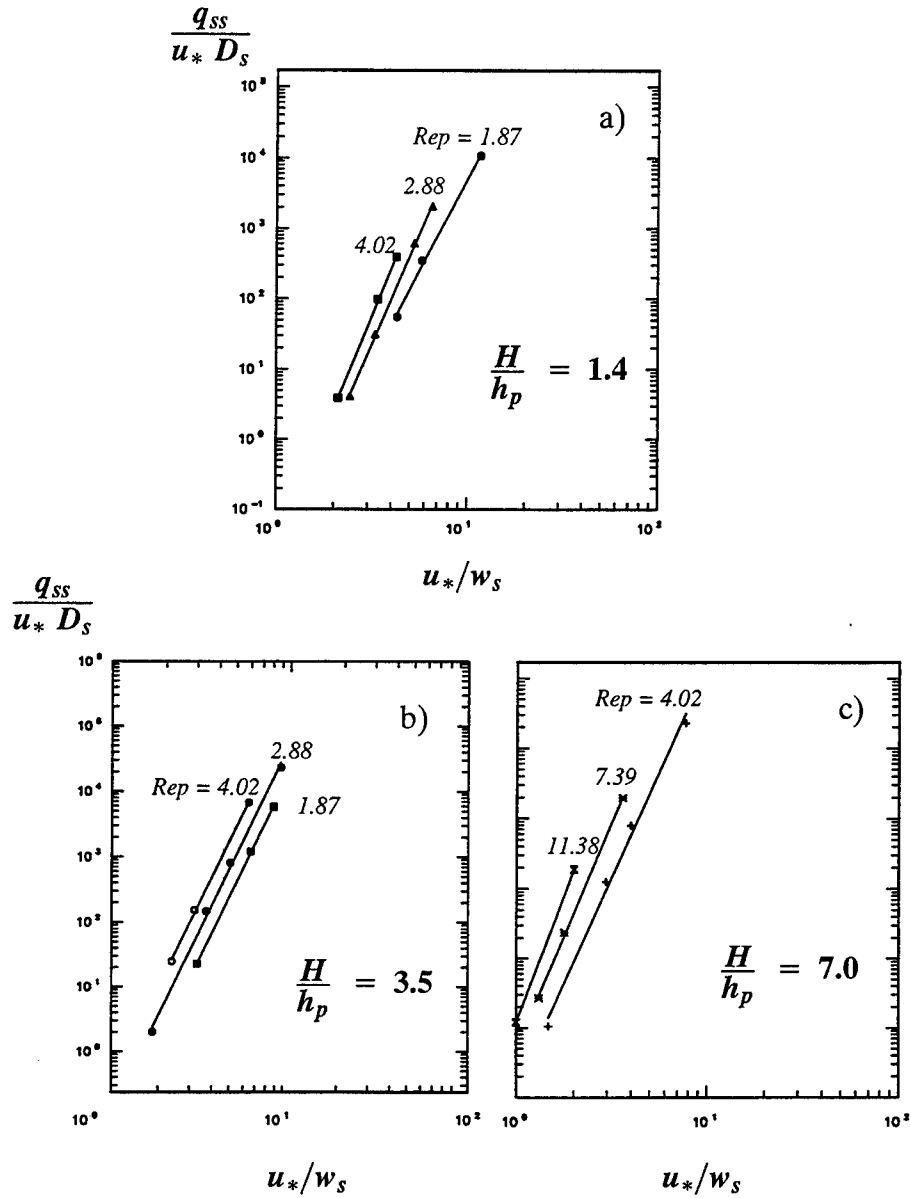


Figure 7.4 Computed suspended transport capacity as a function of  $u_*/w_s$ ,  $Rep$  and  $H/h_p$ , for  $Ha = 0.70$

It was observed that, as expected, transport capacity was a function of both  $u_*/w_s$  and  $R_{ep}$  for each value of the ratio  $H/h_p$ , so that:

$$\frac{q_{ss}}{u_* D_s} = f \left( R_{ep}^b \frac{u_*}{w_s} \right) \quad (94)$$

where the function  $f$  will depend on  $H/h_p$  (and  $Ha$ ). Using this approach, the data could then be collapsed onto a single curve for each  $H/h_p$  ratio. Results are shown in Figure 7.5. Moreover, since all curves in the previous figure are parallel, it is easy to make them all collapse into one single curve writing:

$$\frac{q_{ss}}{u_* D_s} = f \left[ R_{ep}^b \frac{u_*}{w_s} \left( \frac{H}{h_p} \right)^c \right] \quad (95)$$

Figure 7.6 illustrates results for the best fit value of  $c = 0.38$ .

### Suspended Sediment Transport Capacity as function of $Ha$

Following similar procedures as before, values of mean flow depth and plant height were kept constant in the numerical study ( $H = 0.25$  m and  $h_p = 0.071$  m), while plant density was allowed to vary, namely  $a = 0.5, 2.8$  and  $5.0$   $m^{-1}$ . Notice that for  $a = 2.8$   $m^{-1}$ ,  $H/h_p = 3.5$  and  $Ha = 0.7$ , which corresponds to one of the cases studied in the previous section, namely in Figure 7.4 b). Since in both cases values of these two parameters were equal, although the value of each dimensional variable was different, similar relations were expected then between the dimensionless transport capacity and  $u_*/w_s$  for each  $R_{ep}$ . Results are illustrated in Figure 7.7, which shows a good collapse of the computed curves for both cases. Figure 7.8 depicts estimated values of dimensionless transport capacity as a function of both  $u_*/w_s$  and  $R_{ep}$  for each value of the parameter  $Ha$  ( $H/h_p$  was kept constant and equal to 3.5).

### Relative Transport Capacity of Suspended Sediment

The influence of vegetation in reducing the suspended transport capacity of a channel was studied by computing the ratio  $q_{s-veg}/q_{s-oc}$  as a function of plant density for five different sediment sizes. Both water discharge,  $q_w$ , and plant height were kept constant. Here  $q_{s-veg}$  is the computed suspended sediment transport capacity of the vegetated waterway and  $q_{s-oc}$  is the capacity for an open channel of the same slope without vegetation and same water discharge. Results are illustrated in Figure 7.9. Note that in keeping  $q_w$  and  $h_p$  constant both  $Ha$  and  $H/h_p$  were allowed to vary. It is interesting to note that, for very low densities, the ratio  $q_{s-veg}/q_{s-oc}$  becomes slightly larger than unity for the coarsest sediment. This apparent contradiction may be explained by the fact that (at low densities) a small increase in density tends to decrease the momentum transfer toward the bed only by a small amount while at the same time requiring a small increase in flow depth due to the increased flow resistance. The combined effect

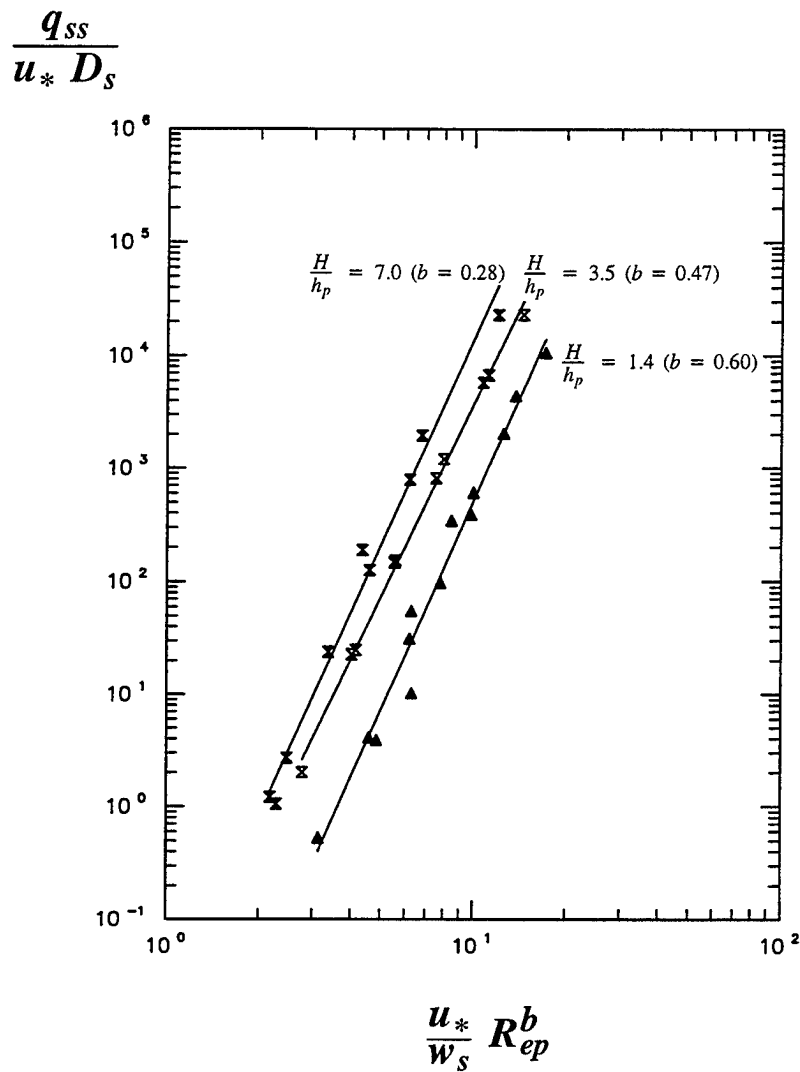


Figure 7.5 Computed suspended transport capacity as a function of the parameters  $u_*/w_s R_{ep}^b$  and  $H/h_p$ , for  $Ha = 0.70$

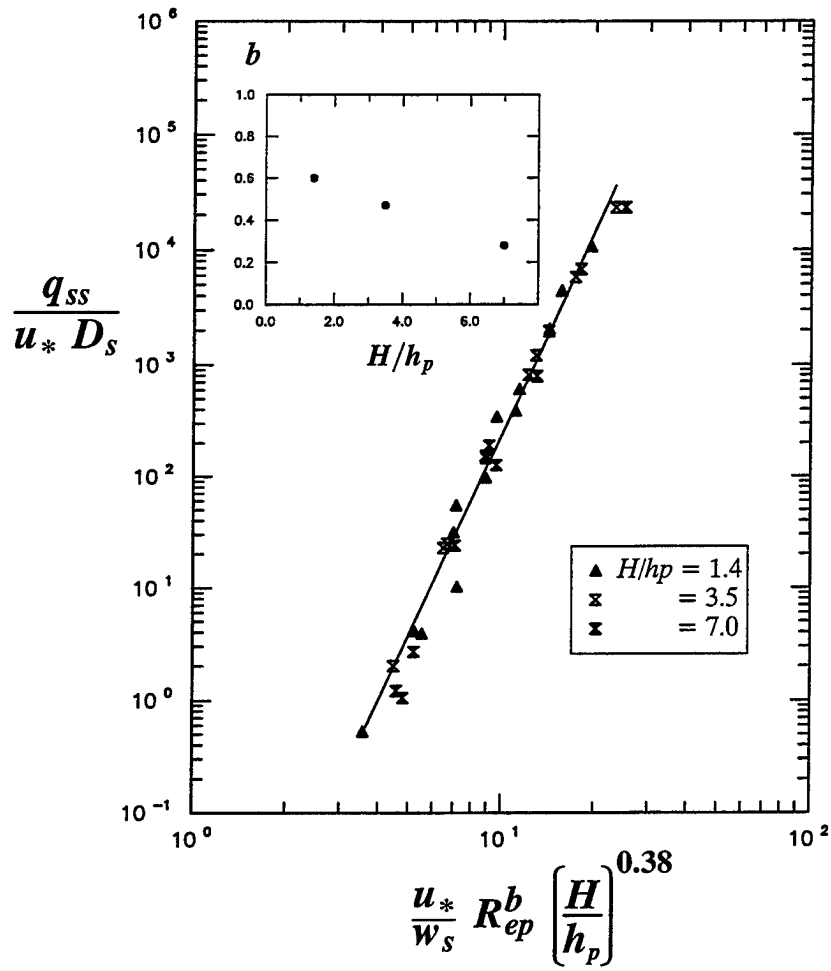


Figure 7.6 Computed suspended transport capacity as a function of parameter  $u_*/w_s R_{ep}^b (H/h_p)^{0.38}$ , for  $H\alpha = 0.70$

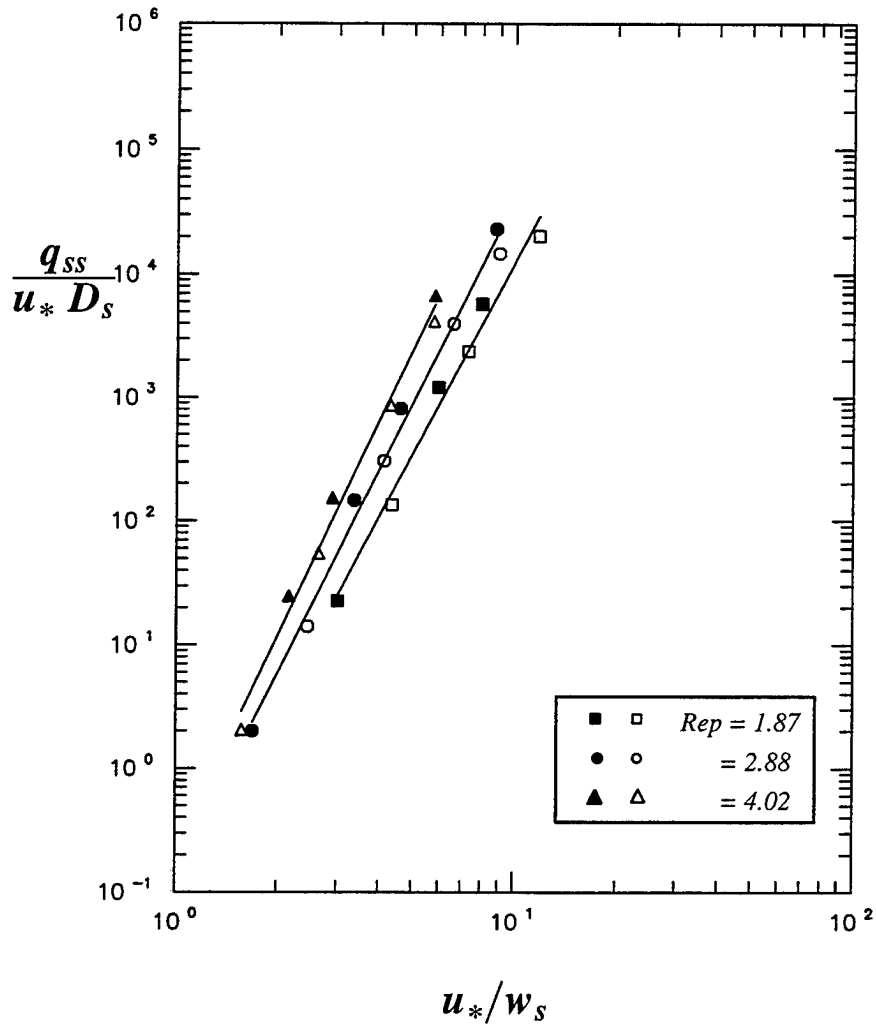


Figure 7.7 Computed suspended transport capacity as a function of  $u_*/w_s$  and  $Rep$ , for  $Ha = 0.70$  and  $H/h_p = 3.5$ . Closed symbols correspond to  $(H, a, h_p) = (0.35 \text{ m}; 2.0 \text{ m}^{-1}; 0.10 \text{ m})$ , whereas open symbols are for  $(H, a, h_p) = (0.25 \text{ m}; 2.8 \text{ m}^{-1}; 0.07 \text{ m})$

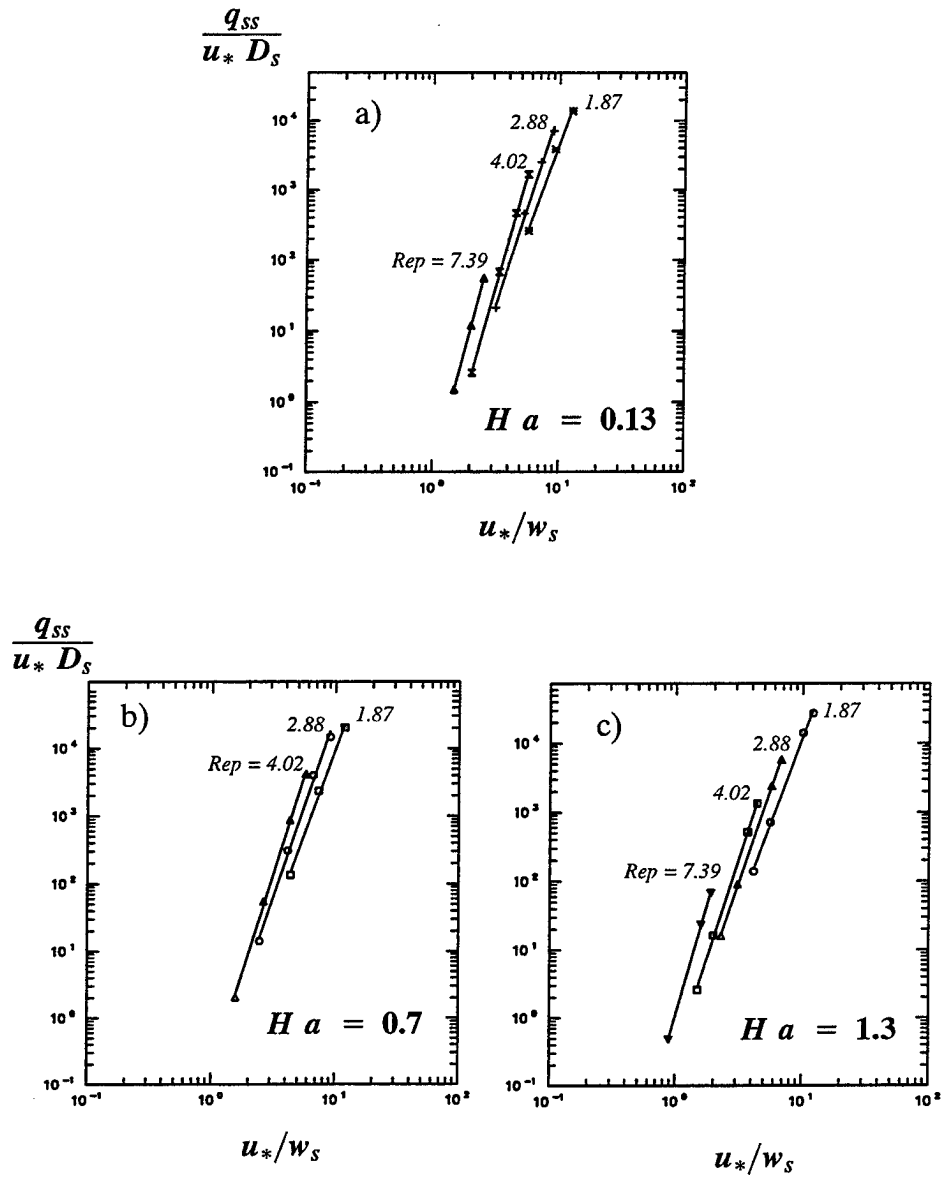


Figure 7.8 Computed suspended transport capacity as a function of  $u_*/w_s$ ,  $Rep$  and  $Ha$ , for  $H/h_p = 3.5$

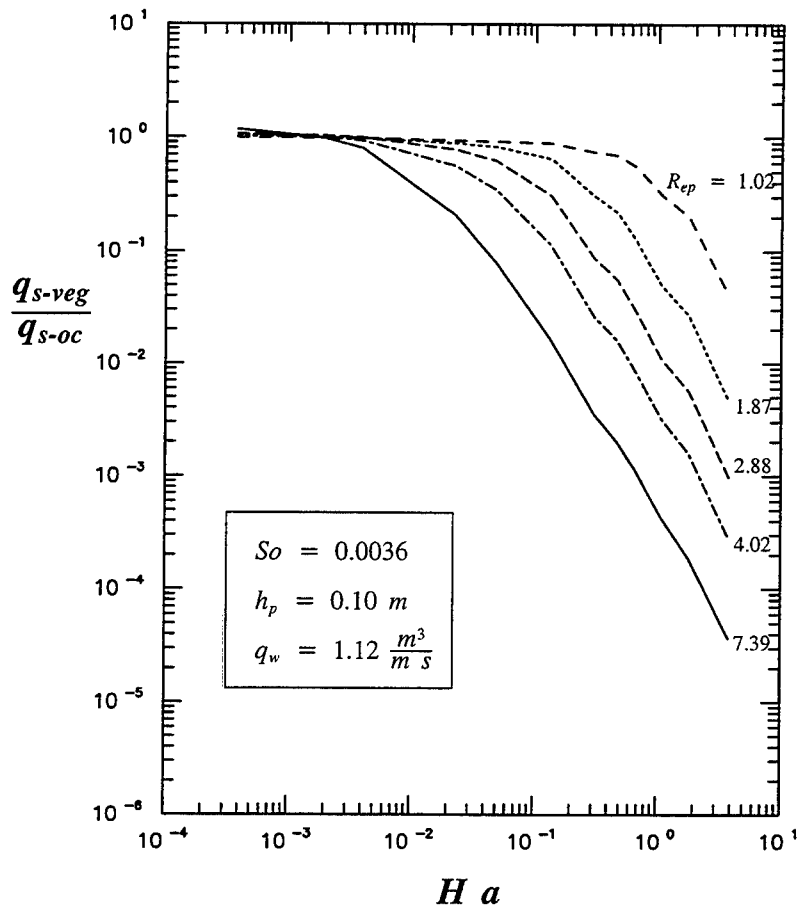


Figure 7.9 Computed relative transport in suspension as a function of density and sediment size for constant water discharge, channel slope, and plant height.

tends to keep the shear stress at the bottom nearly constant, and therefore to entrain as much sediment from the bed as without the plants. Moreover, if it is remembered that the relative sediment concentration profile shows larger values in the presence of vegetation, it can easily be explained why suspended transport capacity may become slightly larger in the presence of plants compared to flow without vegetation.

## Final Remarks

Dimensional analysis helped in identifying the different dimensionless parameters that govern sediment transport processes in vegetated water channels, and the numerical model proved to consistently predict suspended sediment loads under different conditions for the same parameter values. It is worth mentioning that, albeit at a preliminary level, a different type of two-equation model has also been developed as an alternative code, namely a  $k-\omega$  type closure (López and García 1996). Results of both models have been found to provide similar degree of representation to the experimental observations. Only as an example, Figure 7.10 shows the dimensionless sediment transport capacity as computed by the  $k-\omega$  model, compared to the best fit of results obtained with the  $k-\varepsilon$  model.

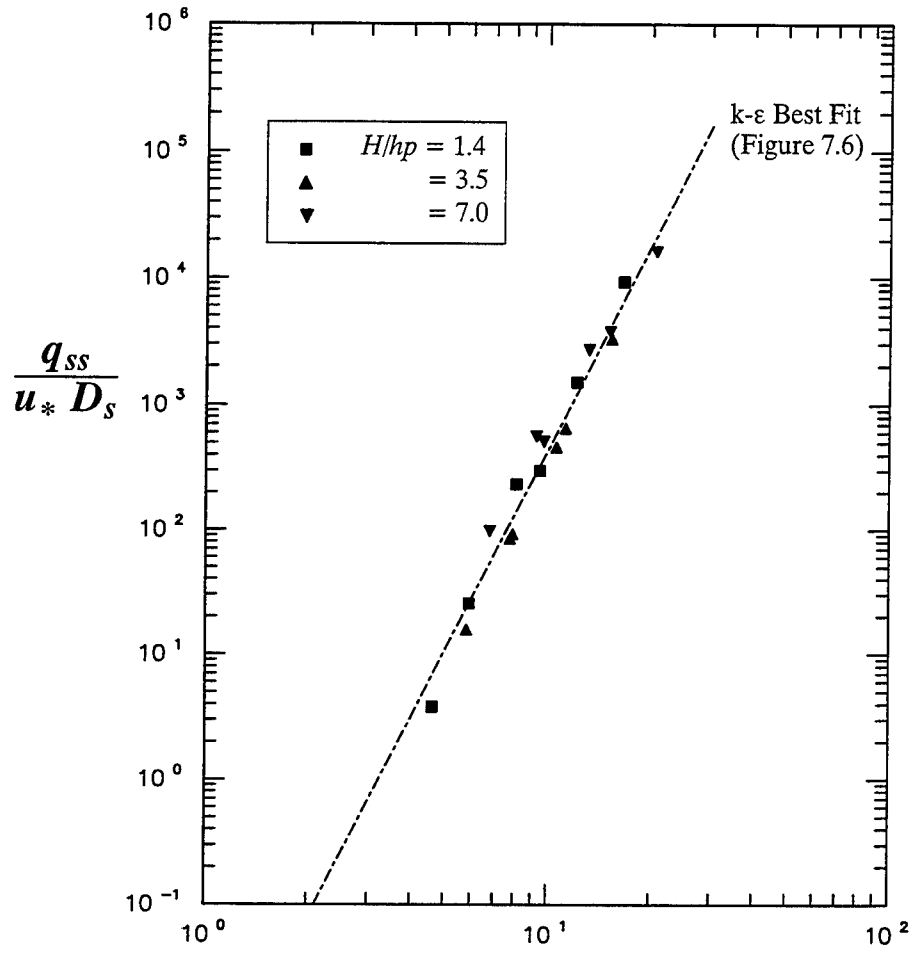


Figure 7.10 Suspended sediment transport capacity as a function of parameter  $\frac{u_*}{w_s} Re_p^b \left( \frac{H}{h_p} \right)^{0.38}$ , for  $Ha = 0.70$ . Computations by the k- $\omega$  model compared to best-fit line to results from k- $\epsilon$  model.

## 8 Summary and Conclusions

---

From the results shown in the previous sections, the following conclusions can be drawn:

- a.* The decrease in suspended sediment transport capacity of channels with vegetation compared to non-vegetated ones at similar water flow rates (i.e. the retention capability of the former) is highly dependent on the reduced ability of flow over a vegetation-covered bed to entrain sediment in suspension. This fact is in turn associated with the decrease in streamwise momentum transferred to the channel bed, due to the absorption of momentum by the plants via drag forces.
- b.* The above-mentioned fact has two important practical consequences, the first one being that any simpler model developed to compute the transport capacity of vegetated channels should be based on a reliable estimate of the average shear stress taken by the bed, which implies a good characterization of the form drag coefficient of plants in water channels. The second one is that laboratory and field studies are needed in order to develop a sediment entrainment function for flow through vegetation. The characteristics of the near-bed turbulence in vegetated open-channel flows are such that wake-generated turbulence might be the main mechanism responsible for sediment entrainment into suspension, playing a role similar to that of turbulent bursts in boundary-layer flows without obstructions.
- c.* The two-equation model of turbulence developed herein provides a good representation of the experimental observations of different turbulence variables, length scales and energy budget terms, hence constituting an

alternative tool for analyzing the influence of different flow and vegetation properties on the overall turbulence structure.

- d. The numerical model consistently predicts the sediment transport capacity under different flow, sediment and vegetation conditions for same values of the governing dimensionless parameters, and proper combination of these parameters further allows for the collapse of all information onto one single relation.
- e. The Rousean profile of relative sediment concentrations, computed with a shear velocity derived from the total action of gravity forces (i.e.  $u_* = \sqrt{g H S_o}$ ), predicts relative distributions very similar to the ones obtained with the numerical model. This might be mainly attributed to the parabolic-type shape of the eddy viscosity profile for both open channels with and without vegetation.
- f. Model results show the Manning's coefficient to remain almost constant (with values close to non-vegetated conditions) up to a critical plant density, and to increase linearly afterwards, in agreement with field studies.
- g. In summary, the two-equation numerical code, based on the k- $\epsilon$  turbulence closure scheme, constitutes a reliable tool for engineering assessments both on the turbulence structure and the suspended sediment transport processes in open channels through vegetation. The challenge for the future consists in extending the capabilities of the model developed for "idealized" vegetation to the case of natural plants.
- h. Future numerical, laboratory, and field work, will also benefit from the dimensional analysis carried out in the previous chapter. Also of particular relevance for future laboratory and field measurements, is the analysis conducted in Chapter 3, where the need to perform spatial as well as temporal averaging of flow measurements in order to obtain meaningful results was clearly demonstrated.

# References

---

1. Arcement, G. J., Jr., and Schneider, V. R. (1989). "Guide for selecting Manning's roughness co-efficients for natural channels and flood plains", Water-Supply Paper 2339, Department of the Interior, U.S. Geological Survey, Reston, VA.
2. Barenblatt, G. I. (1953). "On the motion of suspended particles in turbulent flow". *Prikl. Mat. Mekh.* 16 (1), pp 67-78.
3. Barenblatt, G. I. (1979). "Similarity, Self-Similarity, and Intermediate Asymptotics". Consultants Bureau. New York and London. 218 pp.
4. Barenblatt, G. I., and Golitsyn, G. S. (1974). "Local structure of mature dust storms". *J. Atmos. Sci.*, 31, pp. 1917-1933.
5. Barenblatt, G. I. (1995). "Selected topics in turbulence". Short Course, Department of Theoretical and Applied Mechanics. University of Illinois, Urbana-Champaign.
6. Blackwelder, R. F., and Kovasznay, L. S. G. (1972). "Time scales and correlations in a turbulent boundary layer". *Phys. Fluids* 15(9), 1545.
7. Burke, R. W. (1982). "Free surface flow through salt marsh grass". PhD diss. Massachusetts Institute of Technology Woods Hole Oceanographic Institution, Woods Hole, MA.
8. Burke, R. W., and Stolzenbach, K. D. (1983). "Free surface flow through salt marsh grass". MIT-Sea Grant Report MITSG 83-16, Cambridge, MA, 252 pp.

9. Celik, I., and Rodi, W. (1984). "Simulation of free-surface effects in turbulent channel flows". *Physico-Chem. Hydrodyn.* **5**, 217.
10. Celik, I., and Rodi, W. (1988). "Modeling suspended sediment transport in nonequilibrium situations". *J. Hydr. Eng.* **114**, 1157.
11. Chien, K-Y. (1982). "Predictions of channel and boundary-layer flows with a low-Reynolds-number turbulence model". *AIAA Journal*, Vol. **20**, No. 1, pp. 33-38.
12. Christensen, B. A. (1985) "Open channel and sheet flow over flexible roughness". *Proc. of the Int. Assoc. for Hydr. Res. (IAHR) 21st Congress*. Melbourne, pp 463-467.
13. Coleman, N. L. (1981) "Velocity profiles with suspended sediment". *J. Hydr. Res.*, **19**, pp. 211-229.
14. Corrsin, S. (1974). "Limitations of gradient transport models in random walks and in turbulence". *Turbulent diffusion in environmental pollution*. Proceedings of the Symposium, Charlottesville, VA. Vol 18A. (Frenkiel and Munn, ed.) Academic Press.
15. Dawson, F. H., and Charlton, F. G. (1988). "Bibliography on the hydraulic resistance or roughness of vegetated watercourses". Freshwater Biological Association, Occasional Publ. No. 25.
16. Demissie, M. (1990). "Sediment yield and accumulation in the Cache River". *Proc. National Hydr. Eng. Conf.*, 814.
17. Dietrich, W. E. (1982). "Settling velocities of natural particles". *Water Resour. Res.* **19**(3), 211.
18. Dunn, C., López, F., and García, M. (1996). "Mean flow and turbulence structure induced by vegetation: experiments". Hydraulic Engineering Series No. 51, UILU-ENG 96-2009, Department of Civil Engineering, University of Illinois at Urbana-Champaign.
19. Dunn, C. J. (1996). "Flow structure and resistance in a laboratory channel with simulated vegetation". M. S. thesis., University of Illinois, Urbana-Champaign. 146 pp.
20. Einstein, H. A. (1950) "The bed-load function for sediment transportation in open channel flows". *U.S. Dept. Agric., Soil Conserv. Serv.*, T.B. No. 1026.

21. Einstein, H. A., and Chien, N. (1955). "Effects of heavy sediment concentration near the bed on velocity and sediment distribution". Univ. Calif. Inst. Eng. Res. No. 8.
22. Freeman, G. E., Hall, B. R., and Abraham, D. D. (1994). "Flow resistance and sediment retention for bulrushes in wetland environments". *Proceedings American Society of Agricultural Engineers*, Winter 1993 Meeting, Chicago IL.
23. García, M. (1992). Boundary conditions for sediment-laden flows. *Proc. of Water Forum '92*. Baltimore, MA. American Society of Civil Engineers, New York.
24. García, M., and Parker, G. (1991). "Entrainment of bed sediment into suspension". *J. Hydr. Engrg.* **117** (4), 414.
25. Gourlay, M. R. (1970). Discussion on: "Flow retardance in vegetated channels", by N. Kowen and T. E. Unny, *J. of the Irrig. and Drainage Div.*, Proc. Paper 7498, **96**, 351.
26. Graf, W. H. (1971). "Hydraulics of sediment transport". McGraw-Hill, New York, 513 pp.
27. Happel, J., and Brenner, H. (1965). "Low Reynolds number hydrodynamics". Prentice-Hall, Englewood Cliffs, NJ.
28. Haslam, S. M., and Wolseley, P. A. (1981). "River vegetation: Its identification, assessment and management". Cambridge University Press.
29. Hino, M. (1981). *Ecohydrodynamics*. Advances in Hydrosience. Vol. **12**, pp. 143-193.
30. Hinze, J. O. (1975). "Turbulence". McGraw-Hill. 790 pp.
31. Jones, W. P., and Launder, B. E. (1972) "The prediction of laminarization with a two-equation model of turbulence". *Int. Journal of Heat and Mass Transf.*, Vol. **15**, pp 301-314.
32. Kadlec, R. H. (1990). "Overland flow in wetlands: Vegetation resistance". *J. Hydr. Eng.* **116**, 691.
33. Kim, J., Moin P., and Moser R. (1987). "Turbulence statistics in fully developed channel flow at low Reynolds number", *J. Fluid Mech.* **177**, 133.

34. Kolmogorov, A. N. (1942). "The equation of turbulent motion of an incompressible viscous fluid". *Izv. Akad. Nauk SSSR, Ser.Fiz.* VI(1-2), 56.
35. Kowen, N., Unny, T. E., and Hill, H. M. (1969). "Flow retardance in vegetated channels", *J. Irrig. and Drainage Div.* **95** (IR 2), 329.
36. Kowen, N., and Unny, T. E. (1973). "Flexible roughness in open channels", *J. Hydr. Div.* **99**, 713.
37. Kowen, N., and Li, R. (1980). "Biomechanics of vegetative channel linings", *J. Hydr. Div.* **106** (HY 6), 1085.
38. Launder, B. E., Reece, G. J., and Rodi, W. (1975). "Progress in the development of a Reynolds-stress turbulence closure", *J. Fluid Mech.*, **68** (3), 537.
39. Li, R., and Shen, H. (1973). "Effect of tall vegetation on flow and sediment", *J. Hydr. Div.* **99**, 793.
40. López, F. (1994). "Near-wall turbulent coherent structures and their role on sediment transport in smooth-bed open channel flows", M. S. thesis., University of Illinois, Urbana-Champaign. 200 pp.
41. López, F., and García, M. (1996). "Turbulence and sediment transport in vegetated open channels: Simulation using two-equation turbulence models". RIVERTECH96. First International Conference on New/Emerging Concepts for Rivers. Chicago, Illinois, September 22-26. pp. 12-19.
42. López, F. (1997). "Open-channel flow with roughness elements of different spanwise aspect ratios: Turbulence structure and numerical modelling" Ph.D. diss. University of Illinois. Urbana-Champaign.
43. McComb, W. D. (1990). "The physics of fluid turbulence". Clarendon Press, Oxford.
44. Monin, A. S., and Yaglom, A. M. (1971). "Statistical fluid mechanics: Mechanics of turbulence". Vol 1. The MIT Press, Cambridge, MA, 769 pp.
45. Nezu, I. (1977). "Turbulent structure in open-channel flows", (Translated from Japanese), Ph.D. diss., Kyoto University, Kyoto, Japan.
46. Nezu, I., and Rodi, W. (1986). "Open-channel flow measurements with a laser Doppler anemometer", *J. Hydr. Eng.* **112**, 335.

47. Nezu, I., and Nakagawa, H. (1993). "Turbulence in open-channel flows". IAHR Monograph, A.A. Balkema, Rotterdam, 281 pp.
48. Niño, Y. (1995). "Particle motion in the near bed region of a turbulent open channel flow: implications for bedload transport by saltation and sediment entrainment into suspension". Ph.D. diss. University of Illinois. Urbana-Champaign. 295 pp.
49. Palmer, V. J. (1945). "A method for designing vegetated waterways". *Agric. Eng.* **26**, 516.
50. Pantom, R. L. (1984). "Incompressible flow". A Wiley-Interscience Publication, Wiley, 780 pp.
51. Parker, G. (1978). "Self-formed straight rivers with equilibrium banks and mobile bed: Part 1. The sand-silt river", *J. Fluid Mech.*, **89** (1), 109.
52. Patankar, S. V., and Spalding, D. B. (1970). "Heat and mass transfer in boundary layers". Intertext, London.
53. Petryk, S. (1969). "Drag on cylinders in open channel flow". Ph.D. diss. Colorado State University, Fort Collins, CO.
54. Petryk, S., and Bosmajian, G. (1975). "Analysis of flow through vegetation". *Journal of Hydr. Engrg.* Vol. 101, No. 7, pp. 871-884.
55. Piomelli, U. (1994) "Large-eddy simulation of turbulent flows" TAM Report No. 767. UILU-ENG-94-6023. University of Illinois at Urbana-Champaign. 55 pp.
56. Prandtl, L. (1945). "Über ein neues formelsystem für ausgebildete turbulenz". Nachrichten von der Akad. der Wissenschaft in Göttingen, Math-Phys. Kl. 6.
57. Raupach, M. R., and Shaw, R. H. (1982). "Averaging procedures for flow within vegetation canopies", *Bound.-Layer Meteorol.* **22**, 79.
58. Raupach, M., and Thom, A. S. (1981). "Turbulence in and above plant canopies", *Ann. Rev. Fluid Mech.* **13**, 97.
59. Raupach, M. R., Coppin, P. A., and Legg, B.J. (1986). "Experiments on scalar dispersion within a model plant canopy. Part I: The turbulence structure". *Boundary-Layer Meteorology*, **35**, 21-52.

60. Ree, W. O., and Palmer, V. J. (1949). "Flow of water in channels protected by vegetative linings". *U.S. Soil Conservation Bulletin* No. 967, Feb., 115 pp.
61. Reid, R. O., and Whitaker, R. E. (1976). "Wind-driven flow of water influenced by a canopy", *J. Waterw. Engrg.* **102** (1), 67.
62. Rodi, W. (1976). "A new algebraic relation for calculating Reynolds stresses", *Z. Angew. Math. Mech.* **56**, 219.
63. Rodi, W. (1984). "Turbulence models and their applications in hydraulics: a state-of-the-art review". International Association for Hydraulic Research, The Netherlands.
64. Rotta, J. C. (1951). "Statistische Theorie nichthomogener Turbulenz", *Z. für Physik* **129**, 547.
65. Rotta, J. C. (1962). "Turbulent boundary layers in incompressible flow", *Prog. Aero. Sci.* **2**, 1.
66. Rouse, H. (1937). "Modern conceptions of the mechanics of turbulence". *Trans. Am. Soc. Civil Engrs.*, **102**, pp. 436-505.
67. Saowapon, C., and Kowen, N. (1989). "A physically based model for determining flow resistance and velocity profiles in vegetated channels". In: Symposium on Manning's Equation. B.C. Yen Ed., Virginia, pp. 559-568.
68. Schlichting, H. (1979). "Boundary-layer theory", 7th ed. McGraw-Hill, New York.
69. Shimizu, Y., and Tsujimoto, T. (1993). "Comparison of flood-flow structure between compound channel and channel with vegetated zone", *Proceedings XXV IAHR Congress*, Tokyo, Vol I, 97.
70. Svensson, U. (1986). "Program for boundary layers in the environment", The Swedish Meteorol. and Hydr. Inst. S-601, Norrköping, Sweden.
71. Tollner, E. W. (1974). "Modeling the sediment filtration capacity of simulated, rigid vegetation", M. S. thesis. University of Kentucky, Lexington, KY.
72. Tollner, E. W., Barfield, B. J., and Hayes, J. C. (1982). "Sedimentology of erect vegetal filters", *J. Hydr. Div.*, **108** (12), 1518.

73. Townsend, A. A. (1976). "The structure of turbulent shear flow". Cambridge University Press, Cambridge, MA.
74. Tsujimoto, T., Shimizu, Y., and Nakagawa, H. (1991<sup>a</sup>). "Concentration distribution of suspended sediment in vegetated sand bed channel". *Int. Symp. on the Transport of Susp. Sed. and its Math. Mod.* Florence, Italy.
75. Tsujimoto, T., Kitamura, T., and Okada, T. (1991<sup>b</sup>). "Turbulent structure of flow over rigid vegetation-covered bed in open channels", KHL Progressive Report 1, Hydr. Lab., Kanazawa University, Japan.
76. Tsujimoto, T. (1993). "Unstable phenomena appearing at flow with vegetation", *Proc. Intl. Conf. on Hydr-Sci. and Eng*, Washington, DC, 1390.
77. Tsujimoto, T., and Shimizu, Y. (1994). "Flow and suspended sediment in a compound channel with vegetation". KHL Hydraulic Research '94. Hydr. Lab., Kanazawa Univ. Japan. Also in: *Proc. 1st Int. Symp. Habitat Hydraulics*, Trondheim, Norway. August, 1994.
78. Uberoi, M. S. (1957). "Equipartition of energy and local isotropy in turbulent flows", *J. Appl. Phys.* **28**, 1165.
79. U.S. Department of Agriculture. (1987). "Agricultural resources: Cropland, after and conservation situation and outlook report". *Economic Research Service, USDA*, Washington, DC. 39 pp.
80. U.S. Environmental Protection Agency (1993). "Created and natural wetlands for controlling nonpoint source pollution". Olson R.K. Ed. Office of Research and Development and Office of Wetlands, Oceans, and Watersheds. C.K. Smoley. 216 pp.
81. Vanoni, V. A. (1946) "Transportation of suspended sediment by water". *Trans. A. Soc. Civil Engrs.*, Vol **111**.
82. Wilson, N. R., and Shaw, R. H. (1977). "A higher-order closure model for canopy flow", *J. Appl. Meteorol.* **16**, 1198.
83. Yalin, M. S. (1977). *Mechanics of sediment transport*. 2nd Ed. Pergamon Press, New York, 298 pp.

# Appendix A Notation

---

$\overline{(\cdot)}$	Time-averaged operator over turbulence
$\langle \cdot \rangle$	Spatially averaged operator
$(\cdot)'$	Fluctuation over time-averaged value
$(\cdot)''$	Fluctuation over space-averaged value
$(\cdot)_+$	Variable made dimensionless using wall units ( $U_*$ and $v$ )
$\nabla$	Laplacian operator
$a$	Ratio between the sum of the differential frontal areas of the obstacles divided by the differential volume of fluid
$\alpha$	Dimensionless parameter defining flexibility of vegetation
$b$	Distance equal to five percent of the flow depth measured from the bottom
$b_p$	Plant spacing
$B$	Bouyancy parameter $B = -gR (k^2/\varepsilon^2) ( \partial C/\partial z )$
$C$	Suspended sediment concentration
$C_b$	Bottom sediment concentration
$Cc'$	Model parameter for temperature stratification effects on Prandtl-Schmidt number
$C_D$	Drag coefficient of plants
$C_{Ds}$	Drag coefficient of sediment particles
$C_\mu$	Eddy-viscosity coefficient in the $k$ - $\varepsilon$ turbulence model
$C_o$	Averaged suspended load concentration
$C_1, C_2$	Weighting coefficients for production- and dissipation-related terms
$C_{IR}$	Pressure-strain coefficient
$C_\varepsilon$	Coefficient modifying the traditional wall function for $\varepsilon$
$C_k$	Coefficient modifying the traditional wall function for $k$
$C_{vel}$	Coefficient modifying the traditional wall function for $U$

$C_{fk}, C_{f\varepsilon}$	Weighting coefficients for production- and dissipation-related drag-terms
$D$	Horizontal diameter of the (vertically oriented) plants
$D_s$	Mean sediment diameter
$\delta_{ij}$	Kronecker delta
$\Delta t, \Delta z$	Time and vertical spacing on the numerical grid
$E$	Roughness parameter approximately equal to 9 for hydraulically smooth conditions and $30\nu/u_*'/k_s$ for fully rough conditions where $k_s$ = equivalent sand roughness
$EI$	Stem flexural rigidity
$\varepsilon$	Dissipation rate of turbulent kinetic energy
$Fr$	Froude number
$f_x$	Pressure Force per unit length in z on the perimeter s
$f_i$	Drag force per unit volume, i-direction component
$\phi_c, \phi_c'$	Model parameters for temperature stratification effects on Prandtl-Schmidt number
$\phi_s^G$	Modified version of Grass' parameter
$g$	Gravitational acceleration
$g_i$	Gravitational acceleration component in the i-direction.
$\gamma$	Pressure-strain coefficient
$hp$	Plant height
$H$	Mean flow depth
$\eta$	Kolmogorov microscale
$k_c$	Measure of roughness in the Einstein's (1950) equation for suspended load
$k_e$	Einstein's viscosity constant
$k_s$	Equivalent sandgrain roughness
$\kappa$	Von Karman's constant (0.40)
$k_w$	One-dimensional wave number in the streamwise direction
$k$	Turbulent kinetic energy
$k_o$	Turbulent kinetic energy evaluated at the first grid point from the bed
$l$	Mixing length
$L_s$	Length scale for momentum transfer
$L_x$	Macro-length scale for streamwise velocity fluctuations
$\lambda$	Taylor microscale
$\lambda_d$	Plant density in stems per square meter
$M$	Relative density of plants

$N$	Total number of grid points in the vertical direction
$n$	Manning's resistance coefficient
$\mathbf{n}$	Vector normal to the perimeter of the object
$n_x$	Component of $\mathbf{n}$ in the $x$ -direction
$n_{xu}, n_{xd}$	Vector $n_x$ in the upstream and downstream faces of the object, respectively
$\nu$	Fluid kinematic viscosity.
$\nu$	Kinematic viscosity of sediment-water mixture
$\nu_w$	Kinematic viscosity of clear water
$\nu_T$	Kinematic eddy viscosity
$\mu$	Fluid dynamic viscosity
$P$	Instantaneous pressure
$P, P_w$	Shear- and wake-production terms
$\Psi$	Modified version of Grass' parameter
$Q$	Total water discharge
$q_w$	Specific water discharge
$q_{ss}$	Suspended sediment transport capacity
$q_{s-oc}$	Suspended sediment transport capacity without vegetation
$q_{s-veg}$	Suspended sediment transport capacity with vegetation
$Re$	Flow Reynolds number
$Re_p$	Dimensionless particle size defined as $Re_p = D_s \sqrt{g R D_s} / \nu$
$R_h$	Hydraulic radius
$R_s$	Equivalent hydraulic radius
$R$	Submerged specific gravity of sediment, defined as $= (\rho_s - \rho) / \rho$
$\rho$	Fluid density
$\rho_s$	Sediment density
$\rho_w$	Clear water density.
$s$	Perimeter of a cylinder
$S_\psi$	Generalized source term
$S_o$	Bed slope
$S(k_w)$	One-dimensional normalized spectra for streamwise velocity
$\sigma$	Prandtl-Schmidt number
$\sigma_c$	Prandtl-Schmidt number for sediment particles
$\sigma_{co}$	Prandtl-Schmidt number for non-stratified conditions
$t$	Time

$Tt$	Turbulent transport of turbulent kinetic energy
$T_s$	Time-scale of momentum transfer
$u_1 (u), u_2(v), u_3(w)$	Instantaneous streamwise, spanwise and wall-normal velocities, respectively
$U, V, W$	Mean streamwise, spanwise and wall-normal velocities, respectively
$u', v', w'$	Streamwise, spanwise and wall-normal velocity fluctuations, respectively
$u_{rms}, v_{rms}, w_{rms}$	Root-mean square values of streamwise, spanwise and wall-normal velocity fluctuations, respectively
$U_o$	Value of $U$ at first grid point from the bed
$u_*$	Mean bed shear velocity
$U_{*hp}$	Square-root of the Reynolds stress per unit density at the top of the canopy
$x, y, z$	Right-handed coordinate system representing streamwise, spanwise and wall-normal axis, respectively.
$w_s$	Terminal fall velocity of sediment particle
$Z_u$	Garcia and Parker's parameter ( $Z_u = u_*/w_s R_{ep}^{0.6}$ )
$z_o$	First grid point away from the bed
$\chi$	Generalized variable characterizing sediment transport process

# REPORT DOCUMENTATION PAGE

*Form Approved*  
OMB No. 0704-0188

Public reporting burden for this collection of information is estimated to average 1 hour per response, including the time for reviewing instructions, searching existing data sources, gathering and maintaining the data needed, and completing and reviewing the collection of information. Send comments regarding this burden estimate or any other aspect of this collection of information, including suggestions for reducing this burden, to Washington Headquarters Services, Directorate for Information Operations and Reports, 1215 Jefferson Davis Highway, Suite 1204, Arlington, VA 22202-4302, and to the Office of Management and Budget, Paperwork Reduction Project (0704-0188), Washington, DC 20503.

<b>1. AGENCY USE ONLY (Leave blank)</b>	<b>2. REPORT DATE</b> August 1997	<b>3. REPORT TYPE AND DATES COVERED</b> Final report	
<b>4. TITLE AND SUBTITLE</b> Open-Channel Flow Through Simulated Vegetation: Turbulence Modeling and Sediment Transport		<b>5. FUNDING NUMBERS</b> Work Unit 32752	
<b>6. AUTHOR(S)</b> Fabian Lopez, Marcelo Garcia			
<b>7. PERFORMING ORGANIZATION NAME(S) AND ADDRESS(ES)</b> Hydrosystems Laboratory Department of Civil Engineering University of Illinois at Urbana-Champaign Urbana, IL 61801		<b>8. PERFORMING ORGANIZATION REPORT NUMBER</b> Technical Report WPR-CP-10	
<b>9. SPONSORING/MONITORING AGENCY NAME(S) AND ADDRESS(ES)</b> U.S. Army Engineer Waterways Experiment Station 3909 Halls Ferry Road, Vicksburg, MS 39180-6199; U.S. Army Corps of Engineers Washington, DC 20314-1000		<b>10. SPONSORING/MONITORING AGENCY REPORT NUMBER</b>	
<b>11. SUPPLEMENTARY NOTES</b> Available from National Technical Information Service, 5285 Port Royal Road, Springfield, VA 22161.			
<b>12a. DISTRIBUTION/AVAILABILITY STATEMENT</b> Approved for public release; distribution is unlimited.		<b>12b. DISTRIBUTION CODE</b>	
<b>13. ABSTRACT (Maximum 200 words)</b>  <p>The two-equation turbulence model based on the k-ε closure scheme was developed to simulate the flow and turbulence characteristics of open-channel flows through nonemergent vegetation. Once the performance of the model was verified, the flow structure of vegetated open channels was numerically simulated. Simulated rigid and flexible plants were used to validate the model. Finally, dimensional analysis allowed identification of the dimensionless parameters that govern suspended sediment transport processes in the presence of vegetation, and thus helped in the design of numerical experiments to investigate the role of different flow properties, sediment characteristics, and vegetation parameters upon the transport capacity.</p> <p>The two-equation turbulence model was found to accurately represent the mean flow and turbulence structure of open channels through simulated vegetation, thus providing the necessary information to estimate suspended sediment transport processes. A reduction of the averaged streamwise momentum transfer toward the bed (i.e., shear stress) induced by the vegetation was identified as the main reason for lower suspended sediment transport capacities in vegetated waterways compared with those observed in nonvegetated channels under similar flow conditions. Simulated profiles of kinematic eddy</p> <p style="text-align: right;">(Continued)</p>			
<b>14. SUBJECT TERMS</b> Flow profiles                      Sediment transport Numerical modeling              Turbulence Open-channel flow                Vegetation effects		<b>15. NUMBER OF PAGES</b> 123	<b>16. PRICE CODE</b>
<b>17. SECURITY CLASSIFICATION OF REPORT</b> UNCLASSIFIED	<b>18. SECURITY CLASSIFICATION OF THIS PAGE</b> UNCLASSIFIED	<b>19. SECURITY CLASSIFICATION OF ABSTRACT</b>	<b>20. LIMITATION OF ABSTRACT</b>

**13. (Concluded).**

viscosity were used to solve the sediment diffusion equation, yielding distributions of relative sediment concentration slightly in excess of the ones predicted by the Rousean formula. A power law was found to provide a very good collapse of all the numerically generated data for suspended sediment transport rates in vegetated channels.